A Study of Spherical Solutions in Chameleon Scalar-Tensor Theories

A thesis submitted in conformity with the requirements
for the degree of Master of Science
Department of Pure and Applied Mathematics
Rhodes University

by

Neo Mohapi

February 2014

Abstract

The equivalence principle has proven to be central to theories of gravity, with General Relativity being the simplest and most elegant theory to embody the principle. Most alternative theories of gravity struggle to satisfy the principle and still be distinct from GR. Extensions of cosmological and quantum theories question the irrefutably of the equivalence at every scale. The possibility of an equivalence principle violation at galactic scales would be an exciting prospect. In this thesis, we will carefully examine the equivalence principle through the study of chameleon scalar-tensor theories, this will include solutions for hypothetical stars known as boson stars. Such theories find varied application, especially in cosmology, where they model dark energy and inflation. The AWE hypothesis, is an instance of this. It is a non-universally coupled model in which violations of the equivalence principle on galactic scales may be apparent. We investigate spherically symmetric and static solutions within the framework of this theory. The constraints obtained from galactic rotation curves results in values of the couplings that show no significant violation of the equivalence principle or values consistent with a theory of dark energy.

Acknowledgements

I am deeply grateful for my supervisor Julien Larena. The past two years have opened me up to many more possibilities, experiences, and levels of commitment I never thought were possible. Without his continual encouragement, which was there despite the ever present errors and missed deadlines, I never would have embarked on, nor finished this thesis.

I would also like to thank Landman Bester, Michelle Kogel, Catherine Bartlett, as well as Viroshan Naicker for having the patience for assisting me in the early (and very late) stages of my writing, the Rhodes University Post-Graduate Financial Aid Office and the NRF for the financial support. I would also like to thank every individual member of the Mathematics Department for encouragement and support. I have also greatly benefited from interacting with post-graduate students and staff from the University of Namur. In particular I would like to thank Andre Fuzfa, Jeremy Rekier, and Estelle Collard. I am grateful to the understanding and encouraging recruiters from FNB, especially Kajaal Singh.

To my friends, Ryan Daniels, Ramosamo Raboroko, Tshegofatso Dikoma, thank you.

Finally, I would like to thank my personal pillar of strength, my brother Thato Mohapi. His ever buoyant spirit and cheerfulness have always had a more everlasting effect than any cup of coffee.

When we use mathematics, what are we saying about the nature of nature? It is in this pursuit- the pursuit of meaning- that both the difficulty and pleasure lie.

MARVIN CHESTER

Contents

Chapter 1

Introduction

The concordance model of cosmology, ΛCDM, depends on three main ideas[1]:

- The Cosmological principle is valid.
- The standard model of particle physics is correct.
- General Relativity(GR) is the theory of gravity.

This model explains cosmological phenomena such as the origin of light elements, structure formation, and baryonic acoustic oscillations among others [2]. It has been shown to be in agreement with a large range of other cosmological observations such as the cosmic microwave background (CMB) [3], supernovae data, and direct Hubble rate measurements [4].

Supposing that the three main ideas of the concordance model listed above hold, observational evidence suggests that the universe is currently expanding [5, 6, 7, 8, 9]. This expansion can be generically thought to be driven by "dark energy." Dark energy makes up roughly 70 % of the universes energy content, yet it is not very well understood within the ΛCDM model. Furthermore, a large proportion of the energy budget, almost 25%, is attributed to non-baryonic, weakly interacting and invisible matter, dubbed dark matter.

The underlying assumptions of the concordance model affect the interpretation of cosmological observations and phenomena, especially dark energy and dark matter. Rigorous motivation and tests should underlie the main ideas of the model. For instance, the assumption of homogeneity and isotropy is necessary for a Friedmann Lemaître Robertson Walker (FLRW) universe. Models which do not assume the universe is homogeneous on large scales such as the Lemaitre Tolman Bondi (LTB), and Szekeres compete with the concordance model in explaining the accelerated expansion of the universe or dark energy [10], [11], [12], a primary interest of cosmology today. In the ΛCDM model, the accelerated expansion is attributed to a finely tuned [13] cosmological constant, but could be the result of new physical phenomena as is the case in scalar-tensor theories or the result of an inhomogeneous universe, which is the case in LTB.

It is interesting to consider models which respect the cosmological principle but modify the other two main ideas of GR and the standard model. These ideas are interlinked, especially in high energy physics theories. For example, a violation of the equivalence principle, a central notion in GR, would challenge both assumptions. The equivalence principle (EP) asserts the equivalence of gravitational and inertial mass. The violation can be modelled with non-universal couplings between matter species to a scalar

field. Fifth force effects which result from the additional scalar field can be mitigated by a screening effect, dubbed the chameleon mechanism.

Our motivations are not restricted to modifying an assumption and examining the consequences. A relaxation of the EP, through a non-universally coupled chameleon, sheds light on the two most key areas of cosmology today: dark energy and dark matter. A relaxation of the EP indicates that these are not unrelated problems.

1.1 The Dark Sector and the Violation of the Equivalence Principle

1.1.1 Dark Energy as the Cosmological Constant

To derive the results of ΛCDM cosmology, we first assume and that the gravitational action is given by

$$S = \frac{1}{16\pi G}\int (R+2\Lambda)\sqrt{-g} + S_m(\psi_m, g_{\mu,\nu}),$$

which is the Einstein-Hilbert action of GR (we have set $c=1$). This leads to the following field equations

$$G_{\mu\nu} + \Lambda g_{\mu\nu} = 8\pi G T^{(m)}_{\mu\nu}$$

The ΛCDM model does not provide any explanation for dark energy. It is assumed, in this model, that the cosmological constant can be linked to the average energy density of the vacuum ρ_{vac}. The vacuum can be modelled as a perfect fluid with $\rho_{vac} = -p_{vac}$, in order to be Lorentz invariant [14]. The stress energy tensor for the cosmological constant is given by:

$$T^{(vac)}_{\mu\nu} = -\frac{\Lambda}{8\pi G} g_{\mu\nu} = \rho_{vac} g_{\mu\nu}$$

If we assume that the matter field, ψ_m, is a perfect fluid its stress energy tensor is given by:

$$T^{(m)}_{\mu\nu} = (\rho + p)\, u_\mu u_\nu + p g_{\mu\nu}.$$

Secondly, we assume that the cosmological principal is valid, and as a result the geometry of space-time is described by the Friedmann-Lemaitre- Robertson-Walker (FLRW) line element:

$$ds^2 = -dt^2 + a^2(t)\left(\frac{dr^2}{1-kr^2} + r^2 d\Omega^2\right),$$

as is done in the ΛCDM model, we can satisfactorily explain major cosmological observations, such as the origin of light elements and the CMB. The parameter k, the curvature parameter, takes on the values $+1, 0$ or -1.

Cosmic acceleration in FLRW is then represented by the following acceleration equation:

$$\frac{\ddot{a}}{a} = -\frac{4\pi G}{3}(\rho_m + 3p_m) + \frac{1}{3}\Lambda$$

where ρ_m and p_m are the density and pressure of the matter fluid. The equation of state of a fluid is given by, $\omega = \frac{p}{\rho}$. For dust, $\omega = 0$, and for a generic fluid capable of reproducing cosmic acceleration ($\ddot{a} > 0$) must satisfy the following constraint

$$\omega < -\frac{1}{3}$$

if we are to recover a positive acceleration. The cosmological constant has an equation of state of exactly $\omega = -1$, which reproduces cosmic acceleration.

However, actual observations of the average density of the vacuum suggest that the value of the cosmological constant appears to be finely tuned, with cancellations of up to 120 orders of magnitude [13]. This is the fine-tuning problem of the cosmological constant. There is also a second problem, the coincidence problem, that arises from associating dark energy with cosmological constant. ρ_Λ is comparable to the present critical density $\rho_{c,0} = \frac{3}{8\pi G} H_0^2$. A remarkable coincidence which implies we are living in a period during which the transition to a dark energy universe is about to occur. Alternative models, with a dynamic cosmological constant, have been proposed to account for this fine tuning. Among these are quintessence models, in which the cosmological constant is replaced with a scalar field, but the gravitational theory remains that of GR.

1.1.2 Dark Energy as Quintessence

Quintessence allows for a dynamic cosmological constant. The action is then given by

$$S = \frac{1}{16\pi G} \int \left(R - 2\nabla_\mu \phi \nabla^\mu \phi + V(\phi)\right) \sqrt{-g} + S_m \left(\psi_m, g_{\mu\nu}\right).$$

This provides a mechanism towards justifying the value of the cosmological constant, as the equation of state for dark energy is now

$$\omega = \frac{\rho}{P} = \frac{\dot{\phi}^2 - 2V(\phi)}{\dot{\phi}^2 + 2V(\phi)}.$$

Negative pressures occur when the scalar field is slow rolling. This reduces the problem to finding the correct expression for $V(\phi)$. To coincide with known observations, in particular the fact that dark energy represents 70% of the universes energy content, one needs a scalar field with a very light mass [1]

$$m_\phi \approx H_0 \approx 10^{-33}\text{eV}.$$

1.2 Dark Energy as Extended Quintessence

Although Quintessence introduces a more natural explanation of dark energy, within the framework of standard particle physics the scalar field must couple to matter, thus it is necessary to have the gravitational action

$$S = \frac{1}{16\pi G} \int \left(R - 2\nabla_\mu \phi \nabla^\mu \phi + V(\phi)\right) \sqrt{-g} + \sum_i S_i \left(\psi_i, A_i^2(\phi) g_{\mu,\nu}\right).$$

This non-minimal coupling ($A_i^2 \neq 1$) to matter fields ψ_i leads to extended quintessence theories. Extended quintessence models are identical to scalar-tensor theories as the action above is identical to those of scalar-tensor theories of gravity written in the Einstein frame, as we discuss later in this section.

This makes it clear how a modification of the gravitational theory may extend the cosmological model and provide a more natural explanation of dark energy. The acceleration equation:

$$\frac{\ddot{a}}{a} = -\frac{4\pi G}{3}\sum_i (\rho_i + 3p_i) - \frac{2}{3}(\dot{\phi}^2 - 2V),$$

where ϕ is the scalar field written in the Einstein frame. The acceleration equation written in the Einstein frame seems to imply that $\ddot{a} > 0$ needs $V \neq 0$. If we take it that there are two matter species, ψ_m and ψ_{awe} as in [15], the actual observed Hubble rate $\tilde{H}$, and the other such as the density and pressure of each matter species, ρ_i and P_i, is related to quantities in the Einstein frame (we shall discuss conformal frames in detail in Chapter 3) by the following relations

$$\begin{aligned} H &= A_m^{-1}\left(H + \alpha_m(\phi)\dot{\phi}\right), \\ \tilde{a} &= A_m(\phi)a, \\ \tilde{\rho} &= A_m^{-4}(\phi)\rho_m, \\ \tilde{P} &= A_m^{-4}(\phi)P_m, \end{aligned}$$

and transformations

$$\begin{aligned} \tilde{g}_{\mu\nu} &= A_m^2(\ \phi)\, g_{\mu\nu}, \\ \frac{G}{\tilde{G}} = \tilde{\phi} &= A_m^{-2}(\phi), \\ 3 + 2\omega &= \left(\frac{d\ln A_m(\phi)}{d\phi},\right)^{-2} = \alpha_m^{-2}(\phi), \text{ and} \\ M(\Phi) &= \frac{A_{awe}}{A_m}. \end{aligned}$$

The effect on the actual acceleration equation is then

$$\frac{\ddot{\tilde{a}}}{\tilde{a}} = -\frac{4\pi G}{3\tilde{\phi}}\left(\tilde{\rho}_m + \tilde{\rho}_{awe} + 3\tilde{p}_m + 3\tilde{p}_{awe}\right) - \frac{1}{2}\frac{\dot{\tilde{a}}}{\tilde{a}}\frac{\dot{\tilde{\phi}}}{\tilde{\phi}} - \frac{1}{2}\frac{\ddot{\tilde{\phi}}}{\phi} - \frac{2\omega}{6}\left(\frac{\dot{\tilde{\phi}}}{\tilde{\phi}}\right)^2.$$

The above equation can be simplified using the Friedman and Klein-Gordon equations

$$\begin{aligned} \left(\frac{\dot{\tilde{a}}}{\tilde{a}}\right)^2 &= -\frac{\dot{a}}{a}\frac{\dot{\tilde{a}}}{\tilde{\phi}} - \frac{\ddot{\tilde{\phi}}}{\phi} - \frac{2\omega}{3}\left(\frac{\dot{\tilde{\phi}}}{\tilde{\phi}}\right)^2 - \frac{4\pi G}{3\tilde{\phi}}\left(\rho_m + 3p_m + \rho_{awe} + 3p_{awe}\right), \text{ and} \\ (3+2\omega)\left(\ddot{\tilde{\phi}} + 2\frac{\dot{\tilde{a}}}{\tilde{a}}\tilde{\phi}\right) &= 4\pi G\left(\rho_m - 3p_m + (\rho_{awe} + 3p_{awe})\left(1 - 2\tilde{\phi}\frac{d\ln M(\tilde{\phi})}{d\tilde{\phi}}\right)\right) - \frac{d\omega}{d\tilde{\phi}}\dot{\tilde{\phi}}^2. \end{aligned}$$

In the case of dust where the pressure of each fluid is zero, the above equation can be simplified to

$$\frac{\ddot{\tilde{a}}}{\tilde{a}} = -\frac{4\pi G}{3}\left(1 + 3\alpha_m^2\right)\rho_m - \frac{4\pi G}{3}\left(1 + 3\alpha_m\alpha_{awe}\right)\rho_{awe} + \tilde{H}^2\frac{\tilde{\phi}^2\left(3\frac{d\alpha_m}{d\phi} - 2\right) - 6\alpha_m\dot{\phi}}{3\left(1 + \alpha_m\tilde{\phi}\right)^2}.$$

The acceleration largely driven by the second term, which requires $\alpha_m \alpha_{awe} < 0$. We can thus observe how non-universal couplings, or a violation of the EP, arises from explaining the nature dark energy. The subsequent sections illustrates how non-universal couplings also arise from explaining the nature of dark matter.

Mass varying dark matter candidates have been studied in[16, 17]. In this models, the varying mass is often a result of the DM coupled to dark energy. However, such a coupling, violates the EP, and this violation can be detected for using baryonic matter [18]. Indeed, Eötvös experiments are sensitive to the anomalous acceleration towards dark matter in the galaxy [19]. Evidence for dark matter on galactic scales is supported by the rotation curves of spiral galaxies as we show in 5. Although a modification of gravity on small acceleration scales has been suggested to be rid of the effects of the invisible non-baryonic matter, such theories are unsatisfactory for other reasons 5.5.

1.3 Thesis Outline

This thesis is organised as follows:

Chapter 2 discusses the equivalence principle. We begin with the simplest formulation of the principle. This is followed by an explicit discussion of all the assumptions necessary for the theory to hold in GR, and thus a discussion of the Einstein Equivalence Principle (EEP). We also introduce the parametrised post-Newtonian formalism, in which theories different from GR can be constrained. It is explained why this is especially important within the more generalized principle, the EEP.

We also discuss the most restricted formulation of the equivalence principle the Strong Equivalence Principle, which does not hold in scalar tensor theories. A brief review of the constraints from tests of the equivalence principle in the solar system follows this.

We end the chapter with an introduction to one of the main historical motivations for considering these theories - the variation of physical constants. We consider the possibility of the variation of the fine structure constant and the gravitational constant, and how such a variation is captured by scalar-tensor theories.

Chapter 3 develops the theory of scalar tensor theories more deeply. We briefly examine theories that are equivalent to scalar-tensor theories such as Kaluza-Klein and $f(R)$ theories before we introduce a general scalar-tensor theory. We also make clear the equivalence of conformal frames with explicit calculations of observables in both the Jordan and Einstein frames. We discuss the still persisting confusion in the literature. This is followed by a discussion of the chameleon mechanisms. This is the mechanism that allows scalar tensor theories to be reconcilable with constraints in the solar system, whilst retaining characteristics that make the theory different from GR. The mechanism is demonstrated for both universally and non-universally coupled scalar-tensor theories of gravity. We also examine the history and nature of spherical solutions of the non-universally coupled chameleon model which we study exclusively in the application to galactic rotation curves in chapter 3. It is dubbed the Abnormally Weighting Energy (AWE) hypothesis in which the dark energy (in the form of a Born-Infeld field or a chameleon scalar field) and ordinary matter are non-universally coupled to gravity through the scaler field. The features of AWE remain the same when the non-universal coupling is restricted to two pressure less fluids. We an identify these fluids with baryonic and dark matter.

Finally, we end chapter 3 with a discussion of boson stars. Boson stars are ideal for studying the compact solutions of the scalar-tensor theories. This final section will allow us to easily examine the

nature of spherical solutions across a wide range of chameleon models. Boson stars share generic features in both universally and non-universally coupled chameleon models.

Chapter 4 explores the possibility of forming boson stars in a non-minimally coupled scalar-tensor theory. Boson stars have been suggested to be possible candidates of dark matter. They have been applied in the study of rotation curves. The scalar tensor theory in which we attempt to form boson stars serves as of scalar-tensor theories that unify the dark matter with quintessence.

Chapter 5 explores our non-universally coupled model with galactic rotation curve data. The flat rotation curves of spiral galaxies provide evidence for the existence of dark matter on galactic scales. Thus a likely place to look for the signatures of a violation of the EP between baryonic and dark matter on galactic scales.

This chapter briefly discusses the density profiles used to model the distribution of matter in galaxies, and the evidence for the missing matter, or dark matter, in spiral galaxies. This is followed by a brief discussion of one of the proposed solutions for the missing mass problem, Modified Newtonian Dynamics (MOND).

A brief literature review of the study of rotation curves in scalar-tensor theories follows this, before we investigate the parameter space of non-universally coupled chameleon models. This is done by performing χ^2 fits to galactic rotation curve data, and a Markov chain Monte Carlo (MCMC) sample on the parameter space. It is from this that we discuss the evidence for non-universal coupling, and thus violations of the EP on galactic scales. We conclude the chapter with an examination of scalar field solutions in galaxies and the compatibility of these solutions with solar system constrains and quintessence models.

The final perspectives of the thesis are discussed in the conclusion. An Appendix, A, is provided in which all the field equations used in the thesis are derived from first principles. The appendix also describes the Bayesian and MCMC techniques used in Chapter 5.

Part I

The Equivalence Principle in Astrophysics

Chapter 2

The Equivalence Principle

2.1 Introduction

This chapter will provide an outline of the importance of the equivalence principle (EP) in cosmology today. Particular emphasis will be placed on the EP's formulation in General Relativity (GR). GR obeys three equivalence principles: the weak, the Einstein and the strong equivalence principle. Metric theories of gravity satisfy the first two equivalence principles. Violations of the equivalence principles also arise from high energy theories of physics, quintessence models, and theories with varying fundamental constants.

Ultimately, relaxation of the equivalence principle has to be tested for by observations. We shall discuss the experimental tests of all three equivalence principles. The best direct tests of the weak equivalence principle (WEP) are from Eötvös experiments. These have been performed on local scales and to a limited extent on galactic scales. Tests of the Einstein equivalence principle are briefly mentioned. This principle is embodied in metric theories of gravity. The Parametrized Post-Newtonian formalism, provides a convenient frame work in which metric theories can be compared. We will conclude this chapter with a review of the variation of fundamental constants. In particular, this will consist of a discussion of the tests of the fine structure constant α, and the gravitational constant G. The variation of constants was an important precursor to scalar-tensor theories as will be explained in the review.

2.2 The Weak Equivalence Principle

Galileo's famous leaning tower of Pisa experiment in which two balls are dropped from the top of the tower and reach the ground at the same time provides an intuitive understanding of the WEP. If we restrict our attention to balls of different composition, then the claim that any two balls will always reach the ground at the same time is the WEP. More formally, the formulation of the EP begins with Newton's second law of motion,

$$F = m_i a.$$

The equation relates how an object with an inertial mass, m_i, accelerates when under the influence of a force F. If the force is due to the object interacting with a gravitational field given a potential ϕ, then F is directly proportional to the gradient of the field:

$$\begin{aligned} F &= -m_g \phi_{,x} \\ &= m_g g. \end{aligned}$$

In the above relation, the constant of proportionality m_g is the gravitational mass of the body. It is not obvious that the inertial mass of an object is equivalent to the gravitational mass. The former relates an objects acceleration with the force it experiences, while the second relates the gradient of the gravitational potential with the force the object experiences. The WEP states

$$m_i = m_g$$

for all objects. This is regardless of the objects material composition, orientation, or position in space-time. A direct consequence of this equivalence is that all bodies have the same acceleration in a local region of the gravitational field independently of the quantity of inertial mass they contain. It is thus impossible to distinguish between a uniformly accelerated frame and a gravitational field in a local region of space-time by the use of purely non-gravitational experiments.

Since Newtonian gravity is the weak field limit of GR, which is the case when objects move at speeds much less than the speed of light and when time derivatives are very much smaller than spatial derivatives, the simple formulation of the EP above also holds in GR. However, it does so in a more sophisticated form which takes into account non-Newtonian phenomena. For instance, we will show that failure to reproduce the correct physics for objects that move with relativistic speeds result in the violation of the EP. We will also show that it is necessary to distinguish between gravitational and non-gravitational experiments when testing the EP. Compatibility with special relativity leads to the formulation of the Einstein Equivalence Principle (EEP), which generalises the WEP. A stronger formulation of the EP which has the WEP and the more general EEP as special cases, the Strong Equivalence Principle (SEP) can also be formulated in GR. The SEP places very strong constraints on theories of gravity. Theories that extend GR, such as scalar-tensor theories, violate the SEP.

2.3 Einstein Equivalence Principle

Like the WEP, the EEP can be intuitively grasped through Einstein's elevator *gedaken* experiment. In this experiment an observer in an elevator under a uniform gravitational field on earth would observe the same physics as an observer in an elevator accelerating in empty space. More precisely, the EEP can be broken down to three main ideas: the WEP, Local Lorentz Invariance (LLI) and Local Position Invariance (LPI). The effects due to an accelerated frame of reference and the effects due to gravity cannot be distinguished using the physics of special relativity without a violation of the EEP. It has been conjectured that any complete, self-consistent theory of gravity that embodies WEP necessarily embodies EEP [20]. This is known as Schiff's conjecture. An experiment in which particles rotate under the influence of gravitational field would violate the EEP but not necessarily the WEP [21], [22]. The observer in the *gedaken* experiment would observe this rotation on earth but not in space. Such a possibility, introduces more tests of the equivalence principle, and must be ruled out by experiments.

Attempts to prove the Schiff's conjecture have resulted in criteria necessary for the WEP to imply the EEP, namely the satisfaction of local Lorentz invariance, and local position invariance. These are discussed in subsequent sections.

2.3.1 Local Lorentz Invariance

LLI means that the outcome of any local and non-gravitational experiment is independent of the coordinates of relatively boosted or rotated observers. Special relativity requires that LLI is satisfied. An experimental test of special relativity may also then be a test of the EP. An example of such an experiment would be one that measures the electric force between charged particles.

LLI violating effects are present in unified theories of gravity such as quantum gravity theories [23], [24], [25]. In these theories, the gravitational and gauge couplings are unified [26]. A dilaton scalar field modulates the gauge and gravitational constants. This introduction of this scalar field introduces non-universal couplings, for instance, the mass of the atom is linked to the Coulomb interaction which in turn is linked to a variable fine-structure constant in a composition dependent manner.

As an example, consider a dispersion relation such as

$$E^2 = m^2 + p^2 + E_{pl} f^{(1)} |p| + f^{(2)} p^2 + \frac{f^{(3)}}{E_{pl}} |p|^3 + \frac{f^{(4)}}{E_{pl}} |p|^4 + ...$$

which occur in some quantum gravity theories [24]. If we assume that only $f^{(4)}$ is non-zero and independent of the matter species, then under Hamiltonian dynamics

$$H = m + \frac{p^2}{2m} + f^{(4)} \frac{p^4}{2mE_{pl}^2} + m\phi(x),$$
$$\ddot{x} = -\frac{d\phi}{dx}(1 + 6f^{(4)} \frac{m^2 \dot{x}^2}{E_{pl}}) \implies a = g(1 + \text{velocity dependent term}).$$

The acceleration of an object is thus dependent on the object's velocity. The consequences of which are a violation of the EP. The introduction of matter species dependent terms has similar consequences. Astrophysical observations such as burst of high energy photons from distance sources bound possible values of the $f^{(i)}$'s.

Constraining the LLI violation for dark matter still results in violations of the EP and other observable cosmological signatures. In [27], the violation of the LLI was induced by coupling dark matter to a vector field. This coupling affects the inertial mass of small dark matter halos. However, for large halos, there exists a chameleon mechanism that can restore the inertial mass to its standard value. This work, among others provides motivation to look for similar signatures at the level of galaxies.

A final example of a violation of LLI leading to a violation of the EP is a bi-metric theory of gravity [28] :

$$S = \int \sqrt{-g}(g^{\alpha\beta} \partial_\alpha \phi \partial_\beta \phi + (g^{\alpha\beta} + \tau^{\alpha\beta}) \partial_\alpha \psi \partial_\beta \psi) \; d^4x.$$

In a local frame, where the effects of gravity can be ignored, we may use the action:

$$S = \int \sqrt{-\eta}(\eta^{\alpha\beta} \partial_\alpha \phi \partial_\beta \phi + (\eta^{\alpha\beta} + \tilde{\tau}^{\alpha\beta}) \partial_\alpha \psi \partial_\beta \psi) \; d^4x,$$

where τ^{ab} and g^{ab} are different metrics. Under a Lorentz transformation Λ, $\phi'(x') = \phi((\Lambda^{-1})^{\mu}_{\nu}x^{\nu})$ and $\psi'(x') = \psi((\Lambda^{-1})^{\mu}_{\nu}x^{\nu})$ and the action may be rewritten as

$$S = \int \sqrt{-\eta}(\eta^{\alpha\beta}\partial_{\alpha}\phi'\partial_{\beta}\phi' + (\eta^{\alpha\beta} + (\Lambda^{-2})\tilde{\tau}^{\alpha\beta})\partial_{\alpha}\psi'\partial_{\beta}\psi')\ d^4x'.$$

This makes clear the coordinate dependence on the second part of the action. The action thus violates the LLI, and different physics results for the ψ sector. Experimental tests of special relativity limit such a possibility.

2.3.2 Local Position Invariance

Local position invariance means that experiments are not dependent on where and when they are performed. The first proposed experimental tests of GR, gravitational red-shift, tests this principle. This is because any theory that satisfies the EEP, will produce gravitational red-shift predictions identical to those of GR. Other tests include experiments that measure the variation of fundamental constants. The gravitational mass of an object, such as an atom, is a result of the interactions of the couplings between gravity and the fields that bind the atom. If these fields are not position invariant, then gravity would not couple to mass in a universal manner. We discuss the variation of fundamental constants separately at the end of this chapter, in section 2.7.

The interpretation of experimental tests of LLI and LPI violation can be understood within the framework of the Parametrized Post-Newtonian formalism, which will be introduced in the next section.

2.3.3 Frameworks to test the EEP

When testing the WEP, one is only concerned with the experiments that test for the difference between the accelerations produced by two bodies constituted from different materials. Experimental tests of the EEP, which are tests of the LLI and LPI, are more varied [29, 24]. Tests of the EEP include:

- tests of the speed of light
- tests of time dilation
- gravitational redshift experiments
- tests of the variation of fundamental constants.

Theories that satisfy the EEP, are necessarily metric theories. Metric theories are theories of gravity that satisfy the following postulates [30]:

- Spacetime is endowed with a symmetric metric **g**.
- The trajectories of freely falling bodies are geodesics of that metric (WEP).
- In local freely falling frames, the non-gravitational laws of physics are those of special relativity (LLI and LPI).

As a consequence, in metric theories all non-gravitational fields couple universally to the metric. In addition to matter, the metric itself, may also be generated by other "gravitational fields," such as scalar, vector and tensor fields. GR and *universally coupled* scalar-tensor theories are metric theories, and both satisfy the EEP. Although the GR and *universally coupled* scalar-theories both satisfy the EEP, solar system experiments are able to distinguish between them. This is done using the Parametrized Post-Newtonian (PPN) framework.

2.4 PPN Framework

The PPN framework provides a succinct scheme in which different theories of gravity may be analysed. The basis of the PPN framework rests on the work of Eddington [31], Robertson [32], and Schiff [33] in which the framework was created to interpret the results of solar system tests of gravity. These works introduced the two parameters PPN β and γ, that will be of interest to us in this thesis. The framework has since been extended by the works of Nordtvedt and Will [34, 35, 36] to eight other parameters $\xi, \alpha_1, \alpha_2, \alpha_3, \zeta_1, \zeta_2, \zeta_3$ and ζ_4.

The γ and β parameters are the only non-zero parameters in GR and scalar-tensor theories. These are the parameters used to describe the classical tests of GR, such as the time delay of light, the perihelion shift of mercury and so on. The parameter ξ, is used to describe preferred location effects. The three parameters $\alpha_1, \alpha_2, \alpha_3$ describe preferred frame effects. The α_1 along with the last four parameters $\zeta_1, \zeta_2, \zeta_3$ and ζ_4 are used to describe the violations of the conservation of total angular momentum.

The PPN framework rests on two main assumptions [34]:

- Space-time is a four-dimensional manifold. It need not have an intrinsic metric or affine connection. Each point on the manifold corresponds to a physical event.
- The theory of gravity can be cast in a covariant form.

It also has the following two constraints on any theory of gravity [34]:

- Gravity is associated, at least in part, with fields of tensorial nature.
- The field equations must be derivable from an invariant action principle.

The PPN formalism rests on the following two assumptions [1]:

- There exists a metric $\mathbf{g}$, which denotes proper length and proper time intervals by

$$ds^2 = g_{\mu\nu} dx^\mu dx^\nu$$

- The stress-energy momentum tensor, T, for all matter and non-gravitational fields is conserved,

$$\nabla \cdot T = 0$$

Theories of gravity that have mathematical representations satisfying these postulates can be cast using the PPN metric. This metric is only valid in the slow motion and weak field limit. In this limit gravitational theories have the same structure, and can be seen as an expansion around the Minkowski metric in terms of powers of the gravitational potential.

The PPN metric is typically represented in an isotropic coordinate system for the space-time around a spherical, non rotating object. The only non-zero parameters in GR and scalar-tensor theories are γ and β. To experimentally distinguish GR and scalar-tensor theories, it is sufficient to consider a framework

[1] These consequences are the result of one assumption: the existence of local Lorentz frames in which special relativity holds at every point in space-time

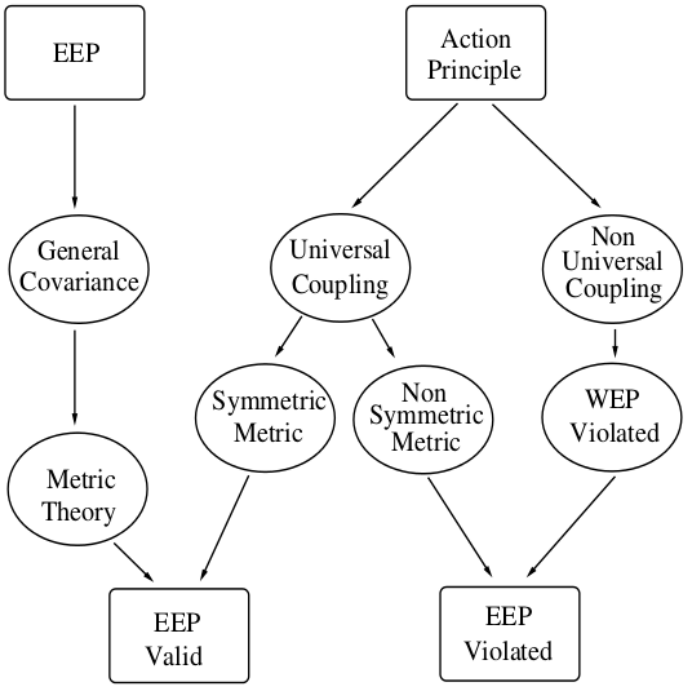

Figure 2.1: An illustration of what considerations lead to the EEP in gravitational theories. This figure is adapted from [30]

.

with only these two parameters. They affect the isotropic Schwarzschild metric in the following way [37], [29]

$$ds^2 = -\left(1 - \frac{2GM}{r} + \frac{2\beta GM^2}{r^2}\right)dt^2 + \left(1 + \frac{2\gamma GM}{r}\right)\left(dr^2 + r^2 d\Omega^2\right).$$

The derivation for this form is as follows: the Schwarzschild metric,

$$ds^2 = -\left(1 - \frac{2GM}{r}\right)dt^2 + \left(1 - \frac{2GM}{r}\right)^{-1} dr^2 + r^2 d\Omega^2,$$

is the appropriate spherically symmetric weak field limit. In isotropic coordinates the spatial part of the metric takes the form

$$ds_3^2 = f^2(r)(dr'^2 + r' d\Omega^2).$$

As a result of comparing coefficients, we derive the following

$$r' = \frac{r}{f}$$
$$\frac{dr}{dr'} = f\left(1 - \frac{1}{f}\frac{df}{dr}r\right)^{-1}.$$

This is sufficient to solve for f

$$\begin{aligned} f &= \frac{2r}{r - GM + \sqrt{r^2 - 2GM}} \\ &= \left(1 + \frac{GM}{2r'}\right)^2. \end{aligned}$$

Hence, we obtain the isotropic Schwarzchild:

$$ds^2 = -\left(1 - \frac{2GM}{r'}\left(1 + \frac{GM}{2r'}\right)^{-2}\right)dt^2 + \left(1 + \frac{GM}{2r'}\right)^4 (dr'^2 + r' d\Omega^2).$$

We note that

$$\left(1 - \frac{2GM}{r'}\left(1 + \frac{GM}{2r'}\right)^{-2}\right) \approx 1 - \frac{2GM}{r'} + \frac{\beta}{2}\left(\frac{2GM}{r'}\right)^2 + \text{ higher order terms}$$

$$\left(1 + \frac{GM}{2r'}\right)^4 \approx 1 + \gamma\frac{2GM}{r'} + \text{ higher order terms}$$

The Schwarzschild metric written in the PPN formalism, requires that $\gamma = 1$, and $\beta = 1$ exactly. It is not always convenient to use the isotropic metric. We will therefore also make use of the PPN metric in regular coordinates by making use of the following relation

$$r \approx r'(1 + \gamma GM),$$

and the transformation

$$r' \to r(1 - \gamma\frac{GM}{r}).$$

We are thus able to write the line element as:

$$ds^2 = -\left(1 - \frac{2GM}{r} + \frac{(\beta - \gamma)GM^2}{2r^2}\right)dt^2 + \left(1 + \frac{2\gamma GM}{r}\right)dr^2 + r^2 d\Omega^2. \tag{2.1}$$

Solar system experiments, as shown in 3, constrain *universally coupled* scalar-tensor theories to such an extent as to make them indistinguishable from GR. There exist mechanisms that allow these theories to be compatible with solar system tests, and yet still be distinct from GR. The chameleon mechanism is one such instance. This mechanism is easily extended to the non-universally coupled scalar-tensor theories and allows for an WEP violating theory to be consistent with known experimental results.

We have been careful to emphasise that *universally coupled* scalar-tensor theories satisfy the EEP. This is because *non-universally coupled* theories do not satisfy the more general equivalence principle. The fields couple to different metrics, and follow different geodesics. However, it is possible to recover the experimental results of special relativity for at least one of the one of the matter fields. This is the case when the units of measurements for the observables in the experiment are based clocks and rods made up from the matter field we wish to recover the result of special relativity for. As far as experimental observations can discern, all baryonic matter in the solar system satisfies the EEP. A non-universally coupled chameleon theory will therefore have to couple to all baryonic matter in the same way. The non-universally coupled chameleon theory we will investigate in this thesis, introduces two

different couplings to baryonic matter and dark matter. This restricts the violation of the EEP to dark matter, and allows for a theory compatible with known observations.

2.5 The Strong Equivalence Principle

The WEP asserts the equivalence of the gravitational mass and the inertial mass. The EEP, places the WEP within the framework of GR and requires the recovery of special relativity in local Lorentz frames. The SEP claims the principle holds even for self gravitating bodies. In the case of self gravitating bodies the gravitational binding energy of the body has a significant contribution to the overall inertial mass energy of the body. The EP would hold if there was no space-time dependence in the gravitational binding energy. This is true in GR. This is not true in most modified theories of gravity, especially scalar-tensor theories in which the fundamental constants of physics may vary (see section 2.7).

An instance of a violation of the SEP would be the Nordtvedt effect [38], [39]. This effect is quantifiable if we suppose that it is due to a variation in the gravitational constant. The subsequent anomalous acceleration due to the self binding gravitational energy of the body can be easily noted within the PPN framework [37], [40]:

$$\begin{aligned}(\text{acceleration of massive body}) - (\text{acceleration of test body}) &= \left(\frac{E_{grav}}{MG_C}\right)\nabla G_C \\ &= \eta_N \frac{E_{grav}}{M}\nabla U,\end{aligned}$$

where U is the external gravitational potential and η_N is a function of PPN parameters:

$$\eta_N = 4\beta - \gamma - 3 - \frac{10}{3}\eta - \alpha_1 + \frac{2}{3}\alpha_2 - \frac{2}{3}\zeta_1 - \frac{1}{3}\zeta_2.$$

In GR we have that $\eta_N = 0$. However, in all scalar-tensor theories η is non-zero as γ and β are not identically one. This makes a violation of the SEP inevitable. Experimental tests of the SEP, such as the Lunar ranging experiments, in which a violation in the SEP would result in the polarisation of the orbit of the Earth-Moon system, set the current best constraints on the SEP [41] of

$$\eta = (4.4 \pm 4.5)\,10^{-4}.$$

Other celestial constraints, such as binary pulsars also provide methods to test for the SEP [42].

2.6 Solar System Tests of The Equivalence Principle

Experiments that constrain the violation of the EP on solar system scales fall broadly into three categories. The first is the classic Galileo drop tower experiment, the first experiment to test the EP. Similar and more modern experiments have been proposed, such as MicroSCOPE and STEP, which will be able to test the difference in the accelerations of two test bodies up to a sensitivity of 10^{-15} [40] using drop experiments in space. A second class of experiments, pioneered by Eötvös, provide the best constraints on the violations of the EP in the solar system today. This experiment probes differences between gravitational mass and the inertial mass using the induced torque of the horizontal component of a given gravitational field.

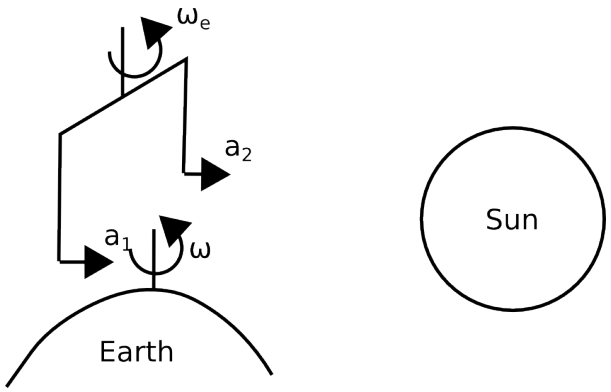

Figure 2.2: A torsion balance experiment. ω is the angular velocity of the earth. Where as a_1 and a_2 are the accelerations towards the sun of two objects of different material composition. A violation of the equivalence principle will induce a periodic variation in the angular velocity of the balance beam ω_e. Diagram adapted from [43]

The third category involves looking for possible effects of the violation of the EP in the orbits of celestial bodies. The second category of experiments is discussed in the subsequent sections.

2.6.1 Eötvös Experiments on Solar System Scales

If two bodies with the same inertial mass fall with different accelerations a_1 and a_2 in a given gravitational field, we can quantify the deviation from the EP with the parameter

$$\eta = \frac{1}{2}\frac{|a_1 - a_2|}{a_1 + a_2}.$$

Newton verified this parameter to an accuracy of 10^{-3} by using pendulums made of different materials. The best tests of the EP in the solar system come from morden forms of the Eötvös experiments, dubbed [40] Eöt-Wash experiments. Historically, these experiments were pioneered by Baron von Eötvös. In these experiments, known as torsion balance experiments, two bodies of known inertial mass are suspended across a beam that is held by a wire. If the gravitational mass is indeed different from the inertial mass, a contribution to the torque along the suspending wire will be induced. These experiments have determined the η parameter to an accuracy of 10^{-13} [40].

2.6.2 Eötvös Experiments on Galactic Scales

Constraints for possible violation of the EP on larger scales of the universe, in which dark matter dominates, and other non-baryonic sectors is fairly weak. Indeed, as little is known about dark matter, violations of the EP cannot be ruled out. However, various experiments to test the equivalence principle in this sectors have not yet shown any evidence of violation. An example is the experiment done in [19], which constrained EP violation in the acceleration of matter towards dark matter using an Eötvös type experiment to constrain η to the order of 10^{-3}. Another category of tests of the EP on larger scales especially probe LLI and LLP. LLI and LLP have been shown to be tightly linked with the WEP. Test of the variation of constants fall into this category. It is hoped that the use of gravitational theories in which the EP may be violated, such as the chameleon models studied in this thesis, may provide cosmological signatures of a violation of the EP, and hence test the EP on larger scales. We shall discuss these in the next section.

2.7 Varying Constants

Dirac [44] was the first to consider the effects of varying constants. His considerations are based on numerical coincidences. He noticed that various physical constants may be grouped together in a dimensionless manner to give a value of approximately 10^{40} [45]. In particular, the gravitational constant is grouped together with quantities that relate to the mass distribution of the universe. This implicitly introduces a variation of the gravitational constant as the mass distribution varies from place to place in the universe. A realisation of this variability by the introduction of dynamical fields in the gravitational action was made by Jordan in [46]. His motivation was to have a gravitational theory which satisfies Mach's principle. Mach's principle states that the inertia of an object is related to the total matter distribution of the universe. That is, motion is only meaningful relative to the total matter of the universe. Mach's principle can also be motivated through dimensional arguments by supposing that the gravitational constant obeys the relation

$$G \sim \frac{R_\nu c^2}{M_\nu},$$

where R_ν and M_ν are the radius and the mass of the universe. This equation implies that the inertial properties of given body, which are determined by the gravitational constant, depend on all the matter in the universe. Unless there is a way to prescribe G explicitly within the theory, its local value is dependent on the distribution of matter around a given body. Other free parameters, besides G can also vary, such as the fine structure constant α_{EM}. A variation of G clearly leads to a violation of the EEP. Variation in other physical constants introduces a variation in the rest mass, which is a function of various fields and their couplings, and thus a variation in the EEP.

Fundamental constants cannot be derived[2] from a smaller set of physical constants. They may only be determined through experiments. Observational constraints on the variation of constants have been obtained from atomic clocks, the Oklo phenomenon and astrophysical observations. A comprehensive review is presented in [47]. On the basis that GR is the theory of gravity and the standard model is the theory of all other interactions there are at least 22 fundamental constants, or 19 dimensionless constants, given 3 fundamental units [48], which have been identified. In principle a variation in any of these fundamental constants will result in the violation of the EP. We will focus on those for which there are good experimental constraints.

2.7.1 Varying The Fine Structure Constant

The fine structure constant is the dimensionless quantity

$$\alpha_{EM} = \frac{e^2}{\hbar c},$$

where e is the value of the electric charge of an electron. It is a free parameter determined by experimental observations in physics. Examples include quasar spectra, atomic clock experiments, the Oklo phenomenon, observations of the hyperfine transition of hydrogen from inter galactic gas, CMB and

[2]It is implicit that we know what the fundamental constants are. This is not immediately obvious as quantities we deem to be fundamental in current theories may be a depended on some dynamical field which is characterised by a set of truly fundamental constants not discernible by current theory or experiments. These constants are candidates for our varying constants.

BBN data [29]. In all these observations, the variation is limited to temporal variations. We use the same convention as in [47]: $\Delta\alpha = \alpha - \alpha_0$ for any constant and $\Delta\alpha < 0$ refers to a value smaller than today's value.

Probing the consequences of a variation in α_{EM} necessitates the introduction of a scalar field. One approach couples the scalar field to the electromagnetic action [49]. This approach has shown that α may vary due to the effects of an inhomogeneous universe and still satisfy local constraints [50].

Constraints on The Variation of α_{EM}

The following table [47] summarises the best available constraints on the temporal variations on α_{EM} at different redshifts:

Limit on $\frac{\dot{\alpha_{EM}}}{\alpha_{EM}}$ (yr^{-1})	Redshift	Method
$(-1.6 \pm 2.3) \times 10^{-17}$	0	Atomic clocks [47]
$< 0.5 \times 10^{-16}$	0.15	Oklo phenomenon [29]
$< 3.4 \times 10^{-16}$	0.45	Meteorites [29]
$< 1.2 \times 10^{-16}$	0.4-2.3	Quasar spectra [29]

In atomic clock experiments, the limit on the variation is obtained by measuring the frequencies, ν_i, of two different atomic clocks which depend on the gyromagnetic factor g_i for each nuclei, the proton to electron mass ratio and the fine structure constant. The effect of variations of other physical constants besides α_{EM} on the measured frequencies can be disentangled by additional non-clock experiments. This need not always be the case, since a direct constraint on α_{EM} is possible using single-ion optical clocks [47].

The Oklo phenomenon and meteorite dating both use isotope ratios to constrain the limit on the variation of α_{EM}. Two billion years ago, a natural nuclear reactor in Oklo, Gabon went critical and fission reactions occurred for a few million years. The isotopic abundances of the yields from the natural reactor allow for the calculation of the rate of reactions that were under-way. An important idea in these calculations is the resonance of a neutron, E_r. E_r is mainly the result of the cancellation of the electromagnetic force and the strong interaction. Many approaches to measure α_{EM} using the Oklo phenomenon have been considered. All are consistent with no variation. Meteorite dating allows us to test for a variation of α_{EM} in the remote past and on times scale as large as the age of the solar system, which is approximately $4 - 5 \times 10^9$ years. Typically in meteorite dating, long lived β decay isotopes are observed. This is a well understood phenomenon described by Gamow theory from which α_{EM} can be extracted. Similarly the β decay rate can be understood in terms of α_{EM}.

Comparing emission spectra on earth and in distant objects of the universe also provides constraints α_{EM} on cosmological scales. At least two transitions with different sensitivities to the fundamental constants must be observed to constrain the variation. Some authors claim that these observations suggests that α_{EM} may have been smaller in the past. However, these claims have been refuted [51], [52]. It is hoped that further observations, from the SKA for example, would be precise enough to detect relative changes in α_{EM} one or two magnitudes higher than present techniques.

The variation of any of the fundamental constants would affect the stellar nucleosynthesis of carbon. In stars carbon is produced when beryllium captures an α particle to produce ^{12}C with a specific resonance energy. The binding energy, B_D, is a function of the fundamental constants. In practice it is difficult to limit the variation of α_{EM} using only the binding energy. Current attempts [53] reduce the variation

to the constants to G, α_{EM}, and a composite constant C which modifies all the nuclear rates. Stellar nucleosynthesis may be able to constrain the variation of these parameters at redshifts smaller than $z \sim 15$.

In the early universe matter was highly ionized and photons were strongly coupled to electrons. When the universe cooled sufficiently, the formation of neutral matter was favoured and the photons decoupled from matter to give rise to the fossil radiation known as the cosmic microwave background (CMB) radiation. Currently, this radiation is seen at a temperature of 2.725K across the entire sky with small anisotropies. These anisotropies mainly depend on G, α_{EM}, and the mass of the electron m_e. G affects the evolution of cosmological perturbations. α_{EM} and m_e affect the temperature at which primordial matter experiences transitions, specifically the temperature at which decoupling and residual ionisation after recombination occur. The constraints obtained from CMB data are dependent on the model of structure formation. Often, CMB data is also combined with 21cm data of intergalactic hydrogen atoms. There is no clear consensus on how to relate these observation to the variation of α_{EM}, [54]. However, the 21 cm signal allows constraints on the variation of α_{EM} to be set on redshifts ranging from $z \sim 1000$ to $z \sim 20$. WMAP-3yr data at 2σ showed no evidence of variation, however WMAP-7yr data, currently at 1σ, indicate that α_{EM}, may have been smaller in the past [55] when only α_{EM} is allowed to vary. No evidence of variation is seen when both α_{EM} and m_e are allowed to vary, with G kept fixed.

The final observational constraints on the variation of α_{EM} is obtained from Big Bang nucleosynthesis (BBN). The light element abundances are largely determined after the universe cooled enough to break the equilibrium between neutrons, protons, electrons, positrons and neutrinos. BBN accounts for this process which depends on Q_{np}, the difference between neutron mass and proton mass, the neutron lifetime τ_n, m_e, m_N, α_{EM}, and the binding energy of the nuclei of interest B_D. WMAP data has been used to determine the parameter η, the baryon to photon ratio, from which the abundances of light element can be determined. The current best estimate of this parameter is [56, 47]

$$\eta = (6.12 \pm 0.15)\, 10^{-19}.$$

Current data points to a discrepancy in the amount of ^7Li produced which is a factor of three lower than predicted. The result is that our understanding of nuclear reactions of stars is either incomplete or our current understanding of BBN will have to be revised. It has been suggested that allowing for the variation of constants may solve the ^7Li problem [47]. Indeed cosmological models with scalar-tensor theories of gravity indicate that this may be the case [57].

2.7.2 Varying The Gravitational Constant

On a local scale, we have a very well tested theory of gravity [29]. Although it is difficult to disentangle the variation of the various constants, since the deviation from general relativity and violation of the weak equivalence principle due to the variation of other constants will have the same qualitative effect.

The mass of any body includes the mass of the elementary particles that constitute it. These are dependent on various fundamental constants of the Standard Model and the binding energy that results from the fundamental interactions. Hence, the mass of any body is a function of fundamental constants. Varying any one fundamental constant results in the mass of any body being space-time dependent. Although the inertial mass of an object is computed as relative to some standard inertial mass kept at a different point in space-time, it is still possible to determine whether there is a spatial variation in

the mass. A standard quantity such as M_P, the mass of the proton, has the advantage of being made purely from fundamental constants. A possible variation will manifest in the dimensionless ratio of M_P and the Planck mass. We may set $\hbar$ and c to one to fix our units and thus explicitly relate the variation of mass to a variation of G [58]. Say the geodesics of the metric g_{ab}, obtained from varying the action $S = -\int m\ ds$ are the observed geodesics and the units of length, time and mass are appropriate for a geometry described by g_{ab}. Then, if the mass of an object is a constant then the geodesic equation is simply

$$\frac{d^2x^a}{ds^2} + \Gamma^a_{bc}\frac{dx^b}{ds}\frac{dx^c}{ds} = 0.$$

A space-time dependence in the mass can be introduced through a scalar field that couples directly to the metric (conformally coupled scalar field) in the following manner

$$m = m_o A_m(\varphi(r)),$$

where m_0 is a constant. The particle now has the following motion

$$\frac{d^2x^a}{ds^2} + \Gamma^a_{bc}\frac{dx^b}{ds}\frac{dx^c}{ds} + \alpha_m(\varphi)\varphi_{,b}\frac{dx^b}{ds}\frac{dx^a}{ds} = 0,$$

which is not the geodesic of the metric g_{ab}, violating the EP.

The other fundamental constants have to be kept constant to disentangle their effects on observations from the variation of G. We shall thus require that the gravitational structure constant

$$\alpha_M = \frac{Gm_P^2}{\hbar c},$$

where m_P is the rest mass of a proton, is fixed.

Constraints on the variation of G, can then be easily written as constraints on the dimensionless constant α_G, which was held fixed in the previous case when the variation of α_{EM} was considered.

There are several methods that can be used to constrain the value of $\frac{\dot{G}}{G}$. Examples include BBN [59], CMB data [60], binary neutron star masses [61], binary pulsar timing [62], and lunar laser ranging (LLR) [41]. We note that these constraints are not always obtained in a model independent manner. In LLR experiments the distance between the earth and the moon is measured precisely. The variation of which can be directly related to the variation of G. The best solar system constraint, where the gravitational energy can be neglected, is found, using LLR [40], to be

$$\frac{\dot{G}}{G} = (4 \pm 9) \times 10^{-13}\ \mathrm{yr}^{-1}.$$

In pulsar timing measurements, where strong gravitation effects are expected, the gravitational binding energy cannot be ignored and model dependent effects may occur. The best model free approach using pulsar data also found no variation in G.

2.8 Summary

This chapter has reviewed the EP in GR in the three forms it takes.

- The WEP, in which all bodies fall with the same acceleration in a given gravitational field, is violated if the acceleration a body experiences is composition dependent.
- The EEP, in which the local reference frame in which is not ignored, is violated if results consistent special relativity cannot be recovered.
- The SEP, in which the inertial mass is explicitly composed of the gravitational binding energy amongst the binding energy from other fields, is violated when the internal structure (even for bodies of the same composition), affects how bodies interact with a given gravitational field.

We have also reviewed the current observational constraints of the violations each of the equivalence principles. This was done in a general way, applicable to a wide variety of theories, for instance the η parameter, from Eötvös experiments, and the γ and β parameters from the PPN framework. The EEP, which is satisfied by metric theories was discussed in detail. This discussion included a literature review of the current status of the variation of fundamental constants.

GR and *universally coupled* scalar-tensor theories of gravity satisfy the EEP. However, solar system constraints of β and γ make it impractical to distinguish these modified theories from GR. The chameleon mechanism, which is explained in detail in 3, results in scalar-tensor theories distinct from GR and yet are compatible with solar system constraints. The mechanism also allows the possibility of an EEP violating theory that is also compatible with constraints.

All scalar-tensor theories violate the SEP. This violation van be related in terms of the PPN parameters. The chapter also provided the current constraints of the SEP.

In the next chapter, we study the spherical solutions of scalar-tensor theories. In particular, a chameleon model first studied in [15] is introduced. It is within this EP violating theory that the original investigations in chapter 5 are undertaken. The EP is explicitly violated in these theories. However, it may still be possible to constrain this violation while observing new signatures in data such as galactic rotation curves.

Chapter 3

Scalar-Tensor Theories

3.1 Introduction

GR is a tensor theory of gravity. The fundamental building block of the theory is the metric tensor field g. Scalar-theories of gravity precede tensor theories simplicity and historical discovery. Newtonian theory is a classical example of a scalar theory of gravity, The scalar field of which can be associated with the gravitational potential. Despite its success and agreement with the WEP, Newtonian theory does not take the physics of special relativity into account nor does it account for all phenomena observed on solar system scales, while GR does. However, GR depends on the SEP which has not been shown to be either favoured nor disfavoured by experiments.

The earliest proposed scalar theory of gravity that took into account special relativity were by G. Nodström. In Nodström's theory, the inertial mass of an object is coupled to a scalar field ϕ, in the following way [45],

$$m = m_0 e^{\phi}.$$

This theory was not successful as it did not predict any deviation of light rays[45]. A scalar theory of gravity provides a way of realising Mach's principle. The principle states that the inertial mass of an object depends on the interaction of all other objects in the universe, and so acceleration can be defined relative to the distribution of mass in the universe. This dependence may be mediated through a scalar field.

GR, a tensor theory of gravity, is consistent with the observed physics of the universe but not Mach's principle. A theory with both a scalar and tensorial field may reproduce the success of GR and also satisfy Mach's principle.

Until recently, observations have constrained the scalar field coupling ω, which appears in the action in the following form

$$S = \frac{1}{16\pi G}\left(\int \Phi R + \frac{\omega(\Phi)}{\Phi}\tilde{g}^{\mu\nu}\partial_\mu\Phi\partial_\nu\Phi\right)\sqrt{-\tilde{g}}d^4x + S_m\left(\psi_m, \tilde{g}_{\mu\nu}\right),$$

to such an extent that these theories were difficult to distinguish from GR. The chameleon mechanism [63] allows for scalar-tensor theories to satisfy all current experimental limits and still be distinguishable from GR.

Other motivations for studying scalar-tensor theories come from the study of modern theories of high energy physics, classical higher dimensional theories, $f(R)$ theories of gravity, quintessence models and inflation theories. The first, higher dimensional theories, often arise in high energy theories of physics. In these theories the compactification of the unobserved dimensions leads to a four dimensional scalar-tensor theory.

While in the second, $f(R)$ theories, the action is assumed to be some arbitrary function of the curvature. The third application of scalar-tensor theories, quintessence models, are an active area of research in modern cosmology. The chameleon model, which refer to as the AWE model, that is the subject of our investigations in chapter 3, is a typical example of a theory that unifies the explanation of dark energy with a modified theory of gravity. Lastly, inflation models have had success in explaining why the universe is almost flat. A class of these models are able to explain inflation with minimal extensions to the Standard Model of elementary physics. We will consider scalar-tensor theories in which the scalar field can be associated with the Higgs field.

3.1.1 Kaluza-Klein Theories

Kaluza-Klein theory [64], a theory with a five dimensional space-time, can be recast as a scalar-tensor theory in four dimensions (see [65] for a review). In general, the theory is set in d extra spatial dimensions. In general, the gravitational action in higher dimension is given by:

$$S = \frac{1}{2\hat{\kappa}} \int \hat{R} \sqrt{|\hat{g}|} d^D x,$$

where $\hat{\kappa}$ is the appropriate generalisation of κ, $\hat{g}_{ab}$ is the D dimensional metric and $\hat{R}$ is the Ricci Scalar formed from the higher dimensional metric. In its original, five dimensional, formulation Kaluza-Klein theory unifies gravity and electromagnetism. For simplicity, we will only discuss the five dimensional theory. The metric can be parametrized in the form [65]

$$\hat{g}_{ab} = \begin{pmatrix} g_{\mu\nu} + \xi A_\mu A_\nu \phi^2 \phi_B & \xi A_\mu \phi^2 \\ \xi A_\nu \phi^2 & \phi^2 \end{pmatrix},$$

with the indices $a, b = 0, .., 4$ and $\mu, \nu = 0, ..., 3$. In this theory, space-time transformations in five dimensions could be associated with electromagnetic gauge transformations. Specifically, the fifth dimensional co-ordinate transformation:

$$x^4 \leftarrow x'^4 = x^4 + k\epsilon(x),$$

alters the off diagonal element

$$A_\mu \rightarrow A'_\mu = A_\mu + \partial_\mu \epsilon.$$

The compactification of a five dimensional Kaluza-Klein theory can to a scalar-tensor theory in four dimensions can be easily shown if we limit the x^4 dependence in the metric to a compactified into S^1 region. For clarity, we will also disregard electromagnetic fields. The metric is then given by

$$\hat{g}_{\mu\nu} = \begin{pmatrix} g_{ab} & 0 \\ 0 & \phi^2 \end{pmatrix},$$

The action is then simply given by

$$\begin{aligned} S &= \frac{1}{16\pi\hat{G}} \int \hat{R}\sqrt{-|\hat{g}|}\; d^{(4+d)}x \\ &= \frac{2\pi}{16\pi\hat{G}} \int R\sqrt{-|g|}\sqrt{\phi}\; d^4x. \end{aligned}$$

For simplicity, we have assumed that the quantity that results from integrating the compact dimension is simply 2π. The above action is that of a scalar-tensor theory. The following conformal transformations (we will discuss this in more detail later in the chapter)

$$\begin{aligned} g_{\mu\nu} &\to g_{\mu\nu}\phi^{-\frac{1}{3}}, \\ \phi &\to \phi^{\frac{2}{3}}, \\ \varphi &= \frac{\kappa^{-1}}{\sqrt{3}} \ln\left(\frac{\phi}{\phi_0}\right), \end{aligned}$$

allow us to write the action in the familiar Einstein frame

$$S = \frac{1}{16\pi\hat{G}} \int \left[R - \nabla^a\varphi\nabla_a\varphi\right]\sqrt{-g}\; d^4x.$$

It was initially assumed that by compactifying from a higher dimensional theory all gauge fields would arise naturally. However, this is not the case. Current High energy theories of physics, such as string theory and quantum gravity often have space-times of high-dimensions with gauge field already present in the higher dimensional space-time. It seems promising that the four dimensional low energy limit of these theories may be a non-universally coupled scalar-tensor theory.

3.1.2 f(R) theories

Modification of General Relativity, such as f(R) theory, Gauss-Bonnet gravity, that introduce higher order terms in the gravitational action, can be theoretically motivated by the need to have a re-normalizable gravitational theory. For instance, quantum corrections to GR adds terms of the type $R\Box^k R$ in the Lagrangian, which leads to the inclusion of $2k+1$ order terms in the field equations [66]. It is also known [67] that a fourth order theory of gravity, in which the curvature term is replaced by a more general term:

$$S = \frac{1}{2\kappa} \int aR^2 + bR_{ab}R^{ab} + kR + \Lambda,$$

could prevent the Big Bang singularity as well as provide a natural explanation to inflation. One realisation of a fourth theory gravity is Gauss-Bonnet gravity. In this theory, the action takes the form

$$S = \int R^2 - 4R_{ab}R^{ab} + R_{abcd}R^{abcd}d^Dx,$$

where D is the number of dimensions in space-time.

There are many ways of formulating higher order gravitational theories. Replacing the curvature scalar with $f(R)$ were f is an arbitrary function is a simple way of studying a large class of these. $f(R)$

theories may also be reduced to scalar-tensor theories of gravity. $f(R)$ theories have the action

$$S = \frac{1}{2\kappa}\int [f(R) + L_m]\sqrt{-g}\ d^4x.$$

There are two ways of deriving the field equations of $f(R)$ gravity: the metric formalism and the Palatini formalism. In the metric formalism the connection coefficients and derived quantities are built the same way from the metric as they are in GR. For instance

$$\Gamma^{\alpha}_{\beta\gamma} = \frac{1}{2}g^{\alpha\beta}\left(\frac{\partial g_{\gamma\lambda}}{\partial x^{\beta}} + \frac{\partial g_{\lambda\beta}}{\partial x^{\gamma}} - \frac{\partial g_{\beta\lambda}}{\partial x^{\lambda}}\right), \text{ and}$$
$$R_{\mu\nu} = \partial_{\gamma}\Gamma^{\lambda}_{\mu\nu} - \partial_{\mu}\Gamma^{\lambda}_{\lambda\nu} + \Gamma^{\lambda}_{\mu\nu}\Gamma^{\rho}_{\rho\lambda} - \Gamma^{\lambda}_{\nu\rho}\Gamma^{\rho}_{\mu\lambda}.$$

We thus have the following field equations

$$F(R)R_{\mu\nu} - \frac{1}{2}f(R)g_{\mu\nu} - \nabla_{\mu}\nabla_{\nu}F(R) + g_{\mu\nu}\Box F(R) = \kappa T_{\mu\nu}$$
$$3\Box F(R) + F(R)R - 2f(R) = \kappa T.$$

In the Palatini formalism in which the connection coefficients $\Gamma^{\lambda}_{\mu\nu}$ and the metric $g_{\mu\nu}$ are independent. The field equations of this action are then given by

$$F(R)R_{\mu\nu}(\Gamma) - \frac{1}{2}f(R)g_{\mu\nu} = \kappa_{\mu nu}, \text{ and}$$
$$F(R)R - 2f(R) = \kappa T.$$

Both representations can be identified with a scalar-tensor theory. The action of the resulting scalar-tensor theory is given by

$$S = \int\left(\frac{1}{2}\phi R - \frac{\omega}{2\phi}\nabla_{\mu}\phi\nabla^{\mu}\phi - U(\phi) + L_m\right)\sqrt{-g}\ dx$$

with

$$\phi = F(R),$$
$$U(\phi) = \frac{R\phi - f(R)}{2\kappa}, \text{ and}$$
$$\omega = 0,$$

in the metric formalism. The following identification

$$\phi = F(R),$$
$$U(\phi) = \frac{RF(R) - f}{2}, \text{and}$$
$$\omega = -\frac{3}{2},$$

in the Palatini formalism also results in a scalar-tensor-theory of gravity.

However, it must be noted that Palatini $f(R)$ has many shortcomings [66]. For instance there are conflicts with the Standard Model of particle and it is unable to reproduce inflation correctly [68]. There

are generalisations of the theory in which other quantities, such as the Riemann tensor are currently being investigated. These may become viable modified gravity models.

As a large class of modified theories gravity, even in higher dimensions, can be reduced to scalar-tensor theories, it is appealing to study these theories as a representative example of modified gravity.

3.1.3 General Action for Scalar-Tensor Theories

In the preceding discussions we provided motivations for investigating scalar-tensor theories of gravity and derived different forms of the action of a scalar-tensor theory of gravity. This was done by allowing fundamental physical constants to vary in GR, compactifying a higher dimensional gravitational theory or changing the variables of another theory were there is at least one extra degree of freedom. This section will introduce a general form of scalar-tensor theories we that will investigate in this thesis. The action of these theories will take the form:

$$S = \frac{1}{16\pi G_*}\int\left[f(\phi,R) - \frac{\omega(\phi)}{2}\nabla^a\phi\nabla_a\phi + V(\phi)]\sqrt{-g} + \sum_i L_m^{(i)}\left(\Psi^{(i)}, h^{(i)}(\phi)\, g_{ab}\right)\right]\sqrt{-g}\; d^4x.$$

In this thesis we will pay particular attention to the following scalar-tensor theories:

- minimally coupled scalar-tensor theories – when $f(\phi,R) = R$
- non-minimally coupled scalar-tensor theories –when $f(\phi,R) = g(\phi)R$
- non-universally chameleon scalar-tensor theories – when $h(\phi)$ is different for different matter species

The function $h(\phi)$ can be absorbed into metric by a conformal transformation for one of the matter species. In the subsequent sections we show that the choice of the conformal frame has no influence on the physical interpretation of the model.

3.2 Conformal Frames

Jordan's formulation theory of a scalar-tensor theory [46], which stems from compactifying a five dimensional space-time is related to the Brans-Dicke scalar-tensor theory by a conformal transformation. The scalar field in this formulation is minimally coupled. This means that the scalar field does not couple to the Ricci scalar in the action. The Brans-Dicke theory is non-minimally coupled. The theory is directly related to a varying gravitational constant, which is represented by a scalar field. The scalar field term therefore couples directly to the Ricci scalar. The Brans-Dicke theory has often been studied as typical scalar-tensor theory of gravity. It is in this frame that quantities in scalar-tensor theories, such as the energy density, can be related to experiments. Modern high energy theories of particle physics, such as M theory, contain scalar fields similar to those of Brans-Dicke theory [69]. It is for these reasons that the Brans-Dicke frame is considered to be the physical frame. The two conformal frames are linked by a conformal transformation.

3.2.1 Conformal Transformations

There had been little consensus on how the scalar field should be incorporated into the gravitational action, until recently [70], [71], [72]. The scalar field could be coupled to the Ricci scalar as in the Jordan frame or to the matter part of the Lagrangian as in the Einstein frame. Historically, it was thought that these formulations or frames described different physical theories. The following section illustrates this is not the case.

Conformal transformations are transformations of the form

$$ds^2 \to \Omega^2(x) ds^2,$$

or equivalently, in terms of the metric:

$$g_{ab} \to \Omega^2(x) g_{ab}$$

as well as a redefinition of the scalar field. These are used to alter the dynamical variables (g_{ab}, ϕ) used in one conformal frame to a new set $(\tilde{g}_{ab}, \tilde{\phi})$, in a different conformal frame. Causality remains intact as a result of the conformal nature of the transformations. When Ω is constant, we have a scale transformation analogous to a change of units, and all physical phenomena remain the same. The result also holds when Ω is not constant. Although, the geodesics in the two frames do not appear to be identical, nor are the matter conservation equations simultaneously conserved in both frames, we will show that physically observable phenomena are the same in either frame.

A conformal transformation of the metric directly affects the Christofell symbols in the following way:

$$\Gamma^c_{ab} \to \Gamma^c_{ab} + \frac{1}{\Omega}(\delta^c_a \Omega, b + \delta^c_b \Omega_{,a} - g_{ab} g^{cd} \Omega, d).$$

This affects subsequent quantities built on these tensors, such as the Riemann, Ricci, Einstein tensors and the Ricci scalar. For example, if the original metric is Ricci-flat $(R = 0)$, the conformally transformed metric is not:

$$\tilde{R} = \Omega^2 R + 6\Omega \Box \Omega - 12 \nabla^a \Omega \nabla_a \Omega.$$

As it is traditional to ascribe a Ricci flat space-time with a vacuum, this may seem surprising. It appears that the conformal transformation leads to the creation of matter. However, it must be noted that it is the absence of a stress energy tensor, and not a vanishing Ricci scalar, that indicates a vacuum. The Einstein tensor transforms in the following way:

$$\tilde{G}_{ab} = G_{ab} - \frac{2}{\Omega}(\nabla_a \nabla_b \Omega - g_{ab} \Box \Omega) - \frac{3}{\Omega^2} g_{ab} \nabla_c \Omega \nabla^c \Omega.$$

This creates a new source to the Einstein tensor. However, as discussed section 3.1 of [73], provided we create a scalar field stress-energy tensor in the original frame dependent on Ω, which vanishes, the transformation to a new conformal frame is also a vacuum. When there are matter sources, the conformal transformation of the stress energy tensor is simply

$$T_{ab} = \Omega^{-4} \tilde{T}_{ab}.$$

This lets us relate the physical components T_{ab} to those of $\tilde{T}_{ab}$, and indicates how quantities in one frame are related to those of another through a change of units. We further note that the Weyl tensor C^d_{abc} is conformally invariant, however, and conformal flatness ($C^d_{abc} = 0$) is preserved.

3.2.2 Physical Conformal Frame in Scalar-Tensor theories

The choice of frame is motivated by mathematical simplicity and not necessarily the need to make certain quantities invariant. The canonical scalar-tensor action in the Brans-Dicke frame is:

$$S = \frac{1}{16\pi G*}\int [\phi R - \frac{\omega(\phi)}{\phi}\nabla^a\phi\nabla_a\phi]\sqrt{-g}\ d^4x + S_m\left(\psi_m, g\right).$$

In this representation the equations of motion take the form

$$\begin{aligned} G_{ab} &= \frac{8\pi}{\phi}T^{(m)}_{ab} + \frac{\omega(\phi)}{\phi^2}(\nabla_a\phi\nabla_b\phi - \frac{1}{2}g_{ab}\nabla^c\phi\nabla_c) + \frac{1}{\phi}(\nabla_a\nabla_b\phi - g_{ab}\Box\phi), \\ \Box\phi &= \frac{1}{2\omega+3}\left(8\pi T^{(m)} - \frac{d\omega}{d\phi}\nabla^c\phi\nabla_c\phi\right), \end{aligned}$$

and the "conservation" equation has the form

$$\nabla^b T^{(m)}_{ab} = 0.$$

The following conformal transformations allows us to move to the Einstein Frame $(\varphi, \tilde{g}_{ab})$:

$$\begin{aligned} g_{ab} \to \tilde{g}_{ab} &= A^2_m(\varphi)g_{ab}, \\ 3 + 2\omega(\phi) &= \alpha_m^{-2}(\varphi), \\ \alpha_m(\varphi) &= \frac{d\ln(A_m(\varphi))}{d\varphi}. \end{aligned}$$

The action in the Einstein frame is thus given by

$$S = \frac{1}{16\pi G_*}\int [\tilde{R} - \frac{1}{2}\nabla^a\varphi\nabla_a\varphi]\sqrt{-\tilde{g}}\ d^4x + S_m\left(\psi_m, g\right).$$

This results in simpler equations of motion:

$$\begin{aligned} \tilde{G}_{ab} &= 8\pi G_*\tilde{T}^{(m)}_{ab} + 2\nabla_a\varphi\nabla_b\varphi - \tilde{g}_{ab}, \nabla^a\varphi\nabla_b\varphi, \\ \tilde{\Box}\varphi &= -4\pi G_*\alpha_m\tilde{T}^{(m)}, \end{aligned}$$

and conservation equations

$$\nabla_a\tilde{T}^{(m)a}_b = \alpha_m(\varphi)\tilde{T}^{(m)}\nabla_b\varphi.$$

A physical frame is a set of variables in which a theory is theoretically consistent and makes testable predictions [74]. Despite the equivalence in conformal frames, until recently, there was confusion in the literature about whether physical predictions are affected by the choice of the representation used and thus which frame is the "physical frame" [75]. We claim that all physical observables in conformal frames are the same and hence all conformal frames represent the same physical reality.

The simplest way to show that the two frames represent the same physical reality is by first noting that the line element ds^2 in the Jordan frame, and the line element $\tilde{ds}^2 = A_m^2(\varphi)\, ds^2$ can both be cast as the PPN line metric 2.1 with the following identifications [76], [29]:

$$\gamma - 1 = \frac{1+\omega(\phi_0)}{2+\omega(\phi_0)} = -2\frac{\alpha_m^2(\varphi_0)}{1+\alpha_m^2(\varphi_0)},$$
$$\beta - 1 = 1 + \frac{d\omega(\phi)}{d\phi}\Big|_{\phi_0} (3+2\omega(\phi_0))^{-2} (4+2\omega(\phi_0))^{-1} = \frac{1}{2}\frac{\alpha_m^2(\varphi_0)}{(1+\alpha_m^2(\varphi_0))^2}\frac{d\alpha}{d\varphi}\Big|_{\varphi_0}.$$

In turn, all weak field, slow moving limit experimental test and observations such as the gravitational deflection of light, the time delay of light, Shapiro time delay and the perihelion shift of Mercury can be cast using the same metric. The only difference being the expression of the PPN parameters. It is also clear that both frames would reduce to the same special relativistic limit.

Finally, we note that the units on which physical observables are based on are invariant to conformal transformations. The mass of an object, which determines the physics of an object in the Jordan frame action

$$S = -\int m\ ds$$

is actually calculated relative to some reference mass m_r. In the Einstein frame, a similar result holds:

$$S = -\int \tilde{m}\ d\tilde{s} = -\int \tilde{m} A(\varphi)\ ds,$$

and the reference mass is $\tilde{m}_r A(\varphi)$. An actual measurement of mass would then be independent of the scalar field. A similar result holds for proper length and proper time. Futhermore, explicit calculations of quantities such as the luminosity distance, [77] further corroborate this fact.

Some authors, see [70] for a review, cite the lack of stable ground states and the appearance of negative energy in the Jordan frame as reasons for supposing the Einstein frame is the physical frame. Also, recent works, such as [78], muddle the concept of physical equivalence by not restricting this to the equivalence of measurable physical observables, but philosophical principles such as the WEP. Papers such as [71] refute this claim and in the spirit of Dicke [58] argue that the choice of conformal frame can be reduced to a choice of units, as we have shown.

We have shown that both frames are admissible and that claims such as the Jordan frame has no stable ground states [79] or that the violation of the EP in the Einstein frame is unacceptable do not favour either frame. *A priori*, it is possible that some variables are unsuitable for describing a physical event. Since in the Einstein frame $\nabla_a \tilde{T}_b^{(m)a} \neq 0$, it is traditional to consider the Jordan frame as the physical frame. It is admissible to prefer one frame over another, analogous to how how one may prefer one coordinate system another. Frameworks that compare different metric theories of gravity, such as the PPN framework work in either frame. There is a growing on the consensus of the equivalence of conformal frames [47], [80] [81].

The subsequent sections and chapters study scalar-tensor theories in both frames depending on mathematical convenience or physical motivation. In particular, we will specifically examine soliton solutions in non-minimally coupled gravity and spherically symmetric solutions in non-universally coupled chameleon models.

3.3 Non-Universally Coupled Scalar-Tensor Theories

3.3.1 Introduction

Although scalar-tensor theories associated directly with the variation of the gravitational constant have found little support from observations, scalar-tensor theories remain a popular approach for modified gravitational models. However, modern theories of inflation propose the use of a hypothetical particle associated with the scalar field, known as the inflaton, to explain inflation. CMB data suggests that the inflaton has a mass of $\approx 10^{13} GeV$ and a small coupling constant [82] $\lambda \approx 10^{-13}$. Scalar fields also occur in string theories. The scalar particle in these theories is known as the dilaton. The coupling between the non-dilaton terms and the curvature is non-universal in these theories. This further prompts a careful study of scalar-tensor theories with non-universal couplings.

Current evidence from the LHC, [83], [84], points to the existence of a Higgs scalar field. Although there are no SM particles with the appropriate mass and coupling constant to produce inflation, a modification of the gravitational interaction through non-minimal coupled Higgs has led to an inflationary model consistent with CMB data [85], [9]. In the unitary gauge, the action of this model will be given by:

$$S = \int \left(-\frac{M^2 + \xi h^2}{2} R + \frac{1}{2} \nabla_a h \nabla^a h - \frac{\lambda}{4} \left(h^2 - v^2 \right)^2 \right) \sqrt{-g} d^4 x$$

for the correct values of ξ and $M \simeq m_{pl}$, where m_{pl} is the reduced Plank mass, one is able to reproduce the main features of inflation. This action forms the basis of some of the spherical solutions studied in this chapter.

We will investigate non-universally coupled scalar-tensor theories in the context of spherically symmetric compact solutions. In this context, it is supposed the object of interest is made of one fluid and thus it is unnecessary to consider non-universal couplings. In contrast to the chameleon models, the first model introduced in this section will not be a chameleon model. This model will enable us to study the properties of solutions in scalar-tensor theories without the chameleon effect. These are still an active area of research, and find applications in soliton solutions where new dark matter candidates may be proposed or new insights into extremely compact objects such as boson stars may be obtained. The final model we consider will be a chameleon model, in which we will show in particular how the chameleon mechanism works.

3.3.2 Chameleon Mechanism

Introduction

The chameleon mechanism is a screening mechanism that enables the scalar field to assume appropriate cosmological value to explain dark energy as well as an appropriate local value in agreement with solar system tests [63], [86], [15],[87]. Such a mechanism allows for a scalar-tensor theory consistent with local solar system tests of the EP, yet with different cosmological behaviour. Most interestingly, non-universal coupling in these models still allow for a violation of the EP between the baryonic and dark matter sectors.

Even when chameleon fields are screened, they still predict non GR phenomena such as scalarisation, which is analogous to ferromagnetism [88], and gravitational memory effects. Our study of scalar-tensor theories will be aimed towards understanding the consequences of a non-universally coupled chameleon fields.

Constraints on Scalar-Tensor Theories

The PPN parameters γ and β distinguish scalar-tensor theories from GR. These parameters constrain the coupling to matter. The current best constraint on the γ parameter [40] is:

$$\gamma - 1 = (2.1 \pm 2.3) \times 10^{-5}.$$

This necessitates that $\omega > 4000$ for scalar-tensor theories written in the Jordan frame, or $\alpha < 10^{-3}$ for scalar-tensor theories written in the Einstein frame. This would then exclude the Kaluza-Klein and $f(R)$ theories introduced as equivalent to scalar-tensor theories. Furthermore, it is necessary that scalar-tensor theories are compatible with free-fall tests of the EP as well. This is measured by the Eot-Wash parameter, the bound of which was discussed in the previous chapter.

If the coupling is assumed to be constant, these constraints suggests rather extreme fine-tuning. In a more natural theory, where the coupling has space-time dependence, mechanism have been proposed to have couplings that are reconcilable with the above constraints, and are low-energy limits of high energy physics theories. Such a mechanism hinges on the fact that the couplings are attracted towards a minimum value compatible with constraints on solar system scales [89, 90]. A density dependent attraction mechanism is a natural way to achieve this effect, and had been investigated in [18, 89, 90]. However, a theory in which this mechanism allows the scalar fields to couple with baryonic matter was first investigated in [91, 63]. The following subsections outline how the mechanism works in universal and non-universally coupled theories.

Chameleons in Universally Coupled Theories

The action for chameleon theories in the Einstein frame is given by [63]:

$$S = \int \left(\frac{M_{PL}^2}{2} R - \frac{1}{2} \nabla_a \phi \nabla^a \phi - V(\phi) \right) \sqrt{-g}\ d^4x + \sum_i S_i(\psi^{(i)}, e^{2\beta_i \frac{\phi}{M_{PL}}} g_{\mu\nu}).$$

In non-universal coupling it is not necessary that all the β_i's are identical. We further note that it is written in the EF, in contrast to the non-minimally coupled scalar-tensor theory studied in the previous sections.

The evolution of the scalar field is derived from the following Klein-Gordon equation:

$$\Box\phi = \frac{\partial V}{\phi} + \sum_i \frac{\beta_i}{M_{PL}} \rho_i e^{\beta_i \frac{\phi}{M_{PL}}}$$

where the matter fields are non-relativistic and ρ_i corresponds to the physical (Jordan frame) energy density. This results in an effective potential

$$V_{eff} = V(\phi) + \sum_i \rho_i e^{\beta_i \frac{\phi}{M_{PL}}}$$

which has a minimum provided $\beta_i > 0$ and V is a monotonically decreasing function. In this mechanism, the minimum of the scalar field is explicitly dependent on local density conditions. For instance the potential could be an inverse power such as the Ratra-Peebles potential [92, 93]:

$$V(\phi) = \frac{\Lambda^{4+\alpha}}{m_{pl}^{\alpha} \phi^4},$$

where Λ and α are free parameters. This self interaction potential has been used in a wide number of scenarios. It has been used to model inflation [92, 93], quintessence [93]. It has also been studied within the context of chameleon cosmologies [63, 77].

From the solution of the Klein-Gordon equation we can deduce the effective coupling α_{eff} that results from the chameleon mechanism. The scalar field solution is given by [63], [94]:

$$\phi(r) = \phi_\infty - \frac{\alpha_{eff}}{r}\frac{M_b}{m_{pl}}e^{-m_\infty(r-R_b)},$$

where R_b is the radius of the object, M_b is its mass. The value of α_{eff} depends on the thin shell parameter [63, 91, 95]

$$\epsilon = \frac{\phi_\infty - \phi_b}{\frac{3}{4\pi}\alpha_m\Phi_b},$$

where Φ_b is the gravitational potential at the boundary of an object, and $\phi_b \approx \phi(r=0)$. If $\epsilon < \frac{1}{2} + \frac{1}{m_\phi^2 R_b}$ [77], where

$$m_\phi^2 = \left.\frac{d^2V_{eff}}{d\phi^2}\right|_{\phi_{min}}, \text{ then}$$
$$\alpha_{eff} \approx 3\alpha_m\epsilon.$$

If

$$\epsilon > \frac{1}{2} + \frac{1}{m_\phi^2 R_b}, \text{ then}$$
$$\alpha_{eff} = \alpha_m.$$

Chameleon Models in Non-Universally Coupled Models

The chameleon effect above is also possible in a theory with non-universal couplings and no additional potential for the scalar field. The effective potential is then:

$$V_{eff} = \sum_i \rho_i e^{\frac{k_i}{2}\frac{\phi^2}{M_{PL}^2}}.$$

If the coupling constants are not all of the same sign, then the scalar field has a minimum ϕ_{min}, as long the following equation is satisfied:

$$\left.\frac{dV_{eff}}{d\phi}\right|_{\phi_{min}} = \sum_i \frac{k_i\phi_{\min}}{m_p^2}\rho_i e^{\frac{k_i}{2}\frac{\phi_{min}^2}{M_{PL}^2}} = 0.$$

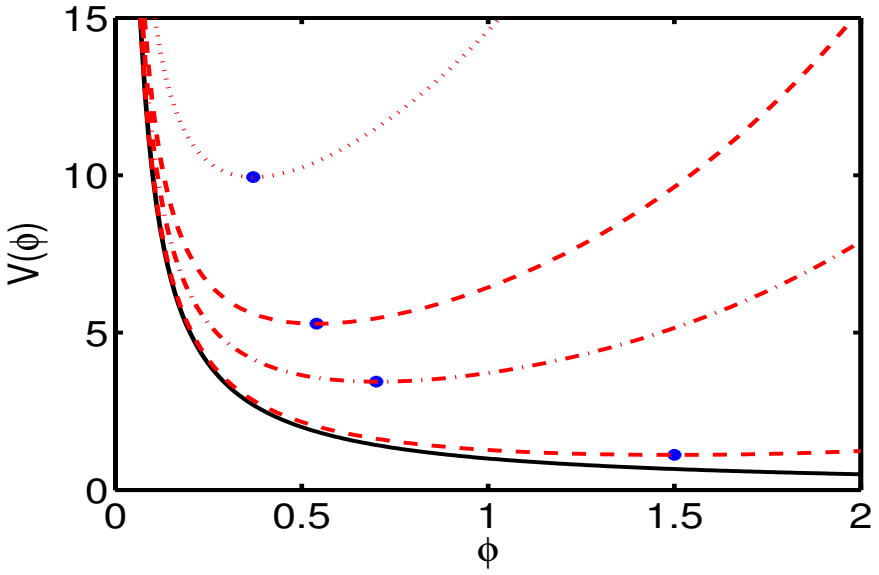

Figure 3.1: An illustration of a density dependent chameleon potential. The solid black line is in the absence of baryons. The blue dots indicate the minimum of the potential.

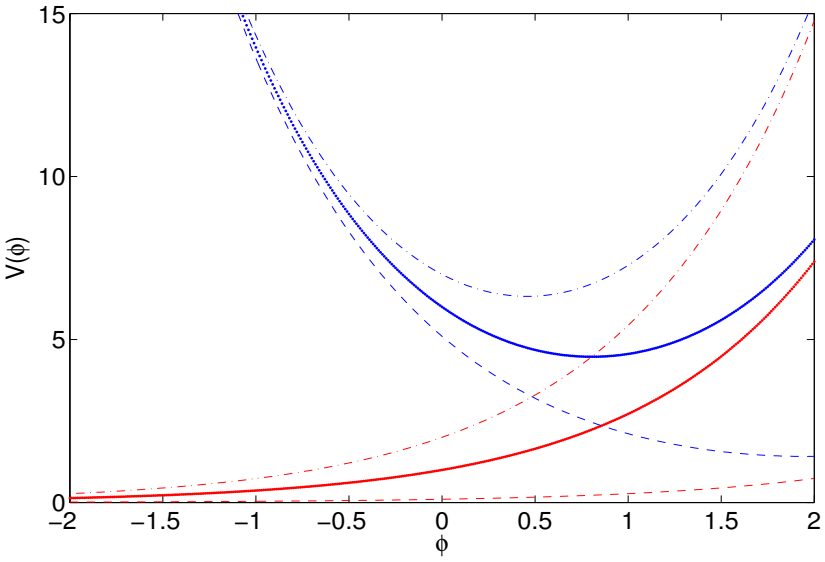

Figure 3.2: An illustration of the effective potential in a non-universally coupled model. The dashed line, which implies the mass of the scalar field is very light, occurs when dark matter dominates. The subsequent arched curves are occurs when the proportion of baryonic increases

Non-universal coupling introduces an explicit violation of the EP. The scalar-tensor theory we use to model non-universally coupled chameleon theories was first investigated by [96, 15]. This model, dubbed the Abnormally Weighting Energy(AWE) model, provides a natural method for explaining dark energy as result of non-universal couplings. The two pressure-less matter species, baryonic matter and dark matter, couple non-universally to the scalar field.

The AWE action of which is given by

$$S=\frac{1}{16\pi G}\left(\int \Phi R\frac{\omega(\Phi)}{\Phi}\tilde{g}^{\mu\nu}\partial_\mu\Phi\partial_\nu\Phi\right)\sqrt{-\tilde{g}}d^4x+S_m\left(\psi_m,\tilde{g}_{\mu\nu}\right)+S_{awe}\left(\psi_{awe},M^2(\Phi)\tilde{g}_{\mu\nu}\right)$$

in the JF frame. The following transformations

$$\begin{aligned}\tilde{g}_{\mu\nu}&=A_m^2(\phi)g_{\mu\nu}\\ 3+2\omega_{BD}&=\left(\frac{d\ln(A_m(\phi))}{d\phi}\right)^{-2}\\ M(\phi)&=\frac{A_{awe(\phi)}}{A_m(\phi)}\end{aligned}$$

allow us to write the action in the EF as

$$S=\int\left[\frac{R}{16\pi G}-2g^{\mu\nu}\partial_\mu\phi\partial_\nu\phi\right]\sqrt{-g}\ d^4x+S_{awe}(\psi_{awe},A_{awe}^2(\phi)g_{\mu\nu})+S_m(\psi_m,A_m^2(\phi)g_{\mu\nu})$$

For convenience, ϕ is dimensionless, as the scaling factor m_{pl} has been absorbed into the definition of ϕ. The field equations are [1],

$$\frac{1}{16\pi G}\left[(R_{\mu\nu}-\frac{1}{2}Rg_{\mu\nu})-2\partial_\mu\phi\partial_\nu\phi+g_{\mu\nu}(g^{\mu\nu}\partial_\mu\phi\partial_\nu\phi)\right]=\frac{1}{2}(T_{\mu\nu}^{(m)}+T_{\mu\nu}^{(awe)}) \tag{3.1}$$

where the matter fields are the perfect fluids

$$\begin{aligned}T_{\mu\nu}^{(m)}&=A_m^4(\phi)\left[(\rho_1+\frac{p_1}{c^2})u_\mu u_\nu+p_1g_{\mu\nu}\right]\\ T_{\mu\nu}^{(awe)}&=A_m^4(\phi)\left[(\rho_2+\frac{p_2}{c^2})\eta_\mu\eta_\nu+p_2g_{\mu\nu}\right]\end{aligned}$$

where u_μ is the four velocity of the matter fluid, and

$$\eta_\mu=\gamma(t,r)\left(u_\mu+v_\mu\right)$$

where η is the peculiar velocity of the AWE fluid. When studying static solutions, as we shall do for galactic rotation curves, we will assume $\gamma(t,r)=1,v_\mu=0$, and $ds^2=-e^{\nu(r)}dt^2+e^{\lambda(r)}dr^2+r^2d\Omega^2$. We can thus explicitly write out the field equations as:

$$\lambda'=8\pi GrA_m^4(\rho_m+\rho_{awe})e^\lambda+r\Psi^2+\frac{1-e^\lambda}{r} \tag{3.2}$$

$$\nu'=8\pi GA_m^4(\phi)(p_m+p_{awe})re^\lambda+r\Psi^2+\frac{e^\lambda-1}{r} \tag{3.3}$$

$$\phi'=\Psi \tag{3.4}$$

$$\Psi'=4\pi GA_m^4(\phi)e^\lambda[\alpha_m(\phi)(\rho_m-3p_m)+\alpha_{awe}(\phi)(\rho_{awe}-3p_{awe}) \tag{3.5}$$

$$+r\Psi(\rho_m+\rho_{awe}-p_m-p_{awe})-\frac{1+e^\lambda}{r}\Psi \tag{3.6}$$

$$p_i'=-(\rho_i+p_i)\frac{\nu'}{2}+\alpha_i(\phi)\Psi)) \tag{3.7}$$

[1] See A.1.1 for derivation of 3.1

The solutions of the above field equations are solved for in 5.

3.4 Summary

The first section showed the relation between $f(R)$ theories, Kaluza-Klein theories and scalar-tensor theories. We then discussed conformal frames in scalar-tensor theories, asserting the equivalence and demonstrating invariance of physical observables with examples. A number of approaches to coupling the scalar field to the gravitational sector as well as the applications thereof were considered. Finally, we showed a derivation of the chameleon mechanism and introduced the equations of motion for spherically chameleon field in AWE. The next part of this thesis will explore the solutions of these equations and those of non-minimally coupled scalar fields and their applications.

Part II

Signatures of The Violations of the EP

Chapter 4

Boson Stars

4.1 Introduction

With vary little modifications, the gravitational action for quintessence theories, introduced in the preceding chapters, can be used to study boson stars. Boson stars are compact solutions of a scalar field. Unlike stars made of baryonic matter, boson stars are gravitationally bound quantum states [97]. They most closely resemble neutron stars, but are mathematically simpler to investigate. Neutron stars support themselves from gravitational collapse by Fermi pressure as a result of Pauli's exclusion principle, while it is the Heisenberg uncertainty principle that keeps boson stars from collapsing.

Boson stars can be created by either a complex or a real scalar fields [98]. They have been shown to exist under the assumption of the following different interactions:

- Self-interactions described by scalar field potentials,
- minimal coupling to gauge fields,
- minimal coupling to gravity(GR), and
- non-minimal coupling to gravity (scalar-tensor theories).

The choice of interaction results in different phenomena. For instance, a violation of the EP may occur, even in the case of universal coupling. Boson stars do not emit any radiation on their own, and do not have a definite interior separate from the vacuum. For an isolated boson star, Cerenkov radiation, which is an acceleration which cannot be made to disappear in a local inertial frame, may signal their existence. This phenomenon would be a testable effect of local Lorentz invariance, and thus the EEP[99].

Boson stars may also be candidates for non-baryonic dark matter. Models of fitted flat rotation curves with bosons stars as dark matter have been proposed [100]. Although boson stars are still hypothetical, evidence for the existence of at least one scalar field, the Higgs, is accumulating [84], [83]. This motivates our study of scalar-tensor theories with the Higgs scalar field. The following sections first we will outline the current understanding of boson stars in GR, before we investigate the possibility of boson stars in a scalar tensor theory non-minimally coupled to the Higgs.

4.2 Boson Star Solutions in GR

4.2.1 Static Solutions

In GR, static solutions are only possible with a complex scalar field. This is because of Derek's theorem, [101, 101]. Albeit, quasi-static solitions known as oscillating soliton stars or oscillons exist [102] if the scalar field is written using the following form [103]

$$\phi(r) = \psi(r)e^{-i\omega t} + \psi(r)e^{i\omega t} = \frac{\psi(r)}{\sqrt{2}}\cos(\omega t).$$

We will restrict ourselves to static solutions and thus complex scalar fields.

The action of boson star in GR is then given by:

$$S = \int \left(\frac{1}{2\kappa} R - \frac{1}{2}\left[g^{ab}\nabla_a \bar{\phi} \nabla_b \phi + V(|\phi|^2) \right] \right) \sqrt{-g}\ d^4x.$$

The scalar field will be assumed to have the form

$$\phi(r) = \psi(r)e^{-i\omega t},$$

rather than

$$\phi(r) = \frac{1}{\sqrt{2}}\left(\psi_R(r) + i\psi_I(r)\right)$$

as the above harmonic time dependent ansatz has been shown in [104] and [105] to result in lowest energy static solutions.

4.2.2 Field Equations

The field equations are then given by

$$G_{ab} = \frac{\kappa}{2}\left[\nabla_a \bar{\phi} \nabla_b \phi + \nabla_a \phi \nabla_b \bar{\phi} - g_{ab}\left(g^{cd} \nabla_v \bar{\phi} \nabla_d \phi + V\left(|\phi^2|\right) \right) \right]$$
$$\Box\phi = -\frac{dV}{d|\phi|^2}\phi.$$

The simplest choice for the potential of the scalar field is simply a potential of the form

$$V(\phi) = m^2|\phi|^2.$$

With the above potential, it has been shown that the critical mass, the mass above which a star cannot resist gravitational collapse, is too small to be of consequence [97]. The addition of a self interaction potential to the action:

$$V(\phi) = m^2|\phi|^2 + \frac{\lambda_c}{2}|\phi|^4,$$

leads to boson stars with masses comparable to those of neutron stars [106]. In the study of boson stars, it will be convenient to use the spherically symmetric static line element:

$$ds^2 = -e^{\nu(r)}dt^2 + e^{\lambda(r)}dr^2 + r^2 d\Omega^2.$$

For convenience, we will use the following transformations to work in dimensionless units:

$$\begin{aligned}\omega &\to m\omega,\\ r &\to \frac{u}{m},\\ \phi &\to m_{pl}\phi.\end{aligned}$$

In the last equation we made use of the reduced Planck mass

$$m_{pl} = \frac{1}{\sqrt{\kappa}}.$$

Furthermore, we will define the dimensionless quantity

$$\Lambda = \lambda_c \frac{m_{pl}^2}{m^2}.$$

The explicit form for the equations of motion then is:

$$\begin{aligned}\lambda' &= \frac{1}{u}\left[\left(\psi^2 e^{\lambda-\nu}\omega^2 + \psi^2 e^{\lambda} + \frac{1}{2}\Lambda\psi^4 e^{\lambda} + \psi'^2\right)u^2 - e^{\lambda} + 1\right]\\ \nu' &= \frac{1}{u}\left[\left(\psi'^2 - \psi^2 e^{\lambda} - \frac{1}{2}\Lambda\psi^4 e^{\lambda} + e^{\lambda-\nu}\psi^2\omega^2\right)u^2 + e^{\lambda} - 1\right]\\ \psi'' &= \left(\psi + \Lambda\psi^3 + \frac{1}{2}\lambda'\psi' e^{-\lambda} - 2\frac{\psi'}{u}e^{-\lambda} - \psi\omega^2 e^{-\nu} - \frac{1}{2}\nu'\psi' e^{-\lambda}\right)e^{\lambda}\end{aligned}$$

The last equation, with the substitution of the previous two, can be simplified to:

$$\psi'' = \psi'\left(e^{\lambda}u\left(\psi^2 + \frac{\Lambda}{2}\psi^4\right) - \frac{e^{\lambda}+1}{u}\right) + \psi e^{\lambda}\left(1 + \Lambda\psi^2 - \omega^2 e^{-\nu}\right)$$

4.3 Boundary Conditions

The first five boundary conditions to solve for a boson star are:

$$\begin{aligned}\psi(0) &= \psi_c,\\ \psi(0) &= 0,\\ \lambda(0) &= 0,\\ \lim_{r\to\infty}\psi(r) &= 0, \text{and}\\ \lim_{r\to\infty}\nu(r) &= -\lim_{r\to\infty}\lambda(r).\end{aligned}$$

The final boundary condition may be given by:

$$\nu(0) = 0.$$

4.3.1 Eigenfrequency

The above condition on ν has been shown to lead to regular solutions. However, it is inconsistent with the fifth boundary condition. Redefining ω and ν solves this inconsistency as they only occur in the

equations of motion as the term $\omega e^{-\nu}$. Thus the solution remains invariant for all non zero k such that

$$\omega \to k\omega$$
$$e^{-\nu} \to e^{-\nu-\ln(k)}.$$

If a solution satisfies all the boundary conditions, except the fifth one. One can find the constant k such that

$$k = \lim_{r\to\infty} e^{-\nu(r)-\lambda(r)}$$

and a new initial condition for ν

$$\nu(0) = \ln(k),$$

that ensures all the boundary conditions are satisfied. The new eigenvalue to the problem will be related to the old one by the relation:

$$\omega_{red} = k\omega$$

As the rescaling cannot be done when $\omega = 0$, the above subsection indicates why a real scalar field does not give rise to boson stars.

The eigenvalue ω determines the number of nodes in the solution. The ground state of a soliton solution correspond to a node less solution. These are known to be stable [104]. As ω increases, the solution has an increasing number of nodes. Furthermore, it appears that if the numerical integration is carried on long enough there always exists a point at which the change in either ν, λ, ψ, or ψ' is below the tolerance level set in the integrator. This rapidly leads to a divergence in ψ towards $\pm\infty$.

We will use this fact to a node-less solution for $\psi(r)$. There exists an interval $\omega_{lo} < \omega < \omega_{hi}$ such that $\lim_{r\to\infty}\psi(r) = \infty$ for ω_{lo} and $\lim_{r\to\infty}\psi(r) = -\infty$ for ω_{hi}. The existence of ω_{lo} is guaranteed, since $\omega = 0$, is a value that leads to the divergence of ψ before it goes through a cusp. Determining the value of ω_{hi} is more involved, since ψ may have crossed more than once before diverging. This leads to the the risk of finding nodal solutions, especially if the eigenvalues between the zero node solution and the rest are close to each other. This is especially true for high values of ϕ_c. In many cases, the algorithm is able to find the value of ω_{hi} that leads to a negative divergence after ψ goes through a single cusp. See figure 4.1 for a graphical illustration.

Once reasonable estimates for the interval $\omega_{lo} < \omega < \omega_{hi}$, has been provided, the algorithm refines this interval using a bisection method until the boundary condition $lim_{r\to\infty}\psi(r) = 0$ is within a given tolerance and the $\omega_{lo} < \omega < \omega_{hi}$ is less than 10^{-10}. If a solution is found, but the latter condition is met but not the former, the algorithm estimates a new interval with an ω_{hi} less than the previous best estimate.

The boson star mass satisfies [98]

$$M = 4\pi\int_0^\infty \rho r^2 dr$$

The mass aspect function may be defined as:

$$\frac{M(u)}{m} = \frac{u}{2}\left(1 - e^{-2\lambda}\right),$$

taking advantage of the fact that this would reach M asymptotically. This mass aspect function corresponds to the ADM mass contained within a sphere of radius u.

4.3.2 Compactification

As all practical domains on a computer are finite in extent, it is difficult to enforce the boundary conditions at spatial infinity. The use of a compactified radial coordinate alleviates the numerical inaccuracies that occur when using a finite grid. We will use the same transformation introduced in [107]:

$$\xi = \frac{u}{1+u}$$

where $0 \leq \xi \leq 1$. This results in the following substitutions

$$\begin{aligned} u &= \frac{\xi}{1-\xi}, \\ \frac{d}{du} &= (1-\xi)^2 \frac{d}{d\xi} \\ \frac{d^2}{du^2} &= (1-\xi)^4 \frac{d^2}{d\xi^2} + 2(1-\xi)^3 \frac{d}{d\xi} \end{aligned}$$

In the case where there is no self-interaction, we were able to obtain results [1] consistent with those of [108] and [109].

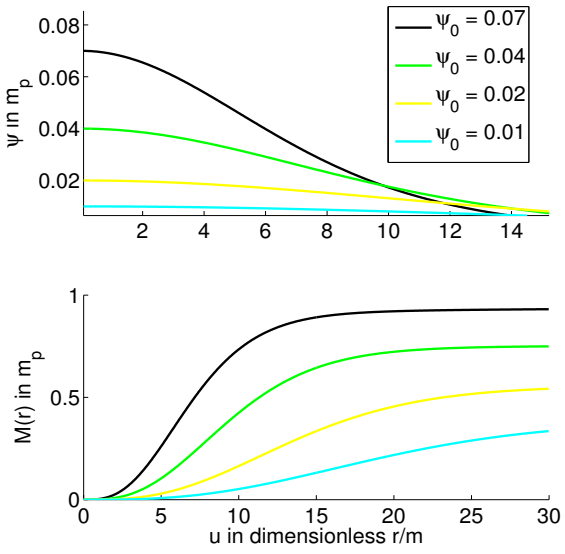

Figure 4.2: Boson star solutions for scalar field potential with no self interaction

[1] The programming code used to produce the results in this chapter as well as subsequent chapters can be made available on request by contacting the mailing the author: N.Mohapi@gmail.com.

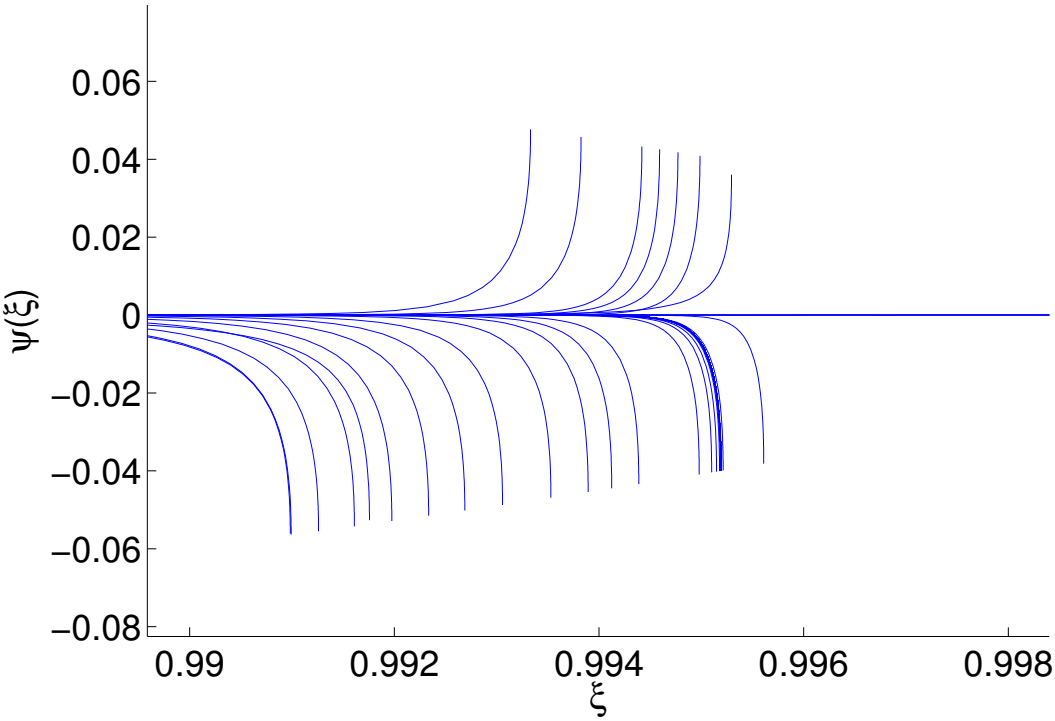

Figure 4.1: An illustration of how the solution searches for the unimodal solution in compactified units. A similar algorithm will be employed in the more complex case with the Higgs field.

4.4 Scalar-Tensor Theory Boson Stars

Boson star solutions can also be shown to exist in scalar-tensor theories [110], [111] , [112], [113], [114], [105], [115]. The simplest extension is to consider a non-minimally coupled scalar field action:

$$S = \frac{1}{16\pi G*}\int [\phi R - \frac{\omega(\phi)}{\phi}\nabla^a\phi\nabla_a\phi]\sqrt{-g} + L_m\sqrt{-g}\ d^4x$$

where

$$L_m = \frac{1}{2}\left(g^{ab}\nabla_a\bar{\varphi}\nabla_b\varphi\right) - V(|\varphi|^2),$$

in which φ is the boson star scalar field. The mass of the boson star in the above case has been shown to differ from the GR value by a few percentage or less for $\omega \geq 6$ in [116]. This result holds even when $\omega = \omega(\varphi)$ [110]. However, there are interesting effects that occur with boson stars in scalar-tensor theories that do not exist in GR, such as memory effects [117] which occurs when the scalar field in a body evolves too slowly to match the cosmological value. This could lead to a body "remembering" a different gravitational constant. A related phenomenon is spontaneous scalarization [118], [105] in which very compact bodies hold a scalar charge or high gradients of the scalar field despite being in an environment in which the effect of the scalar field in negligible.

The structure of a boson stars depends on the cosmological evolution of the scalar field. If the time it takes the boson star scalar field to evolve so as to match the asymptotic scalar field value is larger than the time evolution of the universe, then the star "conserves" the asymptotic value of the field at formation [98].

The Einstein frame scalar field inside a boson stars becomes inhomogeneous once a star's mass increases beyond some critical value (scalarisation). Below this value, the scalar is nearly constant throughout the star. It is necessary that the scalar field satisfies the observational constraints on the PPN parameters γ and β and the inequality

$$\frac{2\phi_B}{(2\omega+3)^2}\frac{d\omega}{d\phi} < -4.$$

The degree of scalarization of an object can be measured by the quantity:

$$Q_s = \lim_{r\to\infty} r^2 \frac{d\phi}{dr},$$

in the Jordan frame.

The effects of non-minimal coupling become apparent with the addition of a second scalar field which couples non-minimally to the Ricci scalar. Often, this additional scalar field can be used to model quintessence if it is non minimally coupled. We will look at the case in which the second scalar field is the Higgs. While the quintessence like scalar fields in the previous section have yet to be discovered, there is accumulating evidence in favour of the existence of the Higgs. Such a theory has been investigated by various authors [119], [120] , [121]. The recent preprint by [121], shows the possibility of soliton like solutions purely form a non-minimally coupled complex Higgs. If we treat the Higgs as a real scalar field and introduce an additional complex scalar field

$$\phi = \Phi(r)e^{-i\omega t}$$

The action for this model takes the following form:

$$S = \int \left(1+\frac{\xi}{m_p^2}H^2\right)\frac{R}{2\kappa} - \frac{1}{2}\nabla_\mu H \nabla^\mu H - V(H) - \frac{1}{2}\nabla_\mu \bar{\phi}\nabla^\mu\phi - U(\phi,H)\ d^4x,$$

where H is the Higgs. In which the potential for the two fields are given by:

$$V(H) = \frac{\lambda_{SM}}{4}\left(H^2-v^2\right)^2, \text{and}$$
$$U(\phi,H) = \frac{\mu_1}{4}H^2|\phi|^2 + \frac{\mu_2}{4}|\phi|^4$$

The above choice of potentials is not arbitrary. The potential for the Higgs has to be a "mexican hat" shape, so that one of the attractors is the vev. The mass term in the potential for the scalar field is determined by the interaction of the scalar field with the Higgs. The self interaction potential is there

The Higgs potential must have the vev as an attractor point, and the mass term for the scalar field is determined through interacting with the Higgs. The interaction of the Higgs with the scalar field may influence these attractor points. The exact influence can be determined from the stationary points of the potential.

The following field equations result

$$\left(1+\frac{\xi}{m_p^2}H^2\right)G_{\mu\nu} = T^{(\xi)}_{\mu\nu} + \kappa T^{(\phi)}_{\mu\nu} + \kappa T^{(H)}_{\mu\nu}.$$

The stress energy tensors for the scalar fields and as a result of non-minimal coupling are given by:

$$
\begin{aligned}
T^{(\psi)}_{\mu\nu} &= \frac{\kappa}{2}\left[\nabla_a\bar{\phi}\nabla_b\phi + \nabla_a\phi\nabla_b\bar{\phi} - g_{ab}\left(g^{cd}\nabla_v\bar{\phi}\nabla_d\phi + U\left(\phi,H\right)\right)\right], \\
T^{(H)}_{\mu\nu} &= \nabla_\mu H\nabla_\nu H - \frac{1}{2}g_{\mu\nu}\left(\nabla_\mu H\nabla^\mu H + V(H)\right), \text{and} \\
T^{(\xi)}_{\mu\nu} &= \frac{2\xi}{m_{pl}^2}\nabla_\mu H\nabla_\nu H + \frac{2\xi H}{m_{pl}^2}\nabla_\mu\nabla_\nu H - g_{\mu\nu}\left(\frac{2\xi}{m_{pl}^2}g^{\alpha\lambda}\nabla_\lambda H\nabla_\alpha H + \frac{2\xi H}{m_{pl}^2}\nabla^\lambda\nabla_\lambda H\right).
\end{aligned}
$$

We can thus derive the following wave equations:

$$
\begin{aligned}
\Box H &= -\frac{2\xi H}{m_{pl}^2}\frac{R}{2\kappa} - \frac{\partial(V_H + U_{\phi,H})}{\partial H}, \text{ and} \\
\Box\phi &= -\frac{\partial U_\phi}{\partial|\phi|^2}\phi.
\end{aligned}
$$

From the above we can explicitly write out the attractors for the boson star:

$$
\phi_{attr} = 0,\ \pm\sqrt{\frac{\mu_1}{\mu_2}H^2}
$$

A zero attractor is compatible with a boson star. We will assume that the scalar field approaches its attractor faster than the Higgs reaches its own attractor. The attractors for the Higgs are then

$$
H_{attr} = 0, \pm\sqrt{v^2 - \frac{2\xi R}{m_{pl}\kappa}}
$$

We can immediately note the presence of the non-minimal coupling term ξ and the interaction with the boson star scalar field, may result in the formation of Higgs monopoles. That is, for a significantly compact object, the Higgs is only attracted towards its vev outside the object. This is reminiscent of the phenomenon of scalarization in scalar tensor theories. We use the term monopoles in the same sense as [120]. If we use the following adimensionalising scheme

$$
\begin{aligned}
H &= m_{pl}\tilde{v}h \\
&= m_{pl}\tilde{v}\left(1+\chi\right) \\
\psi &= m_{pl}\phi \\
v &= Vm_{pl}
\end{aligned}
$$

and let the line element be Schwarzschild. It is interesting to first consider the case $\omega = 0$, which corresponds to a real scalar field for ϕ. In GR, varying the eigenvalue ω was sufficient to find solutions. In a scalar-tensor theory of gravity with the Brout-Englert-Higgs (BEH) field as the scalar-tensor of gravity, the parameters ξ, λ_{SM}, μ, and μ_2 could have an effect of the formation of a boson star without the necessity of a complex scalar field.

4.4.1 Parameter Space Search

It is possible that among the six dimensional space of the parameters ξ, λ_{SM}, μ_1, ϕ_c, h_c and μ_2 a solution with $\omega = 0$. However, it is not obvious what range of parameters, if any, may give rise to a solution. A numerical parameter search, with

$$\begin{aligned}
\xi &\in \left\{0, 3.16 \times 10^{-3}, 1\right\} \\
\lambda_{SM} &\in \left\{10^{-5}, 3.16 \times 10^{-3}, 1, 3.16 \times 10^{2}\right\} \\
\mu_1 &\in \left\{10^{-5}, 3.16 \times 10^{-3}, 1, 3.16 \times 10^{2}, 10^{5}\right\} \\
\mu_2 &\in \left\{10^{-5}, 3.16 \times 10^{-3}, 1, 3.16 \times 10^{2}, 10^{5}\right\} \\
h_c &\in \{0.50, 0.61, 0.72, 0.83, 0.94, 1.06, 1.17, 1.28, 1.39, 1.50\} \\
\phi_c &\in \{0, 0.11, 0.22, 0.33, 0.44, 0.56, 0.67, 0.78, 0.89, 1\}
\end{aligned}$$

4.4.2 Boundary Conditions

At the centre of our coordinate system where $r = 0$, we require the following conditions to hold:

$$\nu(0) = 0, \tag{4.1}$$
$$\nu(0) = 0, \tag{4.2}$$
$$\phi'(0) = 0, \text{ and} \tag{4.3}$$
$$\chi'(0) = 0 \tag{4.4}$$

as a regularity conditions. We will further suppose the values of h and ϕ should be given at the center:

$$h(0) = h_c, \tag{4.5}$$
$$\phi(0) = \phi_c. \tag{4.6}$$

As in the GR case, to recover an asymptotically flat solution we will need to impose conditions at spatial infinity, namely:

$$\lim_{r \to \infty} \nu(r) = -\lambda(r) \tag{4.7}$$

4.4.3 Results

Our criteria for determining whether we may have a possible solution is if the following condition are met

$$\lim_{r \to \infty} h(r) = 1, \text{ and} \tag{4.8}$$
$$\lim_{r \to \infty} \phi(r) = 0. \tag{4.9}$$

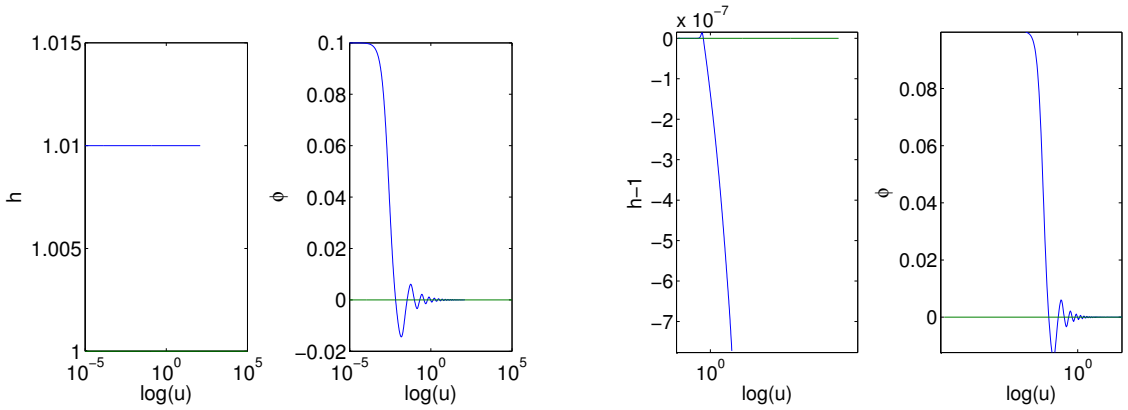

Figure 4.3: A boson star solution would settle the Higgs back to its vev ($h = 1$), if it starts of with a value distinct from it. The graph on the right is for $h_c = 1.01$ and the one for and the one on the left has $h_c = 1$. Neither of the above two figures represent a soliton solution. The following parameters values were used: $\phi_c = 10^{-1}$, $\mu_1 = 10^{-5}$, $\mu_2 = -10^8$, $\xi = 10^{-5}$, and $\lambda_{SM} = 10^8$.

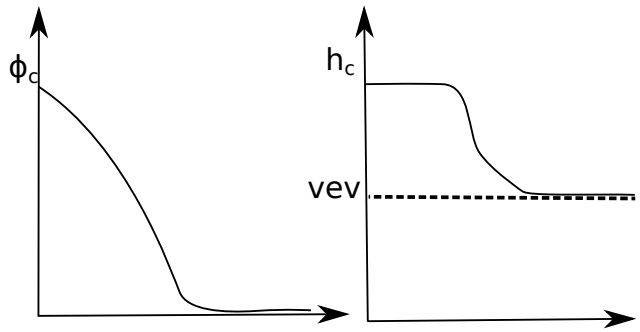

Figure 4.4: An illustration of the hypothesised boson star monopole.

Numerically, this meant checking for candidates within some tolerance of the asymptotic value. We took this tolerance to be 10^{-4}. None of the investigated values in the parameters space had such behaviour.

It is possible that solutions may indeed exist, but the proposed values in the parameter space where not ideal.

4.4.4 Summary

This short chapter introduced boson star solutions. In particular, we demonstrated how boson star solutions are found in GR. It is possible to form boson stars in scalar-tensor theories. Much like in GR, these boson stars are formed from complex scalar fields, with the Brans-Dicke field merely extend GR. We did not seek to reproduce these results, instead we numerically investigated the possibility of producing static solutions using a real scalar field, in action that has been shown to produce particle like distributions of the Higgs around compact objects.

A parameter space search on the coupling constants $\Lambda_{SM}, \mu_1, mu_2, \xi$ and various possible central values of the Higgs and the scalar field, did not yield any boson star like solutions. Despite evidence of what appeared to be a regular multi-modal solutions of the scalar field, the Higgs field always diverged. Our

investigations suggests that the use of a complex scalar field might be warranted, but the time limitations of the thesis prevented such an investigation being undertaken.

Chapter 5

Galactic Dynamics

5.1 Introduction

Galaxies are catalogued by shape, brightness, age, and mass distribution. A well known classification scheme by Edwin Hubble[122] categorises galaxies as either elliptical, normal spiral, barred spiral, or irregular galaxies. These categories are further subdivided according to the nature of the galaxy's bulge, spiral arms and degree of flattening of the galaxies, as Figure 5.1 shows. Elliptical galaxies are represented by the types E0-E7. The number represents the ellipticity of the galaxy with E0 almost spherical and E7 very elliptical. The evolutionary sequence of galaxies does not proceeded from left to right of the figure. Elliptic galaxies, for instance, form from the merger of spiral galaxies [123]. Spiral galaxies are divided into two branches: regular spirals Sa-Sc and barred spirals SBa-SBc. The last letter in the classification scheme of spiral galaxies indicates how tightly wound the spiral arms are around the galactic core. Galaxies that do not fit any of the previous categories, irregular or lenticular galaxies, can be broadly classified as whether they are barred, BIrr, or not, Irr. The galactic dynamics of the three spiral galaxies UGC2259, NGC2403, and NGC2841 will form the basis of this chapter. UGC2259 and NGC2403 are classified as spirals of type Sc and NGC2841 is a type Sb.

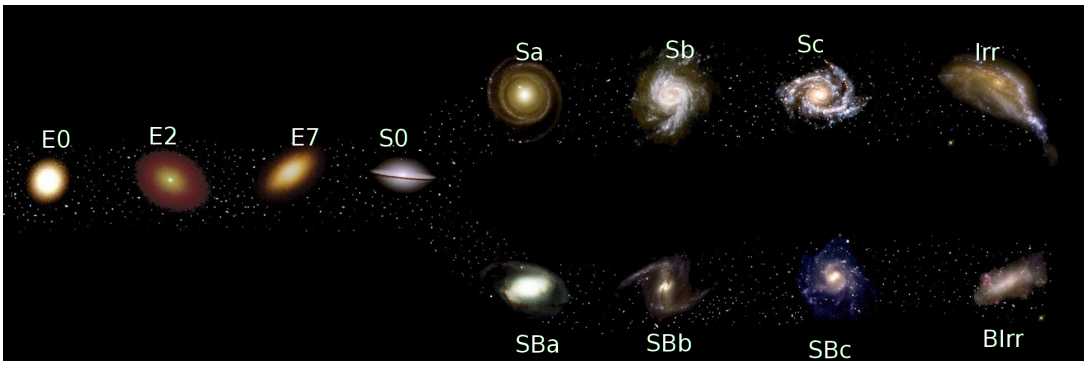

Figure 5.1: The Hubble Classification Scheme. Adapted from [124].

The velocities of stars in galaxies are directly measured from the Doppler shifts of the absorption lines of nuclei that make up the star. In addition, the absorption lines of intergalactic gas also allows us to deduce the kinematics of galaxies. Stars in spiral galaxies are have regular circular orbits around

the galactic center. In contrast to spiral galaxies, the motion of stars in elliptic galaxies is not regular [125]. It is possible to create a graph of the rotational velocities of the stars, or the intergalactic gas as a function of distance from the galactic center as a result of this regularity in the motion. This graph is called a rotation curve. Rotation curves are used to infer the evolutionary history and mass distributions of galaxies. Quite broadly, rotation curves can be classified into four general types [126] as illustrated in figure 5.2.

All the rotation curves observed so far begin with a steep increase in velocity, in line with the expectation that the visible mass increases with radius. Naively, evidence of a Keplerian decay $V \propto \frac{1}{R}$ would be expected far from a spiral galaxy's center, however this has not been observed. In type I rotation curves, the velocity increases monotonically to the extent of the observations, with no discernible maximum. In type II rotation curves, the velocity reaches a maximum and remains flat and steadily within $10-15\%$ of the maximum velocity. In type III curves the velocity decreases after having reached its maximum extent. The decrease in the velocity in type III curves does not follow a Keplerian profile. No rotation curve observed so far has been show to exhibit a Keplerian fall off [125]. Type IV curves display features that are combinations of the first three types of rotation curves.

This chapter will mainly focus on type II curves. These are the types of curves that have been observed in a large number of spiral galaxies. The rotation curves of spiral galaxies are particularly useful when testing toy models of galaxies. Although these models do not capture all the features of spiral galaxies, the essential features of rotation curves can be reproduced. The simplest models only have one component. Although, they can reproduce flat rotation curves, they are unsuitable for investigating non-universally coupled gravitational theories which require at least two components. Bulge-halo or disk-halo models in which the bulge or disk consists of baryonic matter are more suited to our investigations. However, a more realistic model with a bulge, disk and halo in which the contributions from each component can be analysed will be more suited to our investigations.

In our galaxy model, the halo component is made up of dark matter. Theories that modify gravity at galactic scales have been proposed to account for the rotation cures of spiral galaxies without assuming the existence of this invisible mass, dubbed dark matter. One such theory is Modified Newtonian Dynamics(MOND), which has been extensively applied to galactic rotation curves [127, 128]. This includes the rotation curves of the galaxies in this chapter [129, 130]. Because the theory offers an alternative interpretation to rotation curve data, it is briefly reviewed in section 5.5.

Despite the possibility of MOND, there are reasons to assume that the majority of matter in the universe is invisible, non-baryonic and weakly interacting. In principle, it is not obvious what properties dark matter would share with baryonic matter. The known properties of matter arise out of the various interactions of fundamental fields. *A priori*, dark matter may couple non-universally fundamental fields.

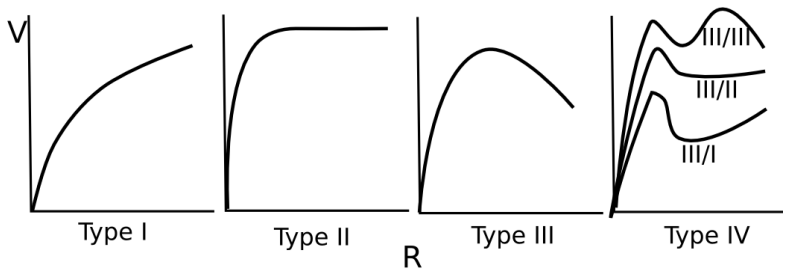

Figure 5.2: Different types rotation curve shapes

Non-universally coupled chameleon scalar-tensor theories are thus ideal in probing the signatures of a violation of the EP that may arise from inclusion of dark matter on galactic scales. As non-universally coupled chameleon models have been used to build cosmological models [15], the overall consistency of these models can be tested for by demanding they satisfy the constraints on the couplings on solar system, galactic and cosmological scales.

5.2 The Data

Rotation curves are inferred from the emission lines of intergalactic gas. The gas is composed of neutral and ionised atoms of various elements and charged particles. Typically, rotation curves have been built from the emission lines of HI and Hα transitions [131]. The data used in this thesis, is exclusively from Hα data. The used in this thesis algorithm (see Appendix B.1.2) failed to converge to a minimum χ^2 value for a combined HI and Hα dataset. This is not an unusual occurrence in fits to rotation curves, as even when searching a four dimensional parameter space optimal χ^2 fits cannot be found [130]. For comparison, figures 5.3 and 5.4 show data from both transitions, HI and Hα. For completeness, we discuss the role that each transition has in the estimation of rotation curves.

5.2.1 HI Rotation Curves

Neutral hydrogen (HI), is a component of the intergalactic medium. The bulk of the medium is made of dust. The environmental conditions of the medium allow for the observation of the hyperfine transition in hydrogen gas. In this transition hydrogen emits and absorbs radiation at the specific wavelength $\lambda = 21.11$cm. The HI line allows us to determine the galactic kinematics up to 3 or 4 times the radial extent of the visible disk of a spiral galaxy. HI rotation curves for the galaxies presented in the figures below, but not used in thesis, were based on 21 cm observations from the Westerbork Synthesis Radio Telescope (WSRT) [132]. The HI rotation curves for the galaxy NGC2841 was obtained from [133] respectively, and that of UGC2259 from [134]. More recent measurement and higher resolution maps of HI rotation curves for these galaxies exist in the literature [135], but these are not included in this thesis as the data to these was not readily accessible.

5.2.2 Hα Rotation Curves

The optical emission lines of Hα are better tracers of galactic dynamics in the inner regions of spiral galaxies as HI rotation curves are affected by beam smearing in these regions [136]. Therefore, the ideal rotation curve combines both HI and Hα data. The Hα rotation curve for the galaxies studies in this thesis are obtained from [137].

5.3 Empirical Density Profiles

5.3.1 Surface Brightness Profiles

The mass of a galaxy $M(R)$ contained within a radius of R is related to the rotational velocity $V(R)$

$$V(R)^2 = \frac{M(R)G}{R}.$$

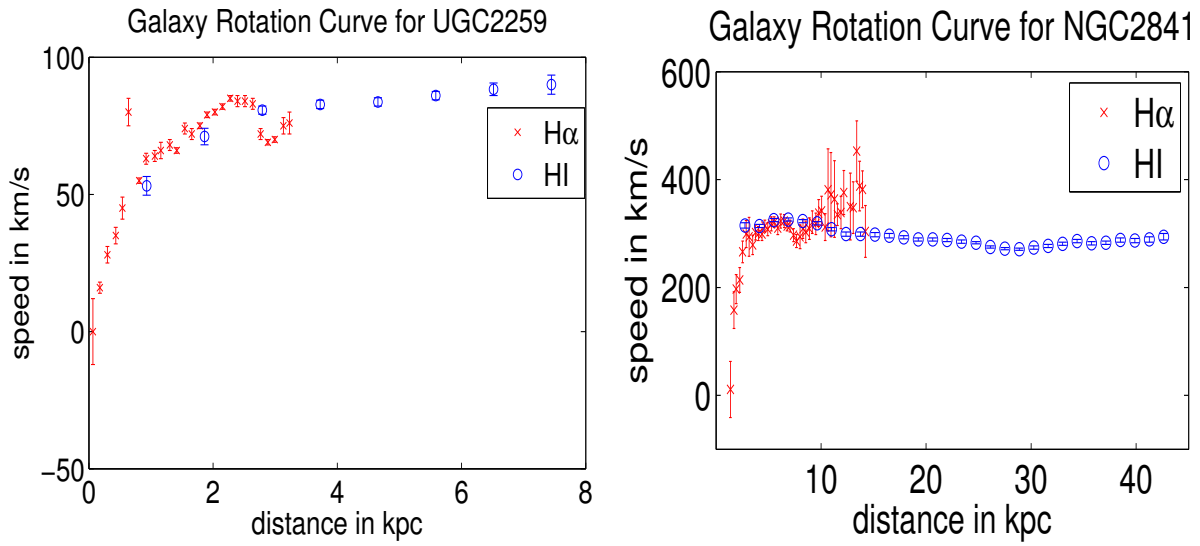

Figure 5.3: Integrated HI and Hα rotation curves. Hα has better resolution in the inner regions of galaxy UGC2259 and NGC2841

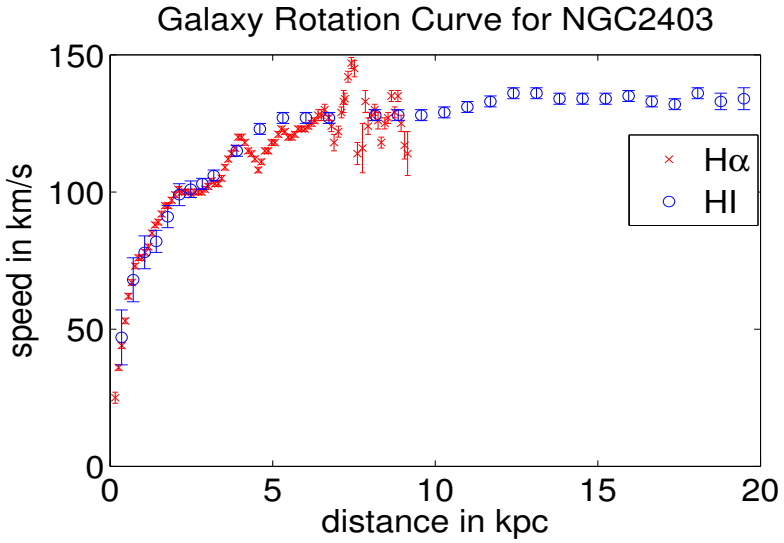

Figure 5.4: Integrated HI and Hα rotation curves for NGC2403

The mass distribution of a galaxy is also expected to be linked to its luminosity distribution

$$L(R) = \frac{M(R)}{\Upsilon^*}$$

where Υ^* is the mass to luminosity ratio and is often taken to be constant. The contributions of the disk and bulge components of spiral galaxies can be discerned in the luminosity profile of galaxies. In the central regions, where a bulge is sometimes visible the luminosity profile follows the law

$$\log I \propto R^{\frac{1}{4}} \tag{5.1}$$

and the disk luminosity has been observed to follow the distribution

$$I \propto e^{-\frac{R}{R_s}} \tag{5.2}$$

where r_s is a characteristic scale [138]. The figure 5.5 shows the surface brightness profiles of the galaxies studies in this thesis. It is common practice to fit a luminosity profile, and then deduce the baryonic matter distribution when fitting rotation curves, as we show when discussing MOND (see 5.5). However, the fits in this chapter will directly assume that the distribution of baryonic matter is distributed with profiles that are known to reproduce these luminosity profiles. These profiles are known to fit a large number of galaxies. It is from the analysis of a large number of luminosity profiles and rotation curves that the bulge is modelled using the Hernquist density profile, the disk by an Einasto density profile, and the galactic halo by the Nevarro-Frenk-White density profile.

5.4 Density Profiles

5.4.1 Isothermal Profile

The simplest density profile that reproduces a flat rotation curve is the isothermal density distribution. The profile does not distinguish between baryonic and dark matter mass distributions, as the total mass is simply directly proportional to the radius and the density distribution is inversely proportional to the square of the radius. The distribution is characterised by two parameters R and ρ_0. The exact form is given as

$$\rho(r) = \rho_0 \left(\frac{R}{r}\right)^2,$$

where ρ_0 is a density parameter and and R is the radius of the sphere.

The isothermal profile can be modified such that the singularity at $r = 0$ is removed and the flat behaviour of the rotational curve becomes apparent some fixed distance away from the galactic center, in accordance with observations:

$$\rho(r) = \rho_0 \left(1 + \left(\frac{r}{R_{DM}}\right)^2\right)^{-1}.$$

The modified isothermal profile does not integrate to a finite mass. Rotation curves typically begin flattening in the disks of spiral galaxies. As the modified isothermal profile does not distinguish between baryonic matter and dark matter it is unsuitable in the investigation of non-universal couplings.

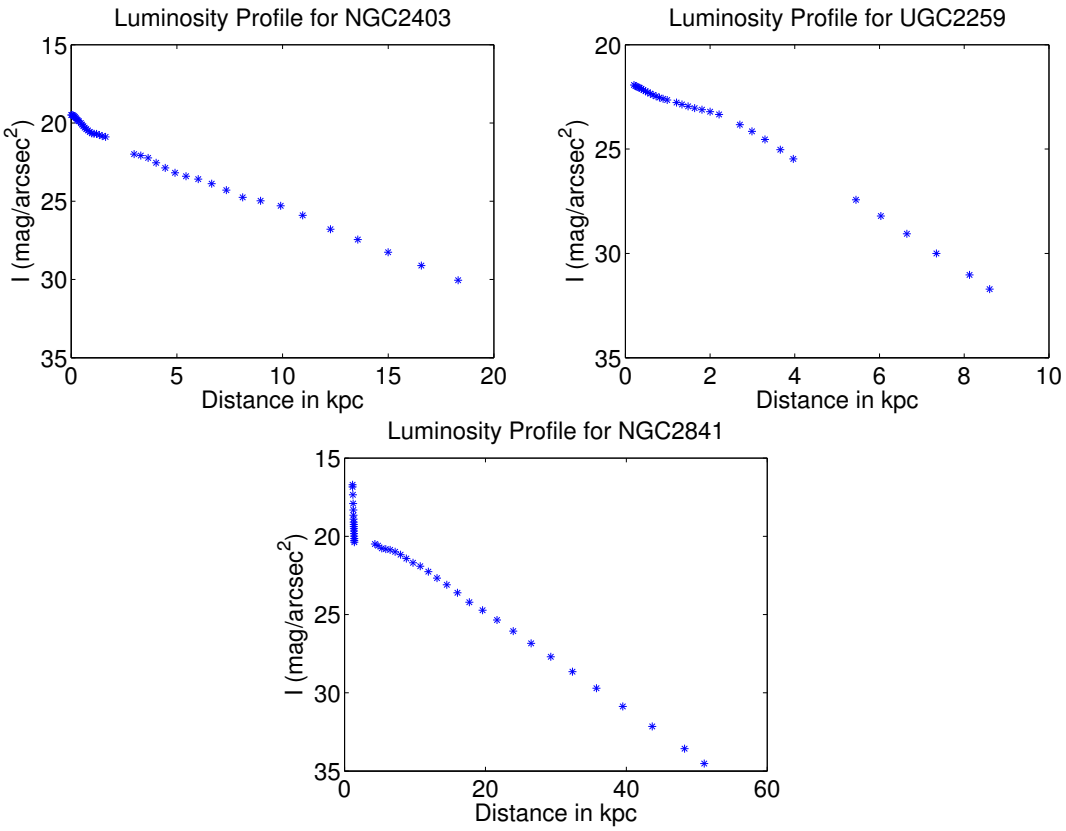

Figure 5.5: Luminosity profile of NGC2403, UGC2259 and NGC2403 from [138].

We will consider density profiles that encapsulate some of the known properties of spiral galaxies. It is known that spiral galaxies have a thin disk consisting of young stars, gas, and dust. They typically have a radius in the order of 10 kiloparsecs but the thickness of the disk is in the order of 100 parsecs. The individual stars in a spiral galaxy follow a circular orbit around the disk. These stars rotate with velocities in the order of 100 km/s. The angular momentum of the disk keep them from collapsing inwards. Some spiral galaxies have over-dense spiral arms in which the majority of new stars are born. Spiral galaxies also have a small spherical collection of stars at their center, referred to as the central bulge. In addition to the disk and bulge, spiral galaxies also contain small clusters of millions of stars (globular clusters) contained in a spherical halo around the galaxy. These will not be included in our models.

5.4.2 Hernquist Density Profile

The properties of the spiral galaxies can vary from one galaxy to another. In particular the surface brightness is not the same for all spiral galaxies. This has led to various ways of classifying spiral galaxies as either galaxies with high surface brightness (HSB) or galaxies with low surface brightness [139]. Such classifications determine the type of density profile appropriate for the spiral galaxy. For simplicity we will first model these galaxies with a spherical bulge and a dark matter halo.

The Hernquist model [140] uses what is known about the luminosity of galaxies to determine their density distribution. The profile is given by:

$$\rho(r) = \rho_0 \frac{1}{\frac{r}{R_0}\left(\frac{r}{R_0}+1\right)^3},$$

where ρ_0 is a proportionality constant and R_0 is a scaling factor which need not correspond to the physical scale length of the galaxy. Despite the singularity at $r = 0$, the model was motivated by empirical law

$$\log_{10}\left[\frac{I(R)}{I(R_e)}\right] = -3.331\left[\left(\frac{R}{R_e}\right)^{\frac{1}{4}} - 1\right]$$

where I is the luminosity as a function of radius R and R_e is the characteristic scale length. This law was discovered by de Vaucouleur [140]. The Hernquist model has the advantage of having simple analytical properties compared to other models based on de Vaucouleur's law. For instance, it is easy to write the cumulative mass distribution function for this profile:

$$M(r) = \frac{2\pi}{3}\rho_0 \frac{r^2}{(r+R_0)^2}.$$

5.4.3 Einasto Density Profile

Two dimensional surface brightness is typically modelled by the Sersic profile [141], [142]. This profile has the form:

$$I(R) = I_e e^{-b_n\left[\left(\frac{R}{R_e}^{\frac{1}{n}}\right)-1\right]},$$

where I_e is the intensity at the effective radius, R_e, that encloses half the total light. The constant b_n is related to the parameter n. When $n = 4$, we can recover de Vaucouleur's law. As the Sersic profile is

inherently a 2D profile it must be de-projected to 3D if we are to remain in spherical symmetry. Such a de-projection to a 3D density $n(r)$ is possible [143], [144], through the use of the Abel Integral for instance:

$$n(r) = -\frac{1}{\pi}\int_r^\infty \frac{1}{\sqrt{R^2 - r^2}}\frac{dI}{dR}\, dR.$$

The evaluation of the above integral is not readily analytically tractable [145]. Various asymptotic [146] and approximate solutions [147] exist. A notable disadvantage of a the Sersic profile is that its de-projections assume an infinite 3D extent, and thus make it difficult to model a galaxy with a truncation radius. De-projections of the Sersic profile are also not well behaved near the center. For these reasons we prefer the Einasto profile, which does not have these disadvantages. It has the form:

$$\rho(r) = \rho_0 e^{\frac{-2}{\alpha}((\frac{r}{R})^\alpha - 1)}.$$

The analytical expression for the mass profile associated with the Einasto profile is not readily derivable. However, the profile is already conveniently expressed in three dimensional spherical symmetry and determining the mass by numerical integration is not difficult.

5.4.4 Navarro-Frenk-White Density Profile

The Navarro-Frenk-White [148] (NFW) model is a generic profile for dark matter halos. It has the form:

$$\rho(r) = \rho_0 \frac{1}{\frac{r}{R_0}\left(\frac{r}{R_0}+1\right)^2}.$$

The mass profile of the NFW profile is as follows:

$$M(R) = 4\pi\rho_0^{(2)} R_2^3 \left(\ln\left(\frac{R}{R_2}+1\right) + \frac{1}{\frac{R}{R_2}+1} - 1\right),$$

where R_2 and $\rho^{(2)}$ are the scaling length for the dark matter profile and characteristic densities respectively.

5.5 Modified Newtonian Dynamics

5.5.1 Introduction

The flat rotation curves seen in spiral galaxies may be accounted for without assuming the existence of dark matter. The theory first introduced by Milgrom in [149], Modified Newtonian Dynamics (MOND), takes this approach by altering the acceleration experienced by objects distances far from the galactic center. Specifically, the asymptotic rotational velocity of spiral galaxies is related to the visible mass of the galaxy by the following relation:

$$V_\infty^4 = a_o G M,$$

known as Milgrom's law. In the above equation V_∞ is the asymptotic velocity of the galaxy, G is the gravitational constant, M is the total mass of the system and a_0 is an acceleration constant appearing in the modified dynamics. The gravitational acceleration is modified in the following way:

$$\mu\left(\frac{g}{a_0}\right)g = g_{MOND},$$

where g_{MOND} is the gravitational acceleration experienced by the body orbiting the galaxy at a radius,

$$g = G\frac{M(r)}{r^2}$$

is the Newtonian gravitational acceleration caused by the mass $M(r)$ of the galaxy, and $\mu\left(\frac{g}{a_0}\right)$ is an arbitrary function chosen such that for $\frac{a}{a_0} >> 1$, $\mu \approx 1$ and for $\frac{a}{a_0} << 1$, $\mu \approx \frac{a}{a_0}$. This leads to different dynamics in the small acceleration regime.

The rotational law in MOND is

$$\begin{aligned}\frac{V(r)^2}{r} &= g_{MOND} \\ &= \mu(x)\frac{GM_b(r)}{r^2}.\end{aligned}$$

Fits in MOND can have have up to three parameters, the mass to luminosity ratio $\Upsilon(r) = \frac{M_b(r)}{L(r)}$ which is constant, the acceleration parameter a_0, and the distance to the galaxy.

5.5.2 The Tully-Fischer relation

At large enough distances, when the baryonic matter does not increase, the gravitational acceleration is small. Due to the nature of μ, once the acceleration approaches a_0, it stays fixed there. A fixed acceleration and a fixed mass then results in an asymptotic value

$$V_\infty^4 = a_0 GM.$$

The above relation is known as Milgrom's law. Replacing the mass with the luminosity we derive the empirically Tully-Fisher relation

$$L \propto v^\alpha,$$

with $\alpha = 4$ exactly.

5.5.3 Galactic Rotation Curve Fits in MOND

The best fit MOND parameters for the HI rotation curves (these are from the same sources as those used in this thesis) of the galaxies UGC2259, NGC2403, and NGC2841 were estimated in [129]. The results are summarized in table 5.1. The results in the table are for only a handful of galaxies for which MOND has been applied. Despite good fits one can already see the difficulties with the theory. For instance, the value of a_0, when allowed to vary, seems to be significantly different for each galaxy. Indeed, a universal a_0 has been shown to be inconsistent with observations [150], [128]. Even with a varying a_0, the theory is overwhelmed with theoretical difficulties.

Galaxy	Υ^* only fit	Υ^* and a_0 fit		Υ^* and distance fit	
	Υ^*	a_0	Υ^*	Distance	Υ^*
UGC2259	2.14 ± 0.11	1.12 ± 0.39	2.28 ± 0.72	0.97 ± 0.22	2.26 ± 1.02
NGC2403	1.43 ± 0.02	1.39 ± 0.06	1.26 ± 0.05	1.09 ± 0.03	1.19 ± 0.06
$NGC2841_1$	14.49 ± 1.31	2.59 ± 0.12	8.01 ± 0.53	2.05 ± 0.08	3.97 ± 0.35

Table 5.1: We only show the best fits for the disk fit. Table adapted from [129]. Υ^* is reported in $\frac{M_\odot}{L_\odot}$, a_0 in $10^{-10}\ m/s^2$

Despite the success of MOND in explaining some rotation curves, such a modification has inconsistencies such as the violation of the conservation of momentum, and the failure of the centre of mass theorem [151]. An internally consistent model of MOND may be produced if Milgrom's law can be derived as a weak field limit of a relativistic theory. The most recent review [127] of theories that attempt to obtain MOND as a limit of a more general relativistic theory states that all attempts have been unsuccessful. However, it is still possible to derive Milgroms law in a classical theory from an action and a variational principle. With this approach, modifications which lead to Milgrom's law are either modifications to the equation of motion [152], modifications to the Poisson equation (Bekenstein-Milgrom MOND, [153]), or modifications to how the gravitational action is written as a function of the potential (QUMOND, [154]). Actual fits to rotation curve data cannot differentiate between these three approaches [155], or provide evidence for a specific form of μ.

5.6 Rotation Curves in Scalar-tensor Theories

Often, cosmological models are ruled out by cosmological constraints, solar system constraints or both. The studies in [156], and [77], show that the inverse power potential $V = \frac{\Lambda^{4+\alpha}}{m_{pl}^4 \phi^\alpha}$ cannot be compatible with both solar system constraints and cosmological constraints.

For theories that survive these constraints, novel signatures may occur on galactic scales. Such as an increase in luminosity due to the contribution of the fifth force to gravitation [87].In [157], it has also been shown that in the presence of a screened galaxy, stellar structure is affected. [158] shows that a violation of the EP occurs even in universally coupled chameleon models as screened and unscreened objects may fall at different rates.

In this chapter, we do not prescribe a specific potential to the scalar field. Instead, we have a completely emergent phenomenon in which non-universal couplings create a density dependent effective potential. This potential mimics chameleon behaviour in regions of high baryonic density as illustrated in chapter 3 and a runaway potential in regions where dark matter dominates. Such a chameleon model could still be compatible with galactic and solar system constraints.

5.6.1 Units and scales

The constants c and $\hbar$ are set equal to unity for computational convenience. It is therefore natural, to further set the Planck mass, M_P equal to unity to make use of the relation

$$8\pi G = c\hbar M_{PL}^{-2}.$$

These are called reduced Planck units. Expressed in conventional units, the length and time scale are as follows

$$L_{scale} = 8.07 \times 10^{-35}\text{m}, \quad T_{scale} = 2.71 \times 10^{-43}\text{s},$$

with

$$M_{PL} = 4.3415 \times 10^{-9}\text{kg}.$$

This length scale is unsuitable for simulations on astrophysical scales, where the distances and time intervals under consideration are many orders of magnitudes higher than these characteristic scales. For numerical convenience we will work with an adimensional scheme in which we will adopt $c = G = 1$, and $L_{scale} = 1$ kpc $= 3.086 \times 10^{19}$ m is the length scale that will be used. This is the results in the characteristic time scale

$$T_{scale} = \frac{L_{scale}}{c} = 1.0293 \times 10^{12} s \approx 3.2 \times 10^{4} \text{ years},$$

and mass scale

$$M_{scale} = \frac{L_{scale}^3}{G T_{scale}^2} = 4.156 \times 10^{46}\text{kg} \approx 2 \times 10^{16} M_{\odot}.$$

For comparisons sake we note that the apparent mass of the Milky Way is approximately 10^{10} $M_{\odot}$. Density and pressure are then scaled as follows:

$$[\rho] = \frac{M_{scale}}{L_{scale}^3} \approx 1.4141 * 10^{-12} \frac{\text{kg}}{\text{m}^3} \text{ and,}$$
$$[p] = \left[\rho c^2\right] = \frac{M_{scale}}{L_{scale} T_{scale}^2} \approx 1.2711 \times 10^{3}\text{Pa}.$$

The scalar field ϕ, can be written in dimensionless form in the Einstein frame action

$$S = \int \frac{1}{16\pi G}[R - 2g^{\mu\nu}\partial_\mu\phi\partial_\nu\phi]\sqrt{-g}\ d^4x + S_{awe}(\psi_{awe}, A_{awe}^2(\phi)g_{\mu\nu}) + S_m(\psi_m, A_m^2(\phi)g_{\mu\nu}),$$

as the field equations imply

$$\left[\phi'^2\right] = \left[8\pi\frac{G}{c^4}T^i\right] = \frac{L_{scale}^3}{M_{scale}T_{scale}^2}\frac{T_{scale}^4}{L_{scale}^4} \times \frac{M_{scale}}{L_{scale}T_{scale}^2}$$
$$\left[\phi'\right] = \frac{1}{L_{scale}}$$

ϕ has the dimensions of mass when the term $\frac{1}{\sqrt{8\pi G}}$ is absorbed into the definition of ϕ:

$$S = \int \left(\frac{R}{16\pi G} - 2g^{\mu\nu}\partial_\mu\phi\partial_\nu\phi\right)\sqrt{-g}\ d^4x + S_{awe}(\psi_{awe}, A_{awe}^2(\phi)g_{\mu\nu}) + S_m(\psi_m, A_m^2(\phi)g_{\mu\nu}).$$

The scalar field is thus associated with the units of the reduced Planck mass. Unless otherwise stated, the quantities in this thesis will be given using the scales discussed above.

5.6.2 Circular Velocities

In spherical symmetry, stars in a galaxy orbit the center with a circular velocity v_{circ}. This velocity can be determined from solving the geodesic equations. Suppose we have a generic metric of the form

$$ds^2 = -A(\tilde{r})d\tilde{t}^2 + B(\tilde{r})d\tilde{r}^2 + \tilde{r}^2 d\Omega^2,$$

the geodesic equation equation is

$$\frac{d^2x^\nu}{ds^2} + \Gamma^\mu_{\nu\sigma}\frac{dx^\nu}{ds}\frac{dx^\sigma}{ds} = 0.$$

When $\nu = 1$, we have

$$\frac{d^2\tilde{r}}{d\tau^2} + \frac{1}{2}\frac{A_{,\tilde{r}}}{B}\left(\frac{dt}{d\tau}\right)^2 + \frac{1}{2}\frac{B_{,\tilde{r}}}{B}\left(\frac{d\tilde{r}}{d\tau}\right)^2 - \frac{\tilde{r}}{B}\left(\frac{d\theta}{d\tau}\right)^2 - \frac{\tilde{r}}{B}\sin^2(\theta)\left(\frac{d\phi}{d\tau}\right)^2 = 0.$$

Without loss of generality, we consider circular orbits along the equatorial plane to describe galactic motion. This results in the following constraints:

$$\frac{d\tilde{r}}{d\tau} = 0,\ \frac{d^2\tilde{r}}{d\tau^2} = 0, \text{ and } \frac{d\phi}{d\tau} = 0.$$

We are thus left with the equation

$$\left(\frac{d\theta}{dt}\right)^2 = \frac{A_{,\tilde{r}}}{2\tilde{r}}.$$

In Schwarzschild co-ordinates we can make the following identifications

$$A(\tilde{r}) = \left(1 - \frac{2GM}{\tilde{r}}\right), \text{ and}$$
$$A(\tilde{r}) = B(\tilde{r})^{-1}.$$

The velocity is then

$$v^2_{circ}(\tilde{r}) = \tilde{r}^2\left(\frac{d\theta}{dt}\right)^2 = \frac{GM}{\tilde{r}},$$
$$v_{circ}(\tilde{r}) = \sqrt{\frac{GM}{\tilde{r}}}.$$

This is the same result derived from Newtonian theory. Once the mass, M has reached a limiting value the velocity will fall off at a rate proportional to $\frac{1}{\sqrt{r}}$. This is refereed to as Keplerian decay. This decay is not observed in spiral galaxies as the velocity remains flat.

In non-universally coupled chameleon theories, baryonic matter follows the geodesic of the metric

$$ds^2 = A^2_m(\phi)\left(e^\nu dt^2 + e^\lambda dr^2 + r^2 d\Omega^2\right).$$

By making the following identifications

$$\begin{aligned}\tilde{r} &= A_m(\phi(r))r,\\ B(\tilde{(r)}) &= \frac{e^{\lambda(r)}}{(1+r\alpha_m(\phi(r))\phi'(r))^2},\\ d\tilde{(t)} &= A_\infty dt,\\ A(\tilde{r}) &= \frac{A_m^2(\phi(r))}{A_\infty^2}e^{\nu(r)},\end{aligned}$$

where $A_\infty = A_m(\phi(r=\infty))$, we can write the circular velocity as

$$v_{circ}^2(\tilde{r}) = \tilde{r}^2\left(\frac{d\theta}{dt}\right)^2 = re^{\nu(r)}\frac{A_m^2(\phi(r))}{2A_\infty^2}\frac{\nu'(r)+2\alpha_m(\phi(r))\phi'(r)}{1+r\alpha_m(\phi(r))\phi'(r)}.$$

The above expression reduces to the GR equivalent when the scalar field is frozen ($\phi' = 0$).

5.6.3 Integration Scheme

The density profiles for our galaxy model do not have a finite extent. By truncating the density profile for the bulge, disk and halo, the field equations 3.2-3.7 can be solved as a boundary value problem. In our integration scheme we will constrain the bulge to region I. While the disk, if present will extend up to region II. The dark matter halo will extend up to region III. While region IV will be a vacuum. The first fluid will model the baryonic matter (regions I and II), which make up the bulge and the disk, while the second will model dark matter halo.

5.6.4 Boundary Conditions

To predict the rotational velocity of a galaxy, we must already have the quantities ν, ν', ϕ, ϕ' and A_m. We will use the same integration regions as shown by Figure 5.6.3 and we will assume the following

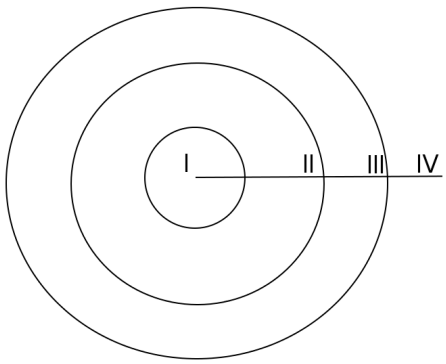

Figure 5.6: The regions used in the integration scheme

boundary conditions:

$$\begin{aligned}
\lambda(r=0) &= 0,\\
\lambda(r=r_3^-) &= \lambda(r=r_3^+),\\
\nu(r=r_3^-) &= \nu(r=r_3^+),\\
\phi(r=0) &= \phi_c,\\
\phi(r=r_3^-) &= \phi(r=r_3^+),\\
\phi'(r=0) &= 0,\\
\phi'(r=r_3^-) &= \phi'(r=r_3^+),\\
p_i(r=r_3^-) &= 0,\\
p_i(r=r_3^+) &= 0.
\end{aligned}$$

r_3 is the extent of the dark matter halo. To ensure that we have a Schwarazschild solution in the vacuum region, we have two choices for the last condition on ν:

$$\begin{aligned}
\nu(r=r_\infty) &= A^2(\phi_\infty)\ln(1-\frac{2GM}{r_\infty}), \text{ or}\\
\nu(r=r_2^+) &= -\lambda(r=r_2^+).
\end{aligned}$$

Without assuming a value ϕ_∞ we can assume that $A_m(\phi_\infty)\approx 1$. We cannot make any assumptions about the total mass of the system M, so the first condition cannot be implemented. Lastly, to integrate we assume values for k_1 and k_2 in addition to the density profiles ρ_1 and ρ_2, which are the Hernquist and NFW profiles.

5.6.5 χ^2 Fits

The best fit to a rotation curve corresponds to minimising the quantity

$$\chi^2\left(\rho_0^{(Bulge)},\rho_0^{(Disk)},\rho_0^{(Halo)},R_{Bulge},R_{Disk},R_{Halo},\phi_c,k_1,k_2\right)=\sum_i\frac{(v_{a,i}-v_{p,i})^2}{\sigma_i^2}.$$

We will minimise χ^2 with respect to each of the following parameters: the value of the scalar field at the center of the galaxy ϕ_c, the coupling constant to matter k_1, the coupling constant to dark matter k_2, the density parameters associated with the distribution of matter and the AWE sector $\rho_0^{(i)}$, and the radius of the bulge, R_{Bulge}, the disk R_{Disk}, and the galactic halo R_{Halo}. This is done using an implementation of the Nelder-Mead Simplex method (See Appendix B.1.2) in MATLAB called fminsearch. This method is a direct search method. It determines the minimum using function evaluations and not derivatives [159]. This method was preferred over a grid search and the Levenberg-Marquardt algorithm (which is a gradient search method) as it converges to a solution faster for our problem.

Estimation of Parameters

In all cases the algorithm returned a best fit for the χ^2 value within 10^{-2}. When comparing GR (in which the parameters $\phi_c=0, k_1=0$ and $k_2=0$) with the chameleon model. We will use the reduced χ^2

statistic, which takes into account the degrees of freedom of the problem. It is given by:

$$\chi^2_{red} = \frac{\chi^2}{N-n}$$

where N is the total number of data points under consideration, and n is the total number of parameters. For the GR model $n = 5$; while for the chameleon model $n = 8$. The number of observed data points N varies for different galaxies. A χ^2_{red} value close to 1 is considered optimal. A value less than this indicates over fitting.

A preliminary examination of the final χ^2_{red} values from the optimisation algorithm indicates that rotation curve fits are poorer in the chameleon model compared to GR. The best fit estimates of the common parameters in both GR and chameleon models are different as the tables below show. We will determine whether this difference is statistically significant in the subsequent sections.

Predictions in AWE must be reconcilable with known data. In [96] it was shown that dark energy observations from the SNe Ia dataset can be accounted for when the couplings k_2 is negative and k_1 is positive. In our analysis, the predictions of the model parameters from $NGC2841$ and $NGC2403$ are consistent with this result. However, in our later analysis, we show that these values are compatible with solar system observations.

The estimated parameters in both the chameleon model and GR, result in the rotation curves shown of figure 5.6.5 and 5.6.5.

The behaviour of a scalar field in cosmology within an object is governed by its density distribution. It may well be possible that the apparently close agreement in the predicted rotation curves occurs because the scalar field is screened. The screening of the scalar field, and other interesting effects such as the shell effects can be related to a single parameter: compactness. It is with this motivation that we present the estimated mass for the galaxies: As all the parameters have been predicted, we are in a position to investigate the scalar field profile. However, we will first investigate the constraints on our best fit parameters, especially the couplings. This may provide new insights into the models.

Constraints on Non-Universally Coupled Chameleon Models

This section uses Bayesian statistics to determine the statistical significance in the parameters predicted by the non-universally coupled chameleon model and what the estimated bounds are. If the data is sufficient to show at an acceptable level of uncertainty that the couplings cannot be identical or trivial, then galaxy rotation curves may provide unambiguous evidence for this models. We note that the posterior for the dataset, D of each galaxy, is given by:

$$P\left(\rho_0^{(Bulge)}, \rho_0^{(Disk)}, \rho_0^{(Halo)}, R_{Bulge}, R_{Disk}, R_{Halo}, \phi_c, k_1, k_2 \middle| D\right) \propto L \times Priors$$

where L is the likelihood as discussed in Appendix B.2.1.

	UGC2259	NGC2403	NGC2841
GR	26.7	12.7	1.6
AWE	32.2	13.2	1.7

Table 5.2: χ^2_{red} for bulge-disk fits to galactic rotation curves

	UGC2259	NGC2403	NGC2841
R_{Bulge}	2.1453	0.7301	5.4933
R_{Disk}	5.7382	3.1442	18.4246
R_{Halo}	12.4592	18.8507	118.4774
$\rho_0^{(Bulge)}$	1.4976×10^{-08}	7.5517×10^{-14}	1.1383×10^{-06}
$\rho_0^{(Disk)}$	8.3762×10^{-11}	4.7141×10^{-15}	2.472×10^{-14}
$\rho_0^{(Halo)}$	4.1856×10^{-08}	1.6288×10^{-07}	2.1274×10^{-6}

Table 5.3: Parameters estimated in GR. R is reported in kpc and ρ in $\frac{2\times10^16M_\odot}{kpc^3} \approx 1.41 \times 10^{-12} kg/m^3$

	UGC2259	NGC2403	NGC2841
R_{Bulge}	2.1537	8.5465	4.9758
R_{Disk}	5.1406	8.9534	13.2649
R_{Halo}	5.1093	8.9572	14.0828
$\rho_0^{(Bulge)}$	1.1107×10^{-08}	3.3502×10^{-09}	7.2675×10^{-07}
$\rho_0^{(Disk)}$	7.9594×10^{-11}	4.1928×10^{-15}	3.2304×10^{-13}
$\rho_0^{(Halo)}$	1.6297×10^{-07}	1.1935×10^{-7}	1.4739×10^{-06}
ϕ_c	8.8534×10^{-05}	4.9466×10^{-04}	7.8406×10^{-05}
k_1	-2.6558×10^{-04}	0.0041	1.9990×10^{-05}
k_2	-1.7768×10^{-04}	-4.7205×10^{-05}	-3.666×10^{-04}

Table 5.4: Parameters estimated in AWE for a galaxy with a disk and bulge. ϕ_c, k_1 and k_2 are dimensionless

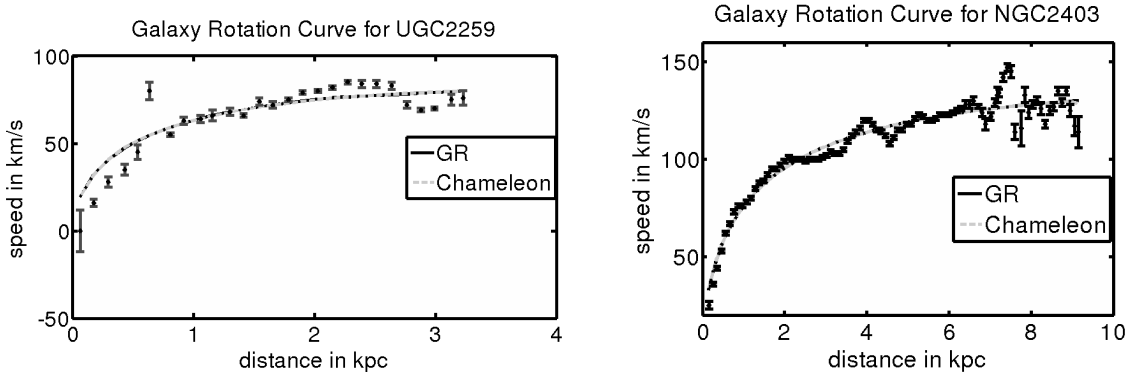

	UGC2259	NGC2403	NGC2841
GR	7.8412×10^{-09}	3.9541×10^{-14}	5.9604×10^{-07}
AWE	5.8155×10^{-09}	2.9916×10^{-14}	3.852×10^{-07}

Table 5.5: Estimated M_{Bulge} in 2 $\times 10^{16} M_\odot$

	UGC2259	NGC2403	NGC2841
GR	6.8202×10^{-08}	5.7409×10^{-07}	1.8772×10^{-06}
AWE	7.0588×10^{-08}	5.7416×10^{-07}	5.5022×10^{-06}

Table 5.6: Estimated M_{Disk} in 2 $\times 10^{16} M_\odot$

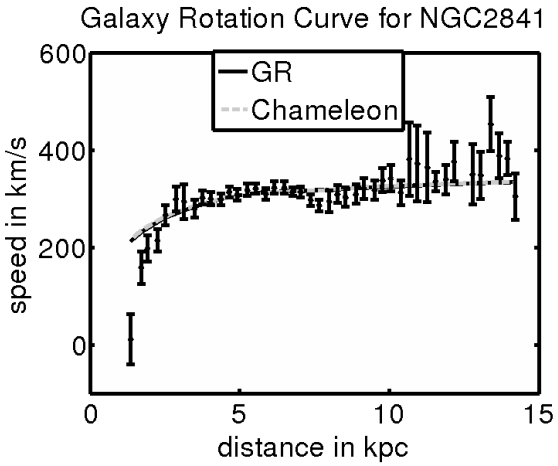

Figure 5.7: Comparison of AWE and GR fits for a disk and bulge model to rotation curves.

	UGC2259	NGC2403	NGC2841
GR	3.9321×10^{-07}	7.6644×10^{-11}	3.7852×10^{-10}
AWE	2.6243×10^{-08}	7.3139×10^{-12}	2.1899×10^{-09}

Table 5.7: Estimated M_{Halo} in 2 $\times 10^{16} M_{\odot}$

	UGC2259	NGC2403	NGC2841
Total Mass	-11.99 %	0.06 %	-31.10 %

Table 5.8: The difference in the estimated mass from the best fit parameters for a galaxy with a disk and a bulge for an AWE model compared to GR

It not obvious what distribution the priors have. In the face of no evidence to point otherwise, a natural guess is that they should be normally distributed around the best fit value and vary enough to include the GR predictions of the best fit parameters. Markov Chain Monte Carlo (MCMC) methods can be used produce samples from the posterior distribution. An implementation of the Metropolis Hastings algorithm in MATLAB, *mhsample*, was used to determine the distribution of each prior. To make sure that the samples converge to the correct stationary posterior we begin the algorithm at different starting points.

Both simple Gaussian distributions and mixed Gaussian distributions were fit to samples marginalised for k_1 and k_2. The mixed Gaussian distribution is suitable for modelling multi-modal data. This is a very real possibility with the data set under consideration. The possible multi-modal nature of the data becomes more apparent with smaller bin sizes in the histogram plots. Despite the different density distributions, the credible intervals each are fit well by either distribution. We will thus always use the simpler model unless a mixed normal distribution displays a far superior fit.

At the 99% level, as shown in table 5.9, either parameter may be zero when all the other parameters have been marginalised. The model will be indistinguishable from GR if both couplings could be zero simultaneously. The joint distribution of k_1 and k_2, provides a test for non-universal coupling in UGC2259 and NGC2841 galaxy rotation curve data. The preceding discussion was important in establishing the suitability of modelling the individual distributions of k_1 and k_2 with normal distributions. The advantage of this is that the joint distribution of both parameters is then easily modelled with a multivariate normal distribution. Because of this, we may use the result

$$\chi_2^2 = (x-\mu)' \Sigma^{-1} (x-\mu)$$
$$\chi_2^2 = \chi_{min}^2 + \Delta\chi_2^2,$$

where μ and Σ are the mean and covariance matrix of the joint distribution of k_1 k_2. It is then a simple matter finding the contours for the $\Delta\chi_2^2$ distribution. Data from the two galaxies UGC2259 and NGC2403 do not favour the chameleon model over GR at the 99% level. As the contours contain regions where the couplings may have the same value at every confidence level that we consider, we also fail to find evidence of non-universal coupling.

5.6.6 Scalar Field Profiles

We now have a realistic profile for the scalar field in a galaxy from galactic rotation fits. The graphs in Figure 5.12 show how the scalar field behaves in relation to the rotation curve of the galaxy. They show very little evidence of spontaneous scalarization of the field in the center of the galaxy. This is very likely due to the weak coupling of the scalar field to matter. A relationship exists between the

	UGC2259	NGC2403
k_1	$-2.6558^{+2.778}_{-2.5032} \times 10^{-4}$	$-2.0898^{+1.9438}_{-2.9722} \times 10^{-4}$
k_2	$-1.7768^{+1.6548}_{-1.6422} \times 10^{-4}$	$-4.7205^{+2.4305}_{-28.780} \times 10^{-05}$

Table 5.9: 95% credible regions for k_1 and k_2

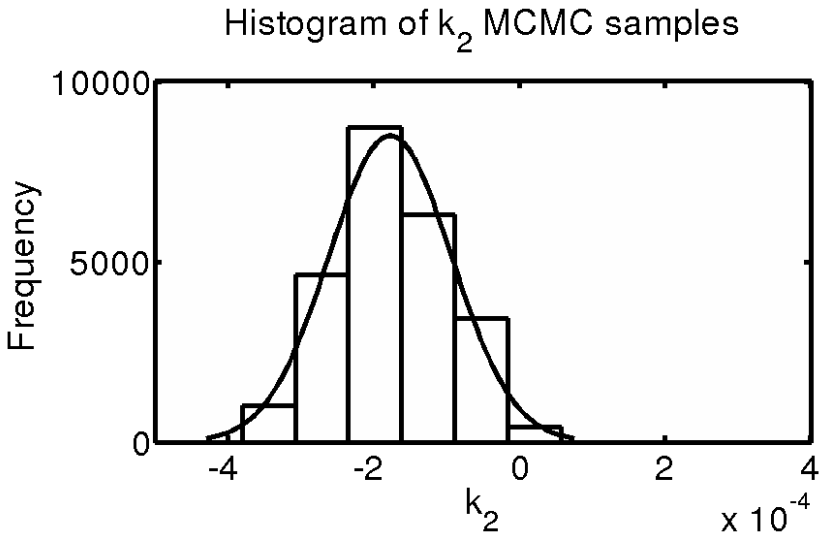

Figure 5.8: A plot of the histogram and the estimated density distribution from MCMC samples of k_2 for UGC2259

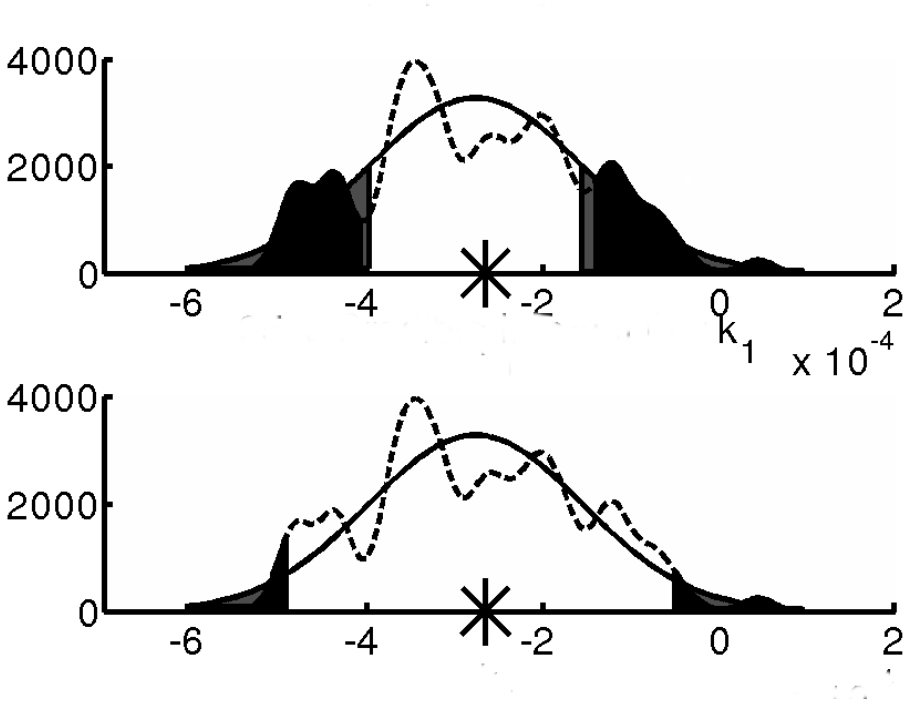

Figure 5.9: Credible intervals for k_1 from UGC2259 galaxy rotation curve data. The dotted plot with the dark areas is obtained using a mixture of Gaussian distributions. The other plot with the lighter areas is obtained from a simple Gaussian fit. The star on each axis shows where the best fit parameter values is.

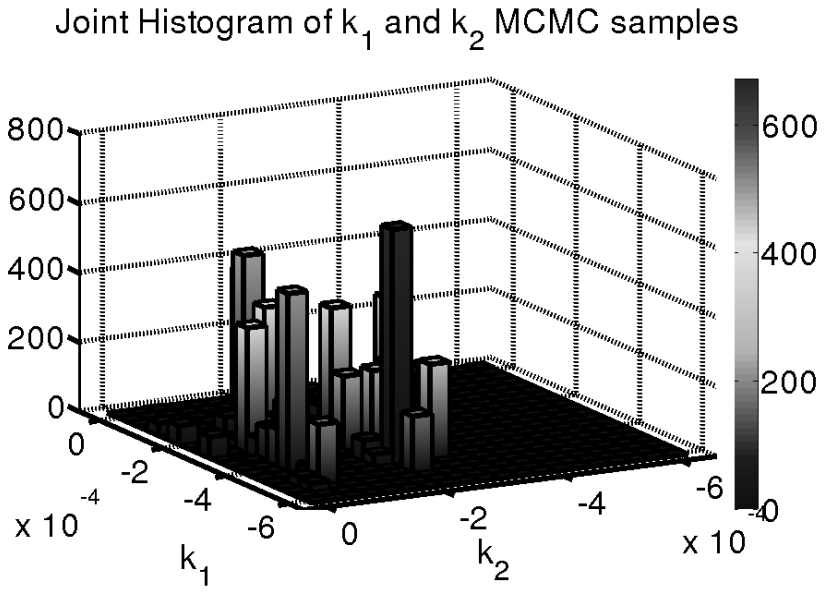

Figure 5.10: A plot of the 3D histogram from MCMC samples from which the joint density distribution of k_1 and k_2 is estimate for UGC2258

	UGC2259	NGC2403	NGC2841
k_1	$-2.6558^{+3.0288}_{-3.2542} \times 10^{-4}$	$-2.0898^{2.7158}_{-3.7442} \times 10^{-4}$	$1.9990^{+0.6207}_{-2.6110} \times 10^{-5}$
k_2	$-1.7768^{+2.1728}_{-2.1602} \times 10^{-4}$	$-4.7205^{+7.3305}_{-33.680} \times 10^{-4}$	$-3.6660^{+8.048}_{-4.3170} \times 10^{-4}$

Table 5.10: 99% credible regions for k_1 and k_2

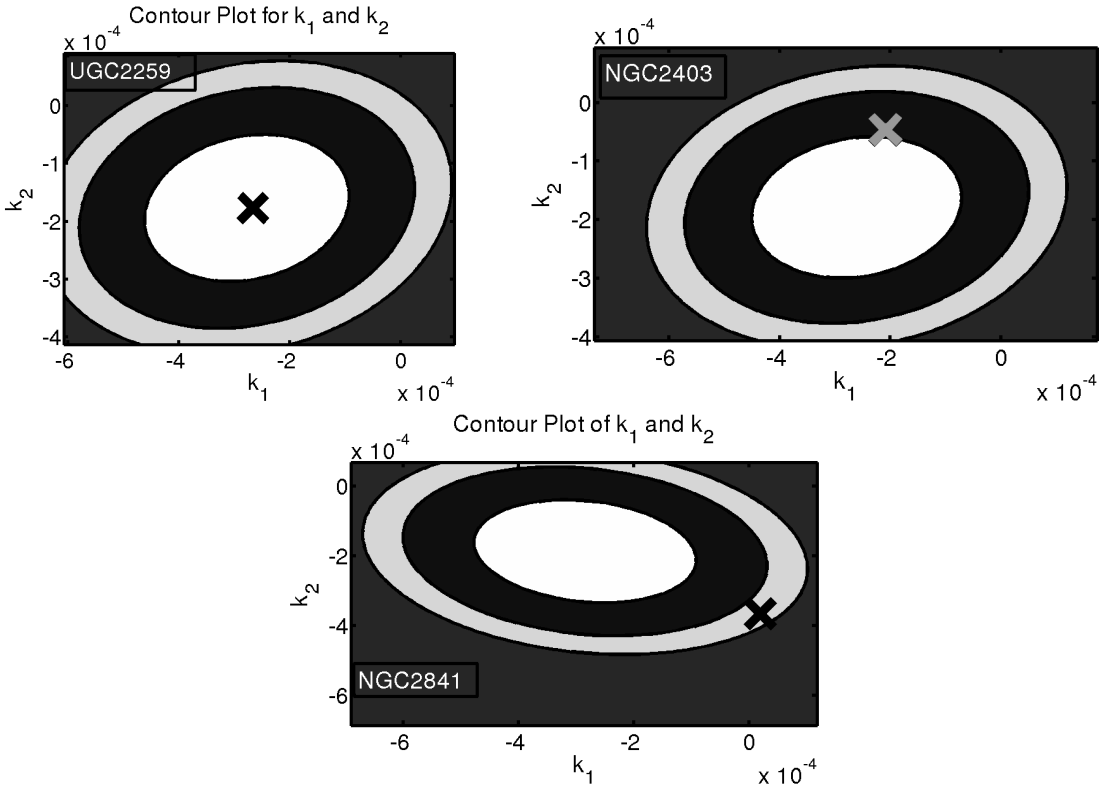

Figure 5.11: The innermost white region represents the 68.3% conditional credible region for k_1 and k_2. The darker region and the light grey region represent the 95.4% and 99% credible regions respectively. The value marked with a star is the best fit value of k_1 and k_2 found using the optimisation algorithm.

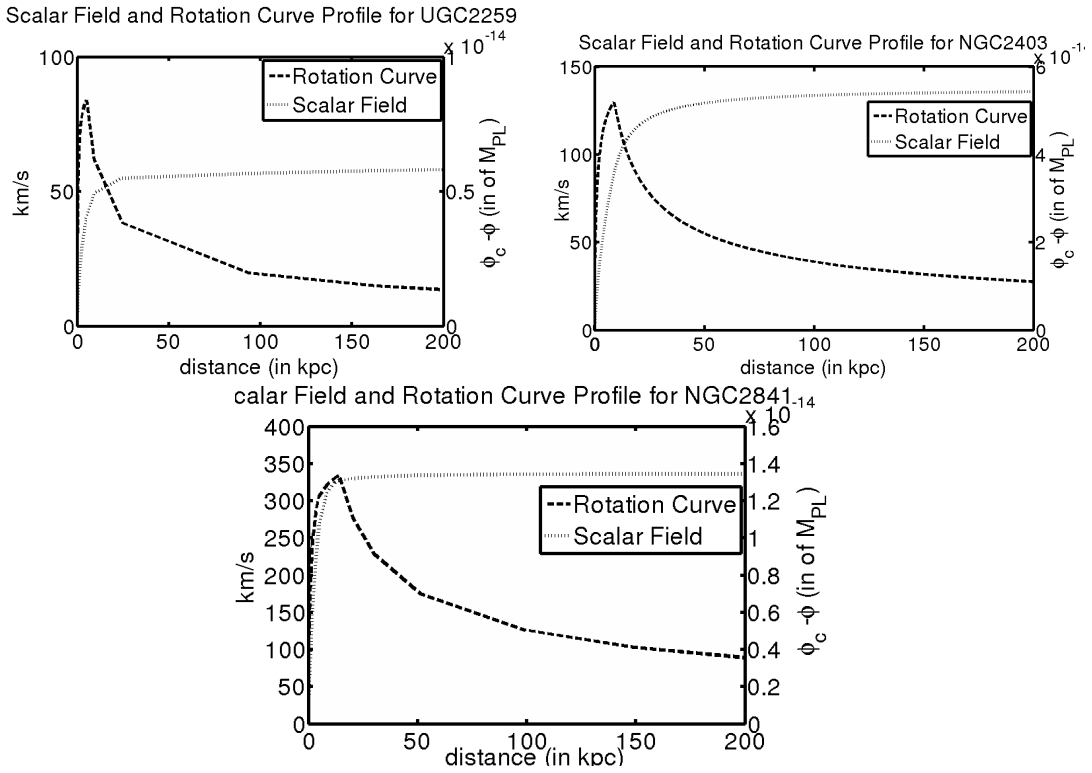

Figure 5.12: A side by side plot of the scalar field $\phi_c - phi$ and galactic rotation curves. The domain on which we did the integration was 200kpc for every galaxy, although the largest galaxy has an extent an order of magnitude smaller.

compactness of an object r_s given by its Schwarzschild radius and the behaviour of the scalar field when we are sufficiently far away from the object, and in a vacuum as is the case in our model:

$$s = \frac{r_S}{2R} \tag{5.3}$$

and its scalar charge α_S , [76], which is defined by the relation

$$\phi \sim \phi_\infty + \alpha_S \frac{r_s}{2r} + O\left(\frac{1}{r^2}\right)$$

where r_S is the Schwarzschild radius.

The best fit parameters can be used to estimate $\phi(r)$, from which the parameters in 5.3 can be calculated.

	UGC2259	NGC2403	NGC2841
ϕ_∞	8.853×10^{-4}	4.9466×10^{-4}	7.8406×10^{-5}
$\alpha_s \times r_s$	-2.4855×10^{-24}	-9.7120×10^{-22}	-6.3283×10^{-25}

Table 5.11: Estimated values of ϕ_∞ and $\alpha_S r_s$ using the best fit parameters of the model.

Table 5.11 corroborates what was inferred from the scalar field plots- that the degree of scalar charge or scalarization of the field is very small.

5.6.7 PPN Parameters

The chameleon effect, allows us to recover a the results of the solar system tests when the baryonic matter density is high. Table 5.12, shows that we do indeed recover the correct parameters. However, the scalar field and couplings are really weak through all the galaxies, and the chameleon mechanism is not necessary.

	UGC2259	NGC2403	NGC2841
$\gamma - 1$	-1.1055×10^{-15}	-8.2264×10^{-12}	-4.913×10^{-18}
$\beta - 1$	-7.3395×10^{-20}	8.432×10^{-15}	2.4553×10^{-23}

Table 5.12: PPN parameters in the galactic center.

5.7 Discussion and Summary

5.7.1 Bulge Disk Decomposition

A bulge, disk and halo were used to model the galaxies in this thesis. This generic model of fitting may not always be appropriate. Indeed, the luminosity profiles of the galaxies indicate that the bulge is not always discernible. An entire class of galaxies, with low luminosities show no indication of bulges. These are known as low surface brightness (LSB) galaxies, and are often dark matter dominated with rotation curve studies only fitting the dark matter halo to these galaxies [160].

The estimated GR bulge of NGC2403, which has a radius of 0.73kpc, may be an example of a galaxy which is unsuitable for such a decomposition. The fit in AWE, found a radically different value of

8.56kpc. We note that in each case the algorithm terminated to a minimum consistent with our criteria. However, without any comparison with the luminosity profile of the galaxy, on cannot decide which fit is better.

It is also noted the radius of the galactic disks is estimated to be close to the halo in the AWE model. We note that for every fit in the AWE model, the initial values we began the algorithm with were close to the GR values. That the the best estimates for the disk turn out to be so close to that of the galactic halo, might again be a result of not including the luminosity profile of each galaxy.

5.7.2 Non-Gaussian Nature of the Priors of NGC2841

The assumption of Gaussian priors was central to finding the credible regions and contour plots of the coupling constants k_1 and k_2 using MCMC methods. If this was indeed the case, then the best-fit value of the parameters would coincide with the peak of the marginalized distribution.

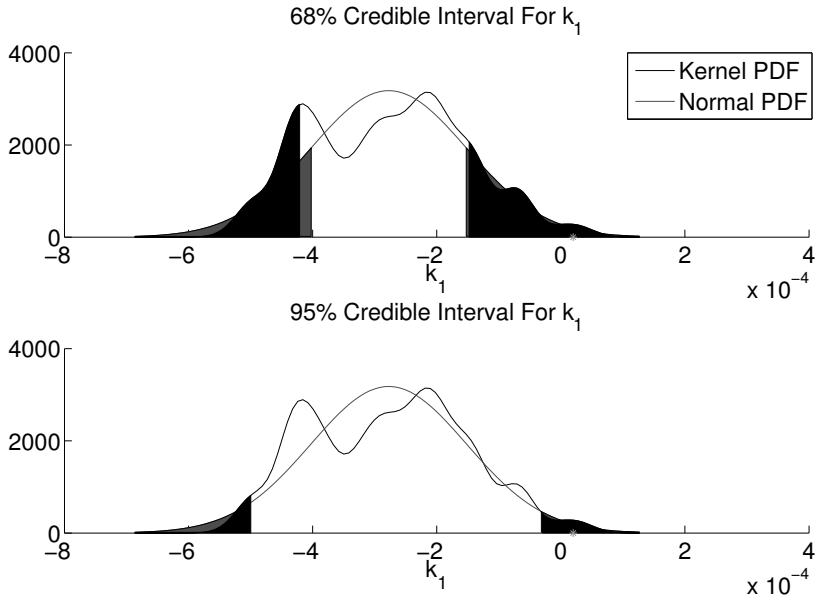

Figure 5.13: The above credible interval plots show how far out the best fit value is from the peak of the distribution. The value is so far out, it is in neither the 65% nor 95% credible regions.

The distribution for k_2 is also likely to be non-gaussian in the galaxy NGC2841, as the best fit value does not coincide with the peak of the distribution of k_2. However, the best fit value of k_2 is not ruled out by the distribution, and thus it can be taken to be a likely value for k_2.

5.7.3 Evidence for Non-Universal Couplings

As shown in Chapter 3, the chameleon mechanism in AWE explicitly requires that $k_2 < 0$ to recover a scalar field which is massive enough to be screened when baryonic matter dominates. In all the galaxies, with high enough credibility, 99 %, the joint distribution does not exclude cases where the coupling may be universally coupled or where the chameleon mechanism is ruled out, such as when $k_2 > 0$ and $k_1 > 0$.

5.7.4 Summary

The first part of this chapter provided a brief introduction to galactic rotation curves. A reviewed known fits of MOND, as well as their limitations, to the galaxies we study on this chapter was done. Chameleon scalar-tensor theories are not an attractive alternative to explaining flat rotation curves. These theories have been shown in chapter 3 to converge towards GR in small scales where baryonic matter dominates. However, they are not obviously distinct from GR on galactic scales. On cosmological scales, with non universal couplings, the inclusion of dark matter results in a violation of the WEP. Interestingly, non-universal couplings alone could also explain dark energy. However, the couplings from galactic scales and lower, do not allow quintessence to occur.

The main result of the investigation was that at the 99% level galactic rotation curves do not distinguish between GR, and non-universally coupled chameleon models. However, the results exclude coupling that could serve to explain dark energy [161].

Conclusions and Perspectives

This thesis has studied static spherical solutions in a specific class of scalar-tensor theories, mainly chameleon scalar-tensor theories. Motivated by high energy theories of physics, we have considered non-universally coupled chameleon models. The general distinguishing feature of non-universally coupled models from GR is that they violate the EP. A review (Chapter 2) of the current literature suggests that there is yet no evidence of violations of the EP.

The scalar-tensor theories we consider are equipped with the chameleon mechanism. This mechanism allows scalar tensor theories to satisfy the known constraints of the EP while retaining couplings constants that distinguish these theories from GR. This is done by introducing a density dependency in the scalar field. The mechanism can be extended, as discussed in Chapter 3, to non-universally coupled models without the addition of a scalar field potential to the action.

Non-universally coupled models are of interest to cosmology as they provide alternative explanations for inflation and dark energy. One of the two models studied in this thesis has been used to explain inflation with a non-minimally coupled Higgs scalar field. The other model, dubbed AWE, takes advantage of the violation of the EP to explain dark energy.

In our investigation of the first model, we restrict ourselves to static boson star solutions. Static boson stars in GR, as a result of Derrick's theorem [98], can only arise from a complex scalar field. We derived these solutions in sections 4.2 and 4.3, in spatially compactified domain, which are consistent with those previously investigated in the literature. It is not clear whether it is possible to obtain static solutions in scalar tensor theories from a real scalar field. We set out to determine the possibility of this in Chapter 4. We supposed the existence of a real scalar field boson star in a non-minimally coupled scalar tensor theory in which gravity is coupled to the Higgs and investigated the parameter space in which solutions may existed. No static solutions were found. It may be that, similar to GR, no static real scalar field boson solutions can be found in scalar tensor theories. However, we provide no formal proof of this. It may be more promising [1] to first investigate more general static boson star solutions from a complex scalar field in scalar-tensor theories before embarking on an extensive numerical simulation program. Such solutions have indeed been studied in the literature, for instance [162]. However, a non-minimally coupled Higgs scalar field and a minimally coupled complex scalar field may result in boson stars with features distinct from those of previous investigations. Indeed scalar-tensor theories in which the Higgs is the scalar field non-minimally coupled to gravity have non-trivial features as investigated in [120], and [121]. A future investigation into the equilibrium points, of which static solutions are special class, of boson stars in this more general setting, will be complementary to the work presented in this thesis.

In our second investigation, in Chapter 5, we made use of a particular scalar-tensor theory, AWE, to examine the effects of scalar-tensor theories on galactic scales. Our galactic model was a toy model with

[1] We would like to thank Prof. Füzfa for his comments on the boson star solutions studied in this thesis, the communicated insight of the results of Chapter 5 as well as recommendations for future work.

three spherical regions fore the core, disk and dark matter halo of a spiral disk. The static solutions of the toy model to galactic rotation data of the galaxies UGC2259, NGC2403 and NGC2841.

In the AWE model non-universal couplings, of order unity, result in a chameleon mechanism. Current evidence from the application of the AWE to dark energy suggested that, on cosmological scales, the non-universal couplings are of opposite sign and of order unity [77]. The coupling constants that arise from the best fit of our toy model to galactic rotation data are very likely negligible and do not conclusively support non-universal couplings in general. Such a result makes it difficult to distinguish AWE from GR through galactic rotation curves. Indeed, such a result may be inferred from the Klein Gordon equations (equations (3.5) - (3.6)) [2], as the the compactness of a galaxy is so small a significant contribution to the evolution of the scalar field in the absence of a potential requires large coupling constants. In future, an investigation in which a scalar field potential is included may yield a signature for a scalar-field on galactic scales.

We admit that the investigation has several shortcomings that directly influence our conclusion. The toy model is fairly simplistic and uses density profiles obtained using only Hα data and n-body simulations in GR. There also remains a possibility that the minimization algorithm used (Nelder-Mead), despite the initial randomization in several starting points, gets trapped in a local minimum. Future works should establish the robustness of the best fit parameters to multiple starting points.

While it is the opinion of the author that the results obtained using galactic rotation curves show that there is no evidence of non-universal couplings on galactic scales, there are several further investigations we propose be undertaken to have any certainty in this result. For instance, we suggest that studies that use both HI and Hα data would strengthen this conclusion. In particular, using a Bayesian approach, the additional data sets which are derived from separate observations would update the current priors, and place more stringent constraints on the coupling parameters. Furthermore, the inclusion of the potential for the scalar field, as well as more general kinetic terms and interactions between the two fluids will provide a surer understanding whether appreciable non-universal couplings exists on galactic scales.

[2] We would like to thank Prof. Füzfa for pointing this out.

Appendix A

Field Equations from The Variational Principle

This appendix derives all the field equations used in this thesis from the action of the theory using the variation of principles.

A.1 Chameleon Action

A.1.1 Introduction

The action in the Einstein Frame is given by:

$$S = \int \left[\frac{R}{16\pi G} - 2g^{\mu\nu}\partial_\mu\phi\partial_\nu\phi \right] \sqrt{-g}\ d^4x + S_{awe}(\psi_{awe}, A^2_{awe}(\phi)g_{\mu\nu}) + S_m(\psi_m, A^2_m(\phi)g_{\mu\nu}).$$

First, we vary the action with respect to the metric $g_{\mu\nu}$

$$\delta S = \delta \int \left[\frac{R}{16\pi G} - 2g^{\mu\nu}\partial_\mu\phi\partial_\nu\phi \right] \sqrt{-g}\ d^4x + \delta S_{awe}(\psi_{awe}, A^2_{awe}(\phi)g_{\mu\nu}) + \delta S_m(\psi_m, A^2_m(\phi)g_{\mu\nu})$$

where

$$\begin{aligned}
&\delta \int \left[\frac{R}{16\pi G} - 2g^{\mu\nu}\partial_\mu\phi\partial_\nu\phi \right] \sqrt{-g}\ d^4x \\
&= \int \left[\frac{\delta R}{16\pi G} - 2\delta\left(g^{\mu\nu}\partial_\mu\phi\partial_\nu\phi\right) \right] \sqrt{-g} + \left[\frac{R}{16\pi G} - 2g^{\mu\nu}\partial_\mu\phi\partial_\nu\phi \right] \delta\sqrt{-g}\ d^4x \\
&= \int \left[\frac{\delta g^{\mu\nu}R_{\mu\nu}}{16\pi G} - 2\delta g^{\mu\nu}\partial_\mu\phi\partial_\nu\phi \right] \sqrt{-g} + \left[\frac{R}{16\pi G} - 2g^{\mu\nu}\partial_\mu\phi\partial_\nu\phi \right] \frac{-\sqrt{-g}g_{\mu\nu}\delta g^{\mu\nu}}{2}\ d^4x \\
&= \delta g^{\mu\nu}\delta \int \left[\frac{1}{16\pi G}\left(R_{\mu\nu} - \frac{1}{2}Rg_{\mu\nu} \right) - 2\partial_\mu\phi\partial_\nu\phi + g_{\mu\nu}\left(g^{\mu\nu}\partial_\mu\phi\partial_\nu\phi\right) \right] \sqrt{-g}\ d^4x
\end{aligned}$$

and

$$\begin{aligned}
\delta S_{(\mathrm{m,awe})}\left(\psi_{(\mathrm{m,awe})}, A^2_{(\mathrm{m,awe})}(\phi)\, g_{\mu\nu}\right) &= \delta \int L_{(\mathrm{m,awe})}\sqrt{-g}\ d^4x \\
&= -\frac{1}{2}\delta g^{\mu\nu} \int T^{(\mathrm{m,awe})}_{\mu\nu}\sqrt{-g}\ d^4x,
\end{aligned}$$

thus

$$\frac{1}{8\pi G}\left(R_{\mu\nu}-\frac{1}{2}Rg_{\mu\nu}\right)-2\partial_\mu\phi\partial_\nu\phi+g_{\mu\nu}\left(g^{\mu\nu}\partial_\mu\phi\partial_\nu\phi\right)=T_{\mu\nu}^{(\mathrm{m,awe})}.$$

The action could also be varied with respect to ϕ, in which case

$$\begin{aligned}
\delta S &= \delta\int\frac{1}{16\pi G}[R-2g^{\mu\nu}\partial_\mu\phi\partial_\nu\phi]\sqrt{-g}\ d^4x+\delta(S_m(\psi_m,A_m^2(\phi)g_{\mu\nu})+S_{awe}(\psi_{awe},A_{awe}^2(\phi)g_{\mu\nu}))\\
&=\frac{1}{16\pi G}\int-\delta(2g^{\mu\nu}\partial_\mu\phi\partial_\nu\phi)\sqrt{-g})\ d^4x+\delta^i\frac{\partial S_i}{\partial g_{\mu\nu}}\frac{\partial g_{\mu\nu}}{\partial A_i^2 g_{\mu\nu}}\frac{\partial A_i^2 g_{\mu\nu}}{\partial\phi}\delta\phi\\
&=\frac{1}{16\pi G}\int 4g^{ab}\nabla_a\nabla_b\phi\sqrt{-g}\delta\phi\ d^4x+\delta^i\frac{\partial S_i}{\partial g_{\mu\nu}}(2g_{\mu\nu}A_iA_i')(A_i^2)^{-1}\delta\phi\\
&=\frac{1}{16\pi G}\int 4g^{ab}\nabla_a\nabla_b\phi\sqrt{-g}\delta\phi\ d^4x+2\delta^i\frac{\partial S_i}{\partial g_{\mu\nu}}g_{\mu\nu}\alpha_i\delta\phi\\
&=\frac{1}{16\pi G}\int 4g^{ab}\nabla_a\nabla_b\phi\sqrt{-g}\delta\phi\ d^4x-2\delta^i g^{\mu\nu}\frac{\partial S_i}{\partial g^{\mu\nu}}\alpha_i\delta\phi\\
&=\frac{1}{16\pi G}\int 4g^{ab}\nabla_a\nabla_b\phi\sqrt{-g}\delta\phi\ d^4x-\delta^i g^{\mu\nu}\alpha_i\int 2L^i\sqrt{-g}\delta\phi\ d^4x\\
&=\frac{1}{16\pi G}\int 4g^{ab}\nabla_a\nabla_b\phi\sqrt{-g}\delta\phi\ d^4x-\delta^i g^{\mu\nu}\alpha_i(-\int T^i_{\mu\nu}\sqrt{-g})\delta\phi\ d^4x
\end{aligned}$$

$$\Box\phi=-4\pi G[\alpha_1T^{(m)}+\alpha_2T^{(awe)}]$$

A.1.2 Schwarzschild Coordinates Geometric Components

As a result of Birkhoff's theorem, the geometry outside a spherical body is described by the line element

$$ds^2=-e^\nu dt^2+e^\lambda dr^2+r^2d\Omega$$

from which we can calculate the following connection coefficients

$$\begin{aligned}
\Gamma^0_{00}&=\frac{1}{2}(-e^{-\nu})(-e^\nu\dot\nu)=\frac{\dot\nu}{2} & \Gamma^0_{10}&=\frac{1}{2}(-e^{-\nu})(-e^\nu\nu')=\frac{\nu'}{2}\\
\Gamma^0_{11}&=\frac{1}{2}(-e^{-\nu})(-e^\lambda\dot\lambda)=e^{\lambda-\nu}\frac{\dot\lambda}{2} & \Gamma^1_{00}&=\frac{1}{2}(e^{-\lambda})(--e^\nu\nu')=e^{\nu-\lambda}\frac{\nu'}{2}\\
\Gamma^1_{10}&=\frac{1}{2}(e^{-\lambda})(e^\lambda\dot\lambda)=\frac{\dot\lambda}{2} & \Gamma^1_{11}&=\frac{1}{2}(e^{-\lambda})(e^\lambda\lambda')=\frac{\lambda'}{2}\\
\Gamma^1_{22}&=\frac{1}{2}(e^{-\lambda})(-2r)=-re^{-\lambda} & \Gamma^1_{33}&=\frac{1}{2}(e^{-\lambda})(-2r\sin^2(\theta))=-e^{-\lambda}r\sin^2\theta\\
\Gamma^2_{21}&=\frac{1}{2}(r^{-2})(2r)=r^{-1} & \Gamma^2_{33}&=\frac{1}{2}(r^{-2})(2r^2\sin\theta\cos\theta)=-r\sin^2\theta\\
\Gamma^3_{23}&=\frac{1}{2}(r^{-2}\sin^{-2}\theta)(2r^2\sin\theta\cos\theta)=\cot\theta & \Gamma^3_{33}&=\frac{1}{2}(r^{-2})(2r\sin^2\theta)=r^{-1}
\end{aligned}$$

and Ricci Tensor and the Ricci Scalar

$$R_{00} = -\frac{\lambda'\nu'}{4}e^{\nu-\lambda} + \frac{\nu''}{2}e^{\nu-\lambda} + \frac{\nu'^2}{4}e^{\nu-\lambda} - \frac{\ddot{\lambda}}{2} + \frac{\dot{\lambda}\dot{\nu}}{4} + r^{-1}\nu'e^{\nu-\lambda} - \frac{\dot{\lambda}^2}{4}$$
$$R_{01} = r^{-1}\dot{\lambda}$$
$$R_{11} = \frac{\dot{\lambda}^2}{4}e^{\lambda-\nu} + r^{-1}\lambda' - \frac{\nu'^2}{4} + \frac{\lambda'\nu'}{4} - \frac{\nu''}{2} - \frac{\dot{\nu}\dot{\lambda}}{4}e^{\lambda-\nu} + \frac{\ddot{\lambda}}{2}e^{\lambda-\nu}$$
$$R_{22} = e^{-\lambda} + r\frac{\lambda'}{2}e^{-\lambda} - \frac{\nu'}{2}re^{-\lambda} + 1$$
$$R_{33} = \frac{\sin^2\theta}{2}(-r\nu'e^{-\lambda} + r\lambda e^{-\lambda} + 2 - 2e^{-\lambda})$$
$$\begin{aligned} R &= g^{00}R_{00} + g^{11}R_{11} + g^{22}R_{22} + g^{33}R_{33} \\ &= \frac{\lambda'\nu'}{2}e^{-\lambda} - \nu''e^{-\lambda} - \frac{\nu'^2}{2}e^{-\lambda} + \ddot{\lambda}e^{-\nu} - \frac{\dot{\lambda}\dot{\nu}}{2}e^{-\nu} + \frac{\dot{\lambda}^2}{2}e^{-\nu} - 2r^{-1}\nu'e^{-\lambda} + 2r^{-1}\lambda'e^{-\lambda} + 2r^{-2} - 2r^{-2}e^{-\lambda} \end{aligned}$$

and finally the Einstein tensor

$$G_{00} = r^{-1}e^{\nu-\lambda}\lambda' + r^{-2}e^{\nu} - r^{-2}e^{\nu-\lambda}$$
$$G_{01} = r^{-1}\dot{\lambda}$$
$$G_{11} = r^{-1}\nu' - r^{-2}e^{\lambda} + r^{-2}$$
$$G_{22} = -r\frac{\lambda'}{2}e^{-\lambda} + r\frac{\nu'}{2}e^{-\lambda} - r^2\frac{\lambda'\nu'}{4}e^{-\lambda} + r^2\frac{\nu''}{2}e^{-\lambda} + r^2\frac{\nu'^2}{4}e^{-\lambda} - r^2\frac{\ddot{\lambda}}{2}e^{-\nu} + r^2\frac{\dot{\lambda}\dot{\nu}}{4}e^{-\nu} - r^2\frac{\dot{\lambda}^2}{4}e^{-\nu}$$
$$G_{33} = \frac{r\sin^2\theta}{2}(\nu'e^{-\lambda} - \lambda'e^{-\lambda} - r\frac{\lambda'\nu'}{2}e^{-\lambda} + r\nu''e^{-\lambda} + r\frac{\nu'^2}{2}e^{-\lambda} - r\ddot{\lambda}e^{-\nu} + r\frac{\dot{\lambda}\dot{\nu}}{2}e^{-\nu} - r\frac{\dot{\lambda}^2}{2}e^{-\nu})$$

A.1.3 Wave Equation

The d'Alembertian

$$\Box\phi = 0,$$

can be calculated explicitly:

$$\begin{aligned} \Box\phi &= \nabla_\mu g^{\mu\eta}\nabla_\eta\phi \\ &= \nabla_\mu g^{\mu\eta}\phi_{,\eta}, \end{aligned}$$

using the geometric quantities calculated above. We note that $X^\mu = g^{\nu\eta}\phi_{,\eta}$ is a tensor quantity with two nonzero components. So

$$\begin{aligned} &= X^\mu_{,\mu} + \Gamma^\mu_{\nu\mu}X^\nu \\ &= e^{-\nu}(\dot{\phi}\dot{\nu} - \ddot{\phi}) + e^{-\lambda}(\phi'' - \phi'\lambda') + \Gamma^\mu_{0\mu}X^0 + \Gamma^\mu_{1\mu}X^1 \\ &= e^{-\nu}(\dot{\phi}\dot{\nu} - \ddot{\phi}) + e^{-\lambda}(\phi'' - \phi'\lambda') - (\Gamma^0_{00} + \Gamma^1_{01})e^{-\nu}\dot{\phi} + (\Gamma^0_{10} + \Gamma^1_{11} + \Gamma^2_{12})e^{-\lambda}\phi' \\ &= e^{-\nu}(\dot{\phi}\dot{\nu} - \ddot{\phi}) + e^{-\lambda}(\phi'' - \phi'\lambda') - \frac{1}{2}(\dot{\nu} + \dot{\lambda})e^{-\nu}\dot{\phi} + \frac{1}{2}(\nu' + \lambda' + 2r^{-1})e^{-\lambda}\phi' \\ &= e^{-\nu}(\frac{1}{2}\dot{\phi}\dot{\nu} - \ddot{\phi} - \frac{1}{2}\dot{\lambda}\dot{\phi}) + e^{-\lambda}(\phi'' - \frac{1}{2}\phi'\lambda' + \frac{1}{2}\nu'\phi' + 2r^{-1}\phi') \end{aligned}$$

A.2 Brout-Englert-Higgs Gravity Action

A.2.1 Introduction

The action in the JF is given by

$$S=\int\left[F(H)\frac{R}{2\kappa}-\frac{1}{2}\nabla_\mu H\nabla^\mu H-V\left(H\right)-\frac{1}{2}\nabla_\mu\psi\nabla^\mu\psi-U(\psi,H)\right]\sqrt{-g}\ d^4x$$

Where

$$\begin{aligned}F(H)&=1+\frac{\xi}{m_p^2}H^2\text{ and}\\V(H)&=\frac{\lambda_{SM}}{4}\left(H^2-v^2\right)^2\\U(\psi,H)&=\frac{\mu}{4}H^2\psi^2\\\kappa&=\frac{8\pi}{m_p^2}\end{aligned}$$

Let

$$\begin{aligned}\mathfrak{f}(R)&=F(H)R\\\mathfrak{F}(R)&=\frac{\partial f}{\partial R}\end{aligned}$$

This allows us the action to appear like that of $f(R)$ gravity. A model in which we can easily derive the field equations of:

$$\begin{aligned}\delta S=&\left[\int\delta\frac{\mathfrak{f}(R)}{2\kappa}-\frac{1}{2}\delta\nabla_\mu H\nabla^\mu H-\delta V\left(H\right)-\frac{1}{2}\delta\nabla_\mu\psi\nabla^\mu\psi-\delta U(\psi,H)\right]\sqrt{-g}\ d^4x\\&+\int\left[F(H)\frac{R}{2\kappa}-\frac{1}{2}\nabla_\mu H\nabla^\mu H-V\left(H\right)-\frac{1}{2}\nabla_\mu\psi\nabla^\mu\psi-U(\psi,H)\right]\delta\sqrt{-g}\ d^4x\end{aligned}$$

focusing on the first term, we can write

$$\begin{aligned}\int\left[\delta\mathfrak{f}\left(R\right)\right]\sqrt{-g}\ d^4x&=\int\left[\frac{\partial\mathfrak{f}}{\partial R}\delta\left(g^{\mu\nu}R_{\mu\nu}\right)\right]\sqrt{-g}\ d^4x\\\delta\left(g^{\mu\nu}R_{\mu\nu}\right)&=\delta g^{\mu\nu}R_{\mu\nu}+g^{\mu\nu}\delta R_{\mu\nu}\\g^{\mu\nu}\delta R_{\mu\nu}&=g^{\mu\nu}\delta R^\rho_{\mu\rho\nu}=\nabla_\sigma\left(g^{\mu\nu}\delta\Gamma^\sigma_{\nu\mu}-g^{\mu\sigma}\delta\Gamma^\rho_{\rho\mu}\right)\end{aligned}$$

In the $g^{\mu\nu}\delta R_{\mu\nu}$ has no contribution since

$$\int\left[\nabla_\sigma\left(g^{\mu\nu}\delta\Gamma^\sigma_{\nu\mu}-g^{\mu\sigma}\delta\Gamma^\rho_{\rho\mu}\right)\right]\sqrt{-g}\ d^4x=0$$

as a result of Stokes theorem. However, in $f(R)$ theories this term has a contribution since

$$\begin{aligned}\int \frac{\partial \mathfrak{f}}{\partial R}\left[\nabla_\sigma\left(g^{\mu\nu}\delta\Gamma^\sigma_{\nu\mu}-g^{\mu\sigma}\delta\Gamma^\rho_{\rho\mu}\right)\right]\sqrt{-g}\;d^4x &= \int \frac{\partial \mathfrak{f}}{\partial R}\left[\nabla_\sigma\left(\nabla^\sigma\delta g^{\mu\nu}-\nabla_\nu\delta g^{\mu\nu}\right)\right]\sqrt{-g}\;d^4x\\ &= -\int\left[g_{\mu\nu}\nabla_\rho\nabla^\rho\frac{\partial \mathfrak{f}}{\partial R}-\nabla_\mu\nabla_\nu\frac{\partial \mathfrak{f}}{\partial R}\right]\delta g^{\mu\nu}\sqrt{-g}\;d^4x\end{aligned}$$

Ultimately,

$$\int\left[\delta\mathfrak{f}(R)\right]\sqrt{-g}\;d^4x=\int\left[\frac{\partial \mathfrak{f}}{R}R_{\mu\nu}-g_{\mu\nu}\nabla_\rho\nabla^\rho\frac{\partial \mathfrak{f}}{\partial R}+\nabla_\mu\nabla_\nu\frac{\partial \mathfrak{f}}{\partial R}\right]\delta g^{\mu\nu}\sqrt{-g}\;d^4x$$

and we can write down the field equations as

$$\begin{aligned}&\mathfrak{F}(R)R_{\mu\nu}-\frac{1}{2}\mathfrak{f}(R)g_{\mu\nu}-\nabla_\mu\nabla_\nu F(H)+g_{\mu\nu}\nabla^\lambda\nabla_\lambda F(H)\\ =&\kappa\left(\nabla_\mu\psi\nabla_\nu\psi-\frac{1}{2}g_{\mu\nu}\left(\nabla_\mu\psi\nabla^\mu\psi+U(\psi,H)\right)\right)+\kappa\left(\nabla_\mu H\nabla_\nu H-\frac{1}{2}g_{\mu\nu}\left(\nabla_\mu H\nabla^\mu H+V(H)\right)\right)\end{aligned}$$

We note that

$$\begin{aligned}\nabla_\mu\nabla_\nu F(H)-g_{\mu\nu}\nabla^\lambda\nabla_\lambda F(H)&=\nabla_\mu\left(\frac{dF}{dH}\nabla_\nu H\right)-g_{\mu\nu}\nabla^\mu\left(\frac{dF}{dH}\nabla_\mu H\right)\\ &=\frac{d^2F}{dH^2}\nabla_\mu H\nabla_\nu H+\frac{dF}{dH}\nabla_\mu\nabla_\nu H-g_{\mu\nu}\left(\frac{d^2F}{dH^2}g^{\alpha\lambda}\nabla_\lambda H\nabla_\alpha H+\frac{dF}{dH}\nabla^\lambda\nabla_\lambda H\right)\end{aligned}$$

A.2.2 Field Equations for a real ψ

$$\begin{aligned}F(H)\left(2r\lambda'+e^{-2\lambda}-1\right)&=r^2\frac{d^2F}{dH^2}H'^2+r^2\frac{dF}{dH}H''-r^2\frac{dF}{dH}H'\lambda'+2\frac{dF}{dH}H'\\ &\quad+e^{2\lambda}\kappa\left(\frac{1}{2}\psi'^2+e^{2\lambda}V(\psi)\right)+e^{2\lambda}r^2\kappa\left(\frac{1}{2}H'^2+e^{2\lambda}U(\psi,H)\right)\\ F(H)\left(2r\nu'-r^{-2}e^{2\lambda}+1\right)&=-r\frac{dF}{dH}H'\left(r\nu'+2\right)+\kappa\frac{r^2}{2}\left(\psi'^2-V(\psi)\right)+\kappa\frac{r^2}{2}\left(H'^2-U(\psi,H)\right)\\ F(H)\left(-\lambda'+\nu'-r\lambda'\nu'+r\nu''+r\nu'^2\right)&=-\left(\frac{dF}{dH}H'\nu'r+r\frac{d^2F}{dH^2}H'^2+r\frac{dF}{dH}H''-rF'H'\lambda'+\frac{dF}{dH}H'\right)\\ &\quad-\kappa\frac{r}{2}\left(\psi'^2+V(\psi)\right)-\kappa\frac{r}{2}\left(H'^2+U(\psi,H)\right)\end{aligned}$$

and

$$\begin{aligned}H''+H'(\nu'-\lambda'+\frac{2}{r})+\frac{\partial F}{\partial H}\left(\frac{R}{2\kappa}\right)&=e^{2\lambda}\frac{\partial V}{\partial H}+e^{2\lambda}\frac{\partial U}{\partial H}\\ \psi''+\psi'(\nu'-\lambda'+\frac{2}{r})&=e^{2\lambda}\frac{\partial V}{\partial\psi}\end{aligned}$$

Appendix B

Parameter Estimation

The chief concern of Chapter 5 is finding the AWE parameters consistent with rotation curves. In particular, the chapter recovered the estimates of ϕ_c, k_1 and k_2 for different rotation curves. Optimal estimates can be determined by minimizing the sum of squared errors between the predicted curve and the actual curve. However, without statistical methods, it is not clear how likely the optimal estimates are, given the data. Monte Carlo methods allow us to recover the probability distribution of the parameters, given the data. The subsequent sections explain the methods used to obtain the optimal values and contours for the coupling constants.

B.1 Parameter Estimation Using Optimisation

B.1.1 Grid Search

In chapter 5, we recovered the parameters that minimise the quantity

$$\chi^2 = \sum_i \frac{\left(v_i^p - v_i^a\right)^2}{\sigma_i^2}$$

where v_i^p and v_i^a are the predicted and actual velocities of the galaxy's rotation respectively, and σ_i is the uncertainty in the measured value. In this section we treat χ^2 as purely a function of the parameters.

The global minimum of a function in a low dimensional space, in which no special assumptions about the behaviour of the function are made, can be easily found using the grid search method. In this method, a provisional global minimum is found by evaluating the function at a number of grid points. A new and more refined grid is then created around the provisional global minimum and the function is evaluated on this new grid and a new provisional global minimum closer to the specified tolerance is obtained. See Figure B.1 for an illustration of the method in two dimensions. This process is repeated, until the grid spacing is less than the specified tolerance. There is a chance that the algorithm may find a local minimum if the initial grid spacing is too large. This danger can be minimised if we begin the algorithm on several successively finer grids. If these also converge to the same global minimum, then we can be confident of having found a global minimum. When the computational costs of evaluating each point in the grid are fairly high, the search method becomes inefficient. This is especially true for in high dimensional space, as is the case in Chapter 5.

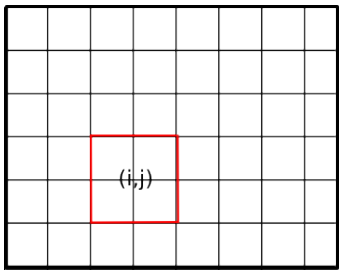

Figure B.1: In the grid search method, the optimal values of the parameters are found by minimising the χ^2 statistic. For the GR rotation curve studies in 5 in which we have to optimise the six parameters R_{Bulge}, R_{Disk}, R_{Halo}, ρ_0^{Bulge}, ρ_0^{Disk}, ρ_0^{Halo}. A very rudimentary grid of ten points for each parameter would require at least 10^6 evaluations of the χ^2 statistic. As the calculation of this statistic takes several hundred milliseconds in MATLAB at best, the grid search method is unsuitable for finding the global minimum. Even if the calculation of the statistic were to be made more efficient, the limitations in memory variable size, make grid spacing of more than thirty points for each parameter intractable

B.1.2 Nedler-Mead Method

In contrast to the grid search method, the downhill simplex method [159] is robust and makes no assumptions about the function to be minimised. The optimisation problem in Chapter 5 has constraints such as weighting the sum of square errors with the standard error at each point and requiring the radius of the galactic halo to be larger than the radius of the disk and requiring the radius of the disk to be larger than that of the bulge that make this optimisation algorithm readily pliable to our problem. The method is implemented using the built in MATLAB function *fminsearch*. Although there is a chance that the algorithm may not find a global minimum, several steps may be taken to minimise this. Firstly, one immediate advantage of the algorithm is that it keeps track of $N+1$ distinct points. Secondly, once a minimum is found, we could re-initialize the algorithm with N random points and the additional point being our provisional global minimum.

The downhill simplex method is based on a geometrical figure known as a simplex. A simplex is a $N+1$ polygon in N dimensions. The initial guess, $\mathbf{P}_0$, provides one vertex of the simplex, with the remaining N points being guessed by a series of λ_i in the following way

$$\mathbf{P_i} = \mathbf{P}_0 + \lambda_i \mathbf{e}_i$$

where the $\mathbf{e}_i$'s are the N unit vectors. Figure B.2 provides a visual illustration of hoe the method works. The method terminates when either the decrease in the cost function value or step size is less than some prescribed value.

B.2 Parameter Estimation Using Statistical Methods

B.2.1 Baye's Theorem

Once the best-fit values of the parameters to a model have been found, it is desirable to provide a statistical measure of how likely are they to take on a range of the values given the data. The probability distribution $P(\rho_0^{(Bulge)}, \rho_0^{(Disk)}, \rho_0^{(Halo)}, R_{Bulge}, R_{Disk}, R_{Halo}, \phi_c, k_1, k_2 | \forall v_i^a, \sigma_i)$ provides such a measure. For convenience, we will write the preceding distribution $P(\theta|X)$. This distribution is known as the posterior distribution, and can be determined using Baye's theorem.

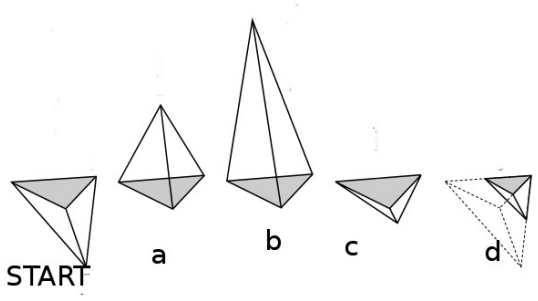

Figure B.2: It is easy to visualise how the simplex method works in 3 dimensions. A step using the method has four possible outcomes for the simplex: a) a reflection, b) a reflection and expansion, c) a contraction in one dimension, d) a contraction in all dimensions. The above diagram obtained from [159]

We treat both the parameters and data as random variables. Although the number of observations is low, we will appeal to the central limit theorem to justify the assumption that each mean measurement of the velocity normally distributed with a mean quantity v_i^{actual} and standard deviation σ_i. The preceding distribution will be identified with the likelihood distribution in Baye's theorem. In particular, for the rotations curves that we study, the likelihood will be given by

$$P(X|\theta) = e^{-\chi^2} \prod_i \frac{1}{\sqrt{2\pi}\sigma_i}.$$

Furthermore, we will assume that the probability distribution of each parameter is normally distributed with a mean identical to the optimal value of the parameter, and a standard deviation equivalent to 50% of the mean value. This distribution is known as the prior distribution.

Our choice for the prior has at least two advantages over choosing uniform distributions. Firstly, it does not prescribe a finite range for the parameters k_1 and k_2, and we can thus be confident the simulation exhaustively determines whether there is evidence of non-universal couplings. For the remaining parameters, we will discard the non-positive values. Secondly, it takes into account the results of our optimisation algorithm. Although the optimal values may not be the modal values of the prior distribution, it is expected that they are no unlikely value.

Baye's theorem relates the posterior distribution to the likelihood and prior:

$$P(\theta|X) = \frac{P(X|\theta)P(\theta)}{P(X)},$$

where $P(X|\theta)$ is the Gaussian likelihood and $P(\theta)$ is a prior distribution [163]. The probability distribution $P(X)$, is known as the evidence and is effectively a normalisation quantity since it can be expressed as

$$P(X) = \int P(X|\theta)P(\theta)\ d\theta.$$

Although, in theory it can be computed simply as a multi-dimensional integral, the computational costs of doing so are prohibitive. It will be convenient to leave out the denominator in Baye's theorem when calculating the posterior. This quantity can be easily recovered, if necessary, by normalising. Indeed,

the biggest challenge with the statistical approach to parameter estimation has been the difficulty of calculating multi-dimensional integrals.

It will be necessary to compute multi-dimensional integrals to produce contour plots and credible intervals. This integrals correspond to the marginalised distributions. A marginal distribution $\alpha \subset \theta = \{\theta_i\}$. It is thus necessary to perform the integration:

$$P(\alpha|X) = \int_{\theta_i \in \alpha} P(\theta|X) d\theta_i.$$

In Chapter 5, this integral is in 6 dimensional space or more. The computational costs of sampling from the marginalised distribution, using a uniform grid are prohibitive. For instance if were to divide the range for each parameter into $N = 100$ nodes. A single sample would require N^6 evaluations of $P(\theta|X)$. Even if we optimistically assume each evaluation takes a millisecond (which is not the case), such a grid would require 32 years to compute! This problem cannot be circumvented by gradually selecting adoptive grids around the maximum likelihood estimates, as we still need to compute a marginalised distribution for each grid. Furthermore, using such an adoptive grid results in a posterior that is rather sensitive to our choice priors. For instance, we may inadvertently select grid spacing that neglects large regions of the parameters space. This practically rules out numerical integration using Riemann sums or related procedures. It is possible to compute these integrals using Monte Carlo methods as shown in the subsequent chapters.

B.2.2 Sampling Using Monte Carlo Methods

Monte Carlo methods avoid having to evaluate the posterior distribution on large multi-dimensional grid, and represent the distribution samples. This is done by taking advantage of the fact that the number of samples in a region θ in the parameter space will be directly proportional to $P(\theta)$.These methods are adaptable, and allow us to produce samples from a wide range of statistical distributions, given a prior $P(\theta)$.

The are various methods of deciding how random exploration in Monte Carlo methods is done such as inverse transform sampling, rejection sampling and Markov chain sampling [164]. The latter is suitable for sampling in high dimensions. A completely random walk, on the contrary, may be unsuitable for producing a sample. It is often preferable to decide on which sample to next draw θ_{i+1}, depending on the likelihood of the current sample θ_i. This is what is done in Markov chain Monte Carlo methods (MCMC). A Markov chain is stochastic process in which future states are independent of past states given the present state. Deciding whether or not to accept the next sample θ_{i+1}, depends on a pre-chosen proposal density $q(\theta_i, \theta_{i+1})$, analogous to a transition probability for a Markov chain. This selection process eliminates sensitivity to our initial priors. The only drawback is that it is not obvious how long the chain must be before the samples drawn are truly from the posterior.

Various methods exist to set up a Monte Carlo Markov chain simulation. The most robust [165] of these is the Metropolis-Hasting algorithm. It is implemented in MATLAB by the routine *mhsample*. The algorithm can be broken into five parts:

- Choose a starting value $\theta^{(0)}$
- At each iteration t, we draw a candidate θ^* from a random walk distribution

- Compute an acceptance ratio

$$r = \frac{P(\theta^*|X)\, q(\theta^*, \theta^{t-1})}{P(\theta^{t-1}|X)\, q(\theta^{t-1}, \theta^*)}$$

- Accept θ^* as θ^t with a probability $\min(r, 1)$, or take $\theta^{(t)}$ as $\theta^{(t-1)}$

- The above steps are repeated until the desired number of samples are drawn. As the parameter space is large in Chapter 5, and the computational power is limited, for simplicity and convenience, the proposal density for each parameter was chosen was chosen to be normally distributed around the optimal values, with a standard error that is 50% of the mean, i.e:

$$q(\theta_{i+1}, \theta_i) = \prod_k \frac{2}{\sqrt{\pi}\theta^k_{opt}} e^{-\frac{\left(\theta_{i+1} - \theta_{opt}\right)}{.25 \times \theta^2_{opt}}}.$$

  Proposal distributions with an explicit θ_i dependence did not appear to converge. The above choice ensures that regions of high likelihood are well explored.

Bibliography

[1] P. Peter and J. Uzan, *Primordial Cosmolgy*. Oxford University Press, New York, 2009. (Cited on pages 2 and 4.)

[2] P. J. E. Peebles, "The standard cosmological model," *ArXiv Astrophysics e-prints* (June, 1998) , arXiv:astro-ph/9806201. (Cited on page 2.)

[3] E. Komatsu, J. Dunkley, M. R. Nolta, C. L. Bennett, B. Gold, G. Hinshaw, N. Jarosik, D. Larson, M. Limon, L. Page, D. N. Spergel, M. Halpern, R. S. Hill, A. Kogut, S. S. Meyer, G. S. Tucker, J. L. Weiland, E. Wollack, and E. L. Wright, "Five-year wilkinson microwave anisotropy probe observations: Cosmological interpretation," *Astrophysical Journals, Supplement* **180** (Feb., 2009) 330–376, arXiv:0803.0547. (Cited on page 2.)

[4] A. Shafieloo and C. Clarkson, "Model independent tests of the standard cosmological model," *Physical Review D* **81** no. 8, (Apr., 2010) 083537, arXiv:0911.4858 [astro-ph.CO]. (Cited on page 2.)

[5] **WMAP Collaboration** Collaboration, C. Bennett *et al.*, "First year wilkinson microwave anisotropy probe (wmap) observations: Preliminary maps and basic results," *Astrophys.J.Suppl.* **148** (2003) 1, arXiv:astro-ph/0302207 [astro-ph]. (Cited on page 2.)

[6] **Supernova Cosmology Project** Collaboration, S. Perlmutter *et al.*, "Measurements of omega and lambda from 42 high redshift supernovae," *Astrophys.J.* **517** (1999) 565–586, arXiv:astro-ph/9812133 [astro-ph]. (Cited on page 2.)

[7] **Supernova Search Team** Collaboration, A. G. Riess *et al.*, "Type ia supernova discoveries at z > 1 from the hubble space telescope: Evidence for past deceleration and constraints on dark energy evolution," *Astrophys.J.* **607** (2004) 665–687, arXiv:astro-ph/0402512 [astro-ph]. (Cited on page 2.)

[8] **SNLS Collaboration** Collaboration, P. Astier *et al.*, "The supernova legacy survey: Measurement of omega(m), omega(lambda) and w from the first year data set," *Astron.Astrophys.* **447** (2006) 31–48, arXiv:astro-ph/0510447 [astro-ph]. (Cited on page 2.)

[9] Planck Collaboration, P. A. R. Ade, N. Aghanim, C. Armitage-Caplan, M. Arnaud, M. Ashdown, F. Atrio-Barandela, J. Aumont, C. Baccigalupi, A. J. Banday, and et al., "Planck 2013 results. xxii. constraints on inflation," *ArXiv e-prints* (Mar., 2013) , arXiv:1303.5082 [astro-ph.CO]. (Cited on pages 2 and 31.)

[10] K. Bolejko, A. Krasiński, C. Hellaby, and M.-N. Célérier, *Structures in the Universe by Exact Methods: Formation, Evolution, Interactions*. Oct., 2009. (Cited on page 2.)

[11] S. February, J. Larena, M. Smith, and C. Clarkson, "Rendering dark energy void," *Monthly Notices of the RAS* **405** (July, 2010) 2231–2242, arXiv:0909.1479 [astro-ph.CO]. (Cited on page 2.)

[12] G. Ellis, "Inhomogeneity effects in cosmology," astro-ph.CO/1103.2335v1. (Cited on page 2.)

[13] S. Weinberg, "The cosmological constant problem," *Rev. Mod. Phys.* **61** (Jan, 1989) 1–23. http://link.aps.org/doi/10.1103/RevModPhys.61.1. (Cited on pages 2 and 4.)

[14] S. M. Carroll, "The cosmological constant," *Living Reviews in Relativity* **4** no. 1, (2001) . http://www.livingreviews.org/lrr-2001-1. (Cited on page 3.)

[15] J.-M. Alimi and A. Füzfa, "The abnormally weighting energy hypothesis: the missing link between dark matter and dark energy," *Journal of Cosmology and Astroparticle Physics* **2008** no. 09, (2008) 014, arXiv:0804.4100v2 [astro-ph]. http://stacks.iop.org/1475-7516/2008/i=09/a=014. (Cited on pages 5, 22, 31, 34, and 51.)

[16] G. R. Farrar and P. J. E. Peebles, "Interacting dark matter and dark energy," *Astrophys.J.* **604** (2004) 1–11, arXiv:astro-ph/0307316 [astro-ph]. (Cited on page 6.)

[17] S. M. Carroll, S. Mantry, M. J. Ramsey-Musolf, and C. W. Stubbs, "Dark-matter-induced violation of the weak equivalence principle," *Physical Review Letters* **103** no. 1, (July, 2009) 011301, arXiv:0807.4363 [hep-ph]. (Cited on page 6.)

[18] G. W. Anderson and S. M. Carroll, "Dark matter with time-dependent mass," in *COSMO-97, First International Workshop on Particle Physics and the Early Universe*, L. Roszkowski, ed., p. 227. 1998. astro-ph/9711288. (Cited on pages 6 and 32.)

[19] G. Smith, E. G. Adelberger, B. R. Heckel, and Y. Su, "Test of the equivalence principle for ordinary matter falling toward dark matter," *Physical Review Letters* **70** (Jan., 1993) 123–126. (Cited on pages 6 and 17.)

[20] A. P. Lightman and D. L. Lee, "Restricted proof that the weak equivalence principle implies the einstein equivalence principle," *Phys. Rev. D* **8** (Jul, 1973) 364–376. http://link.aps.org/doi/10.1103/PhysRevD.8.364. (Cited on page 10.)

[21] S. M. Carroll and G. B. Field, "Einstein equivalence principle and the polarization of radio galaxies," *Physically Review D* **43** (June, 1991) 3789–3793. (Cited on page 10.)

[22] S. Carroll, *Spacetime and Geometry: An Introduction to General Relativity*. Prentice Hall, 2004. (Cited on page 10.)

[23] J. Collins, A. Perez, D. Sudarsky, L. Urrutia, and H. Vucetich, "Lorentz invariance and quantum gravity: An additional fine-tuning problem?," *Phys. Rev. Lett.* **93** (Nov, 2004) 191301. http://link.aps.org/doi/10.1103/PhysRevLett.93.191301. (Cited on page 11.)

[24] D. Mattingly, "Modern tests of lorentz invariance," *Living Reviews in Relativity* **8** no. 5, (2005) . http://www.livingreviews.org/lrr-2005-5. (Cited on pages 11 and 12.)

[25] A. Anisimov, T. Banks, M. Dine, and M. Graesser, "Remarks on noncommutative phenomenology," *Physical Review D* **65** no. 8, (Apr., 2002) 085032, arXiv:hep-ph/0106356. (Cited on page 11.)

[26] T. Damour, "Theoretical aspects of the equivalence principle," *Classical and Quantum Gravity* **29** no. 18, (Sept., 2012) 184001, arXiv:1202.6311 [gr-qc]. (Cited on page 11.)

[27] D. Blas, M. M. Ivanov, and S. Sibiryakov, "Testing lorentz invariance of dark matter," *Journal of Cosmology and Astroparticle Physics* **2012** no. 10, (2012) 057. http://stacks.iop.org/1475-7516/2012/i=10/a=057. (Cited on page 11.)

[28] H. Yilmaz, "On rosen's bi-metric theory of gravitation.," *General Relativity and Gravitation* **6** (June, 1975) 269–276. (Cited on page 11.)

[29] C. M. Will, *Theory and Experiment in Gravitational Physics*. Cambridge University Press. (Cited on pages 12, 14, 19, 20, and 30.)

[30] O. Preuss, *Astronomical Tests of the Einstein Equivalence Principle*. PhD thesis, PhD Thesis, 2003, May, 2003. (Cited on pages 12 and 14.)

[31] A. S. Eddington, *The mathematical theory of relativity*. 1923. (Cited on page 13.)

[32] H. P. Robertson, "Relativity and cosmology," in *Space Age Astronomy*, A. J. Deutsch and W. B. Klemperer, eds., p. 228. 1962. (Cited on page 13.)

[33] L. I. Schiff, "Motion of a gyroscope according to einstein's theory of gravitation," *Proceedings of the National Academy of Science* **46** (June, 1960) 871–882. (Cited on page 13.)

[34] K. S. Thorne and C. M. Will, "Theoretical frameworks for testing relativistic gravity. i. foundations," *Astrophysical Journal* **163** (Feb., 1971) 595. (Cited on page 13.)

[35] C. M. Will, "Theoretical frameworks for testing relativistic gravity. ii. parametrized post-newtonian hydrodynamics, and the nordtvedt effect," *Astrophysical Journal* **163** (Feb., 1971) 611. (Cited on page 13.)

[36] C. M. Will, "Theoretical frameworks for testing relativistic gravity. iii. conservation laws, lorentz invariance, and values of the ppn parameters," *Astrophysical Journal* **169** (Oct., 1971) 125. (Cited on page 13.)

[37] K. S. T. C. W. Misner and J. A. Wheeler, *Gravitation*. W. H Freeman and Company, San Francisco, 1932. (Cited on pages 14 and 16.)

[38] K. Nordtvedt, "Equivalence principle for massive bodies. i. phenomenology," *Physical Review* **169** (May, 1968) 1014–1016. (Cited on page 16.)

[39] K. Nordtvedt, "Equivalence principle for massive bodies. ii. theory," *Physical Review* **169** (May, 1968) 1017–1025. (Cited on page 16.)

[40] C. M. Will, "The confrontation between general relativity and experiment," *Living Reviews in Relativity* **9** no. 3, (2006) . http://www.livingreviews.org/lrr-2006-3. (Cited on pages 16, 17, 21, and 32.)

[41] J. G. Williams, S. G. Turyshev, and D. H. Boggs, "Progress in lunar laser ranging tests of relativistic gravity," *Phys.Rev.Lett.* **93** (2004) 261101, arXiv:gr-qc/0411113 [gr-qc]. (Cited on pages 16 and 21.)

[42] T. Damour and G. Schaefer, "New tests of the strong equivalence principle using binary-pulsar data," *Physical Review Letters* **66** (May, 1991) 2549–2552. (Cited on page 16.)

[43] L. Ryder, *Introduction to General Relativity*. Cambridge University Press, 2009. (Cited on page 17.)

[44] P. Dirac, "The cosmological constants," *Nature* **139** (1937) 323. (Cited on page 18.)

[45] C. H. Brans, "The roots of scalar-tensor theory: an approximate history," *ArXiv General Relativity and Quantum Cosmology e-prints* (June, 2005) , arXiv:gr-qc/0506063. (Cited on pages 18 and 23.)

[46] P. Jordan, "Die physikalischen weltkonstanten," *Die Naturwissenschaften* **25** (1937) 513–517. (Cited on pages 18 and 27.)

[47] J. Uzan, "Varying constants, gravitation and cosmology," *Living Reviews in Relativity* **14** no. 2, (2011) . http://www.livingreviews.org/lrr-2011-2. (Cited on pages 18, 19, 20, and 30.)

[48] K. Nakamura and P. D. Group, "Review of particle physics," *Journal of Physics G: Nuclear and Particle Physics* **37** no. 7A, (2010) 075021. http://stacks.iop.org/0954-3899/37/i=7A/a=075021. (Cited on page 18.)

[49] J. D. Bekenstein, "Fine-structure constant: Is it really a constant?," *Phys. Rev. D* **25** (Mar, 1982) 1527–1539. http://link.aps.org/doi/10.1103/PhysRevD.25.1527. (Cited on page 19.)

[50] D. F. Mota and J. D. Barrow, "Local and global variations of the fine-structure constant," *Monthly Notices of the Royal Astronomical Society* **349** (Mar., 2004) 291–302, arXiv:astro-ph/0309273. (Cited on page 19.)

[51] J. A. King, J. K. Webb, M. T. Murphy, V. V. Flambaum, R. F. Carswell, *et al.*, "Spatial variation in the fine-structure constant – new results from vlt/uves," arXiv:1202.4758 [astro-ph.CO]. (Cited on page 19.)

[52] P. Petitjean, R. Srianand, H. Chand, A. Ivanchik, P. Noterdaeme, *et al.*, "Constraining fundamental constants of physics with quasar absorption line systems," arXiv:0905.1516 [astro-ph.CO]. (Cited on page 19.)

[53] F. C. Adams, "Stars in other universes: Stellar structure with different fundamental constants," *JCAP* **0808** (2008) 010, arXiv:0807.3697 [astro-ph]. (Cited on page 19.)

[54] R. Khatri and B. D. Wandelt, "Reply to flambaum and porsev comment on '21 cm radiation - a new probe of variation in the fine structure constant'," *Phys.Rev.Lett.* **105** (2010) 039002, arXiv:1007.1963 [astro-ph.CO]. (Cited on page 20.)

[55] S. Landau and C. G. Scoccola, "Constraints on variation in α and m_e from wmap 7-year data," *Astron.Astrophys.* **517** (2010) A62, arXiv:1002.1603 [astro-ph.CO]. (Cited on page 20.)

[56] E. Komatsu, J. Dunkley, M. R. Nolta, C. L. Bennett, B. Gold, G. Hinshaw, N. Jarosik, D. Larson, M. Limon, L. Page, D. N. Spergel, M. Halpern, R. S. Hill, A. Kogut, S. S. Meyer, G. S. Tucker, J. L. Weiland, E. Wollack, and E. L. Wright, "Five-year wilkinson microwave anisotropy probe observations: Cosmological interpretation," *Astrophysical Journals, Supplement* **180** (Feb., 2009) 330–376, arXiv:0803.0547. (Cited on page 20.)

[57] J. Larena, J.-M. Alimi, and A. Serna, "Big bang nucleosynthesis in scalar tensor gravity: The key problem of the primordial li-7 abundance," *Astrophys.J.* **658** (2007) 1–10, arXiv:astro-ph/0511693 [astro-ph]. (Cited on page 20.)

[58] C. Brans and R. H. Dicke, "Mach's principle and a relativistic theory of gravitation," *Physical Review* **124** (1961) 925–935. (Cited on pages 21 and 30.)

[59] C. J. Copi, A. N. Davis, and L. M. Krauss, "A new nucleosynthesis constraint on the variation of g," *Phys.Rev.Lett.* **92** (2004) 171301, arXiv:astro-ph/0311334 [astro-ph]. (Cited on page 21.)

[60] R. Nagata, T. Chiba, and N. Sugiyama, "Wmap constraints on scalar- tensor cosmology and the variation of the gravitational constant," *Phys.Rev.* **D69** (2004) 083512, arXiv:astro-ph/0311274 [astro-ph]. (Cited on page 21.)

[61] S. E. Thorsett, "The gravitational constant, the chandrasekhar limit, and neutron star masses," *Phys. Rev. Lett.* **77** (Aug, 1996) 1432–1435. http://link.aps.org/doi/10.1103/PhysRevLett.77.1432. (Cited on page 21.)

[62] V. M. Kaspi, J. H. Taylor, and M. F. Ryba, "High - precision timing of millisecond pulsars. 3: Long - term monitoring of psrs b1855+09 and b1937+21," *Astrophys.J.* **428** (1994) 713. (Cited on page 21.)

[63] J. Khoury and A. Weltman, "Chameleon cosmology," *Physical Review D* **69** no. 4, (Feb., 2004) 044026, arXiv:astro-ph/0309411. (Cited on pages 23, 31, 32, and 33.)

[64] O. Klein, "Quantum theory and five-dimensional theory of relativity. (in german and english)," *Z.Phys.* **37** (1926) 895–906. (Cited on page 24.)

[65] D. Bailin and A. Love, "Review article: Kaluza-klein theories," *Reports on Progress in Physics* **50** (Sept., 1987) 1087–1170. (Cited on page 24.)

[66] A. D. Felice and S. Tsujikawa, "f(r) theories," *Living Reviews in Relativity* **13** no. 3, (2010) . http://www.livingreviews.org/lrr-2010-3. (Cited on pages 25 and 26.)

[67] K. S. Stelle, "Classical gravity with higher derivatives," *General Relativity and Gravitation* **9** (Apr., 1978) 353–371. (Cited on page 25.)

[68] T. P. Sotiriou and V. Faraoni, "f(r) theories of gravity," *Reviews of Modern Physics* **82** (Jan., 2010) 451–497, arXiv:0805.1726 [gr-qc]. (Cited on page 26.)

[69] K. Becker, M. Becker, and J. H. Schwarz, *String Theory and M-Theory.* 2007. (Cited on page 27.)

[70] V. Faraoni, E. Gnzig, and P. Nardone, "Conformal trasformations in classical gravitational theories and in cosmology," *Fund. Cosmic Phys* **20** (1999) 121, arXiv:gr-qc/9811047. (Cited on pages 28 and 30.)

[71] E. Flanagan, "The conformal frame freedom in theories of gravitation," *Classical and Qauntum Gravity* **21** (2004) 3817, arXiv:astro-qc/0403063v3. (Cited on pages 28 and 30.)

[72] V. Faraoni and S. Nadeau, "(pseudo)issue of the conformal frame revisited," *Physical Reviewd D* **75** no. 2, (Jan., 2007) 023501, arXiv:gr-qc/0612075. (Cited on page 28.)

[73] J. Frauendiener, "Conformal infinity," *Living Reviews in Relativity* **3** no. 4, (2000) . http://www.livingreviews.org/lrr-2000-4. (Cited on page 28.)

[74] V. Faraoni, *Cosmolgy in Scalar-Tensor Gravity*. Kluwer Academic, Dordrecht, 2004. (Cited on page 29.)

[75] G. M. L. Sokolowski, "Physical equivalence between nonlinear gravity theories and a general-relativistic self-gravitationg scalar field," *Physical Review D* **50** (1994) 5039. (Cited on page 29.)

[76] T. Damour and G. Esposito-Farese, "Tensor-multi-scalar theories of gravitation," *Classical and Quantum Gravity* **9** no. 9, (1992) 2093. http://stacks.iop.org/0264-9381/9/i=9/a=015. (Cited on pages 30 and 71.)

[77] A. Hees and A. Füzfa, "Combined cosmological and solar system constraints on chameleon mechanism," *Physical Review D* **85** no. 10, (May, 2012) 103005, arXiv:1111.4784 [gr-qc]. (Cited on pages 30, 33, 58, and 75.)

[78] G. F. R. Ellis, R. Maartens, and M. A. H. MacCallum, *Relativistic Cosmology*. Mar., 2012. (Cited on page 30.)

[79] V. Faraoni and E. Gunzig, "Einstein frame or jordan frame," *International Journal of Theoretical Physics* **38** (1999) 217. (Cited on page 30.)

[80] R. Catena, M. Pietroni, and L. Scarabello, "Einstein and jordan frames reconciled: A frame-invariant approach to scalar-tensor cosmology," *Physical Review D* **76** (2007) . (Cited on page 30.)

[81] V. Faraoni and N. Lanahan-Tremblay, "Breakdown of the initial value formulation of scalar-tensor gravity and its physical meaning," *Phys. Rev. D* **78** (Sep, 2008) 064017. http://link.aps.org/doi/10.1103/PhysRevD.78.064017. (Cited on page 30.)

[82] F. Bezrukov and M. Shaposhnikov, "The standard model higgs boson as the inflaton," *Physics Letters B* **659** (Jan., 2008) 703–706, arXiv:0710.3755 [hep-th]. (Cited on page 31.)

[83] S. CMS Collaboration Chatrchyan, V. Khachatryan, A. M. Sirunyan, A. Tumasyan, W. Adam, E. Aguilo, T. Bergauer, M. Dragicevic, J. Erö, C. Fabjan, and et al., "Observation of a new boson at a mass of 125 gev with the cms experiment at the lhc," *Physics Letters B* **716** (Sept., 2012) 30–61, arXiv:1207.7235 [hep-ex]. (Cited on pages 31 and 38.)

[84] G. ATLAS Collaboration Aad, T. Abajyan, B. Abbott, J. Abdallah, S. Abdel Khalek, A. A. Abdelalim, O. Abdinov, R. Aben, B. Abi, M. Abolins, and et al., "Observation of a new particle in the search for the standard model higgs boson with the atlas detector at the lhc," *Physics Letters B* **716** (Sept., 2012) 1–29, arXiv:1207.7214 [hep-ex]. (Cited on pages 31 and 38.)

[85] F. Bezrukov, "The higgs field as an inflaton," *Classical and Quantum Gravity* **30** no. 21, (Nov., 2013) 214001, arXiv:1307.0708 [hep-ph]. (Cited on page 31.)

[86] P. Brax, "Chameleon dark energy," in *AIP Conference Proceedings*, vol. 736, pp. 105–110. AIP, Oct., 2004. arXiv:0410103 [astro-ph]. http://arxiv.org/abs/astro-ph/0410103. (Cited on page 31.)

[87] A.-C. Davis, E. A. Lim, J. Sakstein, and D. J. Shaw, "Modified gravity makes galaxies brighter," *Physical Review D* **85** no. 12, (June, 2012) 123006, arXiv:1102.5278. http://arxiv.org/abs/1102.5278. (Cited on pages 31 and 58.)

[88] T. Damour and G. Esposito-Farèse, "Nonperturbative strong-field effects in tensor-scalar theories of gravitation," *Phys. Rev. Lett.* **70** (Apr, 1993) 2220–2223. http://link.aps.org/doi/10.1103/PhysRevLett.70.2220. (Cited on page 31.)

[89] T. Damour and K. Nordtvedt, "Tensor-scalar cosmological models and their relaxation toward general relativity," *Physics Review D* **48** (Oct, 1993) 3436–3450. http://link.aps.org/doi/10.1103/PhysRevD.48.3436. (Cited on page 32.)

[90] T. Damour and A. M. Polyakov, "The string dilation and a least coupling principle," *Nuclear Physics B* **423** (July, 1994) 532–558, arXiv:hep-th/9401069. (Cited on page 32.)

[91] J. Khoury and A. Weltman, "Chameleon fields: Awaiting surprises for tests of gravity in space," *Physical Review Letters* **93** no. 17, (Oct., 2004) 171104, astro-ph/0309300. (Cited on pages 32 and 33.)

[92] B. Ratra and P. J. E. Peebles, "Cosmological consequences of a rolling homogeneous scalar field," *Phys. Rev. D* **37** (Jun, 1988) 3406–3427. http://link.aps.org/doi/10.1103/PhysRevD.37.3406. (Cited on pages 32 and 33.)

[93] P. J. Steinhardt, L. Wang, and I. Zlatev, "Cosmological tracking solutions," *Physical Review D* **59** no. 12, (June, 1999) 123504, astro-ph/9812313. (Cited on pages 32 and 33.)

[94] D. F. Mota and D. J. Shaw, "Evading equivalence principle violations, cosmological, and other experimental constraints in scalar field theories with a strong coupling to matter," *Physical Review D* **75** no. 6, (Mar., 2007) 063501, arXiv:hep-ph/0608078. (Cited on page 33.)

[95] T. Tamaki and S. Tsujikawa, "Revisiting chameleon gravity: Thin-shell and no-shell fields with appropriate boundary conditions," *Phys. Rev. D* **78** (Oct, 2008) 084028. http://link.aps.org/doi/10.1103/PhysRevD.78.084028. (Cited on page 33.)

[96] J.-M. Alimi and A. Füzfa, "Toward a unified description of dark energy and dark matter from the abnormally weighting energy hypothesis," *Phys. Rev. D* **75** (Jun, 2007) 123007, arXiv:astro-ph/0702478v3. http://link.aps.org/doi/10.1103/PhysRevD.75.123007. (Cited on pages 34 and 63.)

[97] R. Ruffini and S. Bonazzola, "Systems of self-gravitating particles in general relativity and the concept of an equation of state," *Physical Review* **187** (Nov., 1969) 1767–1783. (Cited on pages 38 and 39.)

[98] F. E. Schunck and E. W. Mielke, "Topical review: General relativistic boson stars," *ArXiv e-prints* (Jan., 2008) , arXiv:0801.0307. (Cited on pages 38, 41, 43, and 74.)

[99] T. Damour, O. Darrigol, B. Duplantier, and V. Rivasseau, *Einstein, 1905âĂŞ2005: PoincarÃľ Seminar 2005 /*. BirkhÃďuser Verlag„ Basel :, 2006. (Cited on page 38.)

[100] E. W. Mielke and F. E. Schunck, "Nontopological scalar soliton as dark matter halo," *Physical Review D* **66** no. 2, (June, 2002) 023503. (Cited on page 38.)

[101] G. H. Derrick, "Comments on nonlinear wave equations as models for elementary particles," *Journal of Mathematical Physics* **5** (Sept., 1964) 1252–1254. (Cited on page 39.)

[102] I. I. Tkachev, "Coherent scalar-field oscillations forming compact astrophysical object," *Soviet Astronomy Letters* **12** (Oct., 1986) 305–308. (Cited on page 39.)

[103] E. Seidel and W.-M. Suen, "Oscillating soliton stars," *Physical Review Letters* **66** (Apr., 1991) 1659–1662. (Cited on page 39.)

[104] R. Friedberg, T. D. Lee, and Y. Pang, "Mini-soliton stars," *Phys. Rev. D* **35** (Jun, 1987) 3640–3657. http://link.aps.org/doi/10.1103/PhysRevD.35.3640. (Cited on pages 39 and 41.)

[105] A. Whinnett, "Spontaneous scalarization and boson stars," *Phys.Rev.* **D61** (2000) 124014, arXiv:gr-qc/9911052 [gr-qc]. (Cited on pages 39 and 43.)

[106] M. Colpi, S. L. Shapiro, and I. Wasserman, "Boson stars - gravitational equilibria of self-interacting scalar fields," *Physical Review Letters* **57** (Nov., 1986) 2485–2488. (Cited on page 39.)

[107] C.-W. Lai, *A Numerical Study of Boson Stars*. PhD thesis, PhD Thesis, 2004, Oct., 2004. (Cited on page 42.)

[108] B. C. Mundim, *A Numerical Study of Boson Star Binaries*. PhD thesis, PhD Thesis, 2010, 2010. (Cited on page 42.)

[109] S. L. Liebling and C. Palenzuela, "Dynamical boson stars," *Living Reviews in Relativity* **15** (May, 2012) 6, arXiv:1202.5809 [gr-qc]. (Cited on page 42.)

[110] D. F. Torres, "Boson stars in general scalar-tensor gravitation: Equilibrium configurations," *Physical Review D* **56** (Sept., 1997) 3478–3484, gr-qc/9704006. (Cited on page 43.)

[111] D. F. Torres, F. E. Schunck, and A. R. Liddle, "Brans-dicke boson stars: Configurations and stability through cosmic history," *Class.Quant.Grav.* **15** (1998) 3701–3718, arXiv:gr-qc/9803094 [gr-qc]. (Cited on page 43.)

[112] D. F. Torres, "Boson stars in general scalar - tensor gravitation: Equilibrium configurations," *Phys.Rev.* **D56** (1997) 3478–3484, arXiv:gr-qc/9704006 [gr-qc]. (Cited on page 43.)

[113] S. Yazadjiev, "Tensor mass and particle number peak at the same location in the scalar tensor gravity boson star models: An analytical proof," *Class.Quant.Grav.* **16** (1999) L63–L69, arXiv:gr-qc/9906038 [gr-qc]. (Cited on page 43.)

[114] A. Whinnett and D. F. Torres, "Charged scalar tensor boson stars: Equilibrium, stability and evolution," *Phys.Rev.* **D60** (1999) 104050, arXiv:gr-qc/9905017 [gr-qc]. (Cited on page 43.)

[115] B. Gradwohl and G. Kaelbermann, "Dilaton stars," *Nucl.Phys.* **B324** (1989) 215. (Cited on page 43.)

[116] M. A. Gunderson and L. G. Jensen, "Boson stars in the brans-dicke gravitational theories," *Physical Revied D* **48** (Dec., 1993) 5628–5633, astro-ph/9308014. (Cited on page 43.)

[117] J. D. Barrow, "Gravitational memory\?," *Physical Review D* **46** (Oct., 1992) 3227. (Cited on page 43.)

[118] T. Damour and G. Esposito-Farèse, "Tensor-scalar gravity and binary-pulsar experiments," *Physical Review D* **54** (Jul, 1996) 1474–1491. http://link.aps.org/doi/10.1103/PhysRevD.54.1474. (Cited on page 43.)

[119] J. L. F. Barbón and J. R. Espinosa, "On the naturalness of higgs inflation," *Physical Review D* **79** no. 8, (Apr., 2009) 081302, arXiv:0903.0355 [hep-ph]. (Cited on page 44.)

[120] A. Füzfa, M. Rinaldi, and S. Schlögel, "Particlelike distributions of the higgs field nonminimally coupled to gravity," *Physical Review Letters* **111** no. 12, (Sept., 2013) 121103, arXiv:1305.2640 [gr-qc]. (Cited on pages 44, 45, and 74.)

[121] M. Rinaldi, "The dark aftermath of higgs inflation," *ArXiv e-prints* (Sept., 2013) , arXiv:1309.7332 [gr-qc]. (Cited on pages 44 and 74.)

[122] E. P. Hubble, "Extragalactic nebulae.," *Astrophysical Journal* **64** (Dec., 1926) 321–369. (Cited on page 49.)

[123] L. L. Christensen, R. Y. Shida, and D. de Martin, *Cosmic Collisions: The Hubble Atlas of Merging Galaxies*. Oct., 2009. (Cited on page 49.)

[124] K. Fathi, *Dynamics and morphology in the inner regions of spiral galaxies*. PhD thesis, University of Groningen, 2004. (Cited on page 49.)

[125] J. Binney and S. Tremaine, *Galactic Dynamics: Second Edition*. Princeton University Press, 2008. (Cited on page 50.)

[126] A. V. Zasov and G. A. Kyazumov, "The rotation curves of normal galaxies," *Soviet Astronomy* **27** (Aug., 1983) 384. (Cited on page 50.)

[127] B. Famaey and S. S. McGaugh, "Modified newtonian dynamics (mond): Observational phenomenology and relativistic extensions," *Living Reviews in Relativity* **15** no. 10, (2012) . http://www.livingreviews.org/lrr-2012-10. (Cited on pages 50 and 58.)

[128] F. J. Sánchez-Salcedo, A. M. Hidalgo-Gámez, and E. E. Martínez-García, "Slowly rotating gas-rich galaxies in modified newtonian dynamics (mond)," *Astronomical Journal* **145** (Mar., 2013) 61, arXiv:1301.5847 [astro-ph.CO]. (Cited on pages 50 and 57.)

[129] K. G. Begeman, A. H. Broeils, and R. H. Sanders, "Extended rotation curves of spiral galaxies - dark haloes and modified dynamics," *Monthly Notices of the Royal Astronomical Society* **249** (Apr., 1991) 523–537. (Cited on pages 50, 57, and 58.)

[130] R. H. Sanders and K. G. Begeman, "Modified dynamics / mond / as a dark halo," *Monthly Notices of the Royal Astronomical Society* **266** (Jan., 1994) 360. (Cited on pages 50 and 51.)

[131] Y. Sofue and V. Rubin, "Rotation curves of spiral galaxies," *Annual Review of Astronomy and Astrophysics* **39** (2001) 137–174, arXiv:astro-ph/0010594. (Cited on page 51.)

[132] S. Blais-Ouellette, P. Amram, and C. Carignan, "Accurate determination of the mass distribution in spiral galaxies. ii. testing the shape of dark halos," *Astrophysical Journal* **121** (Apr., 2001) 1952–1964, arXiv:astro-ph/0006449. (Cited on page 51.)

[133] K. G. Begeman, *HI rotation curves of spiral galaxies*. PhD thesis, Kapteyn Institute, (1987), Dec., 1987. (Cited on page 51.)

[134] C. Carignan, R. Sancisi, and T. S. van Albada, "H i and mass distribution in the dwarf 'regular' galaxy ugc 2259," *Astrophysical JOurnal* **95** (Jan., 1988) 37–44. (Cited on page 51.)

[135] W. J. G. de Blok, F. Walter, E. Brinks, C. Trachternach, S.-H. Oh, and R. C. Kennicutt, Jr., "High-resolution rotation curves and galaxy mass models from things," *The Astrophysical Journal* **136** (Dec., 2008) 2648–2719, arXiv:0810.2100. (Cited on page 51.)

[136] S. Blais-Ouellette, P. Amram, C. Carignan, and R. Swaters, "Velocity in 6 spiral galaxies (blais-ouellette+, 2004)," *VizieR Online Data Catalog* **342** (June, 2004) 147. (Cited on page 51.)

[137] D. S. Goldwirth and J. Katz, "A comment on junction and energy conditions in thin shells," *Classical and Quantum Gravity* **12** no. 3, (1995) 769. http://stacks.iop.org/0264-9381/12/i=3/a=014. (Cited on page 51.)

[138] S. M. Kent, "Dark matter in spiral galaxies. ii - galaxies with h i rotation curves," *Astrophysical Journal* **93** (Apr., 1987) 816–832. (Cited on pages 53 and 54.)

[139] S. S. McGaugh, "The number, luminosity and mass density of spiral galaxies as a function of surface brightness," *Monthly Notices of the RAS* **280** (May, 1996) 337–354, arXiv:astro-ph/9511010. (Cited on page 55.)

[140] L. Hernquist, "An analytical model for spherical galaxies and bulges," *Astrophysical Journal* **356** (June, 1990) 359–364. (Cited on page 55.)

[141] J. L. Sérsic, "Influence of the atmospheric and instrumental dispersion on the brightness distribution in a galaxy," *Boletin de la Asociacion Argentina de Astronomia La Plata Argentina* **6** (1963) 41. (Cited on page 55.)

[142] J. L. Sersic, *Atlas de galaxias australes*. 1968. (Cited on page 55.)

[143] M. Baes and G. Gentile, "Analytical expressions for the deprojected sérsic model," *Astronomy & Astrophysics* **525** (Jan., 2011) A136, arXiv:1009.4713 [astro-ph.CO]. (Cited on page 56.)

[144] A. Mazure and H. V. Capelato, "Exact solutions for the spatial de vaucouleurs and sérsic laws and related quantities," *Astronomy and Astrophysics* **383** (Jan., 2002) 384–389, arXiv:astro-ph/0112147. (Cited on page 56.)

[145] B. K. Dhar and L. L. R. Williams, "Surface brightness and intrinsic luminosity of ellipticals," *Monthly Notices of the Royal Astronomical Society* **427** (Nov., 2012) 204–244, arXiv:1112.3120 [astro-ph.CO]. (Cited on page 56.)

[146] L. Ciotti, "Stellar systems following the r exp 1/m luminosity law," *Astronomy and Astrophysics* **249** (Sept., 1991) 99–106. (Cited on page 56.)

[147] P. Prugniel and F. Simien, "The fundamental plane of early-type galaxies: non-homology of the spatial structure.," *Astronomy & Astrophysics* **321** (May, 1997) 111–122. (Cited on page 56.)

[148] J. F. Navarro, C. S. Frenk, and S. D. M. White, "The structure of cold dark matter halos," *Astrophysical Journal* **462** (May, 1996) 563, arXiv:astro-ph/9508025. (Cited on page 56.)

[149] M. Milgrom, "A modification of the newtonian dynamics - implications for galaxies," *Astrophysical Journal* **270** (July, 1983) 371–389. (Cited on page 56.)

[150] C. Carignan, B. S. Frank, K. M. Hess, D. M. Lucero, T. H. Randriamampandry, S. Goedhart, and S. S. Passmoor, "Kat-7 science verification: Using h i observations of ngc 3109 to understand its kinematics and mass distribution," *Astronomical Journal* **146** (Sept., 2013) 48, arXiv:1306.3227 [astro-ph.CO]. (Cited on page 57.)

[151] J. E. Felten, "Milgrom's revision of newton's laws - dynamical and cosmological consequences," *Astrophysical Journal* **286** (Nov., 1984) 3–6. (Cited on page 58.)

[152] M. Milgrom, "Dynamics with a nonstandard inertia-acceleration relation: An alternative to dark matter in galactic systems," *Annals of Physics* **229** (Feb., 1994) 384–415, arXiv:astro-ph/9303012. (Cited on page 58.)

[153] J. Bekenstein and M. Milgrom, "Does the missing mass problem signal the breakdown of newtonian gravity?," *Astophysical Journal* **286** (Nov., 1984) 7–14. (Cited on page 58.)

[154] M. Milgrom, "Quasi-linear formulation of mond," *Monthly Notices of the RAS* **403** (Apr., 2010) 886–895, arXiv:0911.5464 [astro-ph.CO]. (Cited on page 58.)

[155] B. Famaey, G. Gentile, J.-P. Bruneton, and H. Zhao, "Insight into the baryon-gravity relation in galaxies," *Physical Review D* **75** no. 6, (Mar., 2007) 063002, arXiv:astro-ph/0611132. (Cited on page 58.)

[156] R. Gannouji, B. Moraes, D. F. Mota, D. Polarski, S. Tsujikawa, and H. A. Winther, "Chameleon dark energy models with characteristic signatures," *Physics Review D* **82** no. 12, (Dec., 2010) 124006, arXiv:1010.3769 [astro-ph.CO]. (Cited on page 58.)

[157] P. Chang and L. Hui, "Stellar structure and tests of modified gravity," *Astrophysical Journal* **732** (May, 2011) 25, arXiv:1011.4107 [astro-ph.CO]. (Cited on page 58.)

[158] L. Hui, A. Nicolis, and C. W. Stubbs, "Equivalence principle implications of modified gravity models," *Physical Review D* **80** no. 10, (Nov., 2009) 104002, arXiv:0905.2966 [astro-ph.CO]. (Cited on page 58.)

[159] W. H. Press, B. P. Flannery, S. A. Teukolsky, and W. T. Vetterling, *Numerical Recipes in Fortran: The Art of Scientific Computing*. Cambridge University Press, 1992. (Cited on pages 62, 82, and 83.)

[160] R. Kuzio de Naray, S. S. McGaugh, and W. J. G. de Blok, "Mass models for low surface brightness galaxies with high-resolution optical velocity fields," *Astrophysical Journal* **676** (Apr., 2008) 920–943, arXiv:0712.0860. (Cited on page 71.)

[161] A. Füzfa and J.-M. Alimi, "Dark energy as a born-infeld gauge interaction violating the equivalence principle," *Physical Review Letters* **97** no. 6, (Aug., 2006) 061301, astro-ph/0604517. (Cited on page 73.)

[162] J. J. Van der Bij and M. Gleiser, "Stars of bosons with non-minimal energy-momentum tensor," *Physics Letters B* **194** no. 4, (1987) 482–486. (Cited on page 74.)

[163] R. Ellis, J. Huchra, S. Kahn, G. Rieke, and P. B. Stetson, eds., *Practical Statistics for Astronomers*. Nov., 2003. (Cited on page 83.)

[164] M. P. Hobson, *Bayesian methods in cosmology*. Cambridge University Press, 2010. (Cited on page 84.)

[165] W. Bolstad, *Understanding Computational Bayesian Statistics*. Wiley Series in Computational Statistics. Wiley, 2012. http://books.google.co.za/books?id=jqLF-x4t3TwC. (Cited on page 84.)